
Electronic Thesis and Dissertation Repository

7-29-2014 12:00 AM

Curcumin-Loaded Magnetic Nanoaggregates Conjugated with Folic Acid for Targeted Cancer Treatment

Melessa Salem
The University of Western Ontario

Supervisor
Dr. Elizabeth Gillies
The University of Western Ontario Joint Supervisor
Dr. Sohrab Rohani
The University of Western Ontario

Graduate Program in Biomedical Engineering
A thesis submitted in partial fulfillment of the requirements for the degree in Master of Engineering Science
© Melessa Salem 2014

Follow this and additional works at: <https://ir.lib.uwo.ca/etd>

 Part of the [Biomaterials Commons](#)

Recommended Citation

Salem, Melessa, "Curcumin-Loaded Magnetic Nanoaggregates Conjugated with Folic Acid for Targeted Cancer Treatment" (2014). *Electronic Thesis and Dissertation Repository*. 2206.
<https://ir.lib.uwo.ca/etd/2206>

This Dissertation/Thesis is brought to you for free and open access by Scholarship@Western. It has been accepted for inclusion in Electronic Thesis and Dissertation Repository by an authorized administrator of Scholarship@Western. For more information, please contact wlsadmin@uwo.ca.

CURCUMIN-LOADED MAGNETIC NANOAGGREGATES CONJUGATED WITH FOLIC
ACID FOR TARGETED CANCER TREATMENT

(Thesis format: Integrated Article)

by

Melessa Salem

Biomedical Engineering Graduate Program

A thesis submitted in partial fulfillment
of the requirements for the degree of
Masters of Engineering Science

The School of Graduate and Postdoctoral Studies
The University of Western Ontario
London, Ontario, Canada

©Melessa Salem 2014

Abstract

Cancer has been, and still remains, one of the most complicated diseases to treat. As a result of the side effects experienced from current cancer treatment methods, there has been a growing interest in the development of targeted drug delivery systems that can destroy cancer cells, but render healthy tissue unharmed. To address this challenge, magnetite nanoaggregates were synthesized through the precipitation of iron oxide in the presence of polymers, conjugated with folic acid for folate targeting, and loaded with curcumin for cancer treatment. The resulting magnetite nanoparticles were 10 – 20 nm in size and the aggregates formed varied in size depending on the ratio of polymers present. Furthermore, the ratio of polymers on the particle surfaces, in addition to the presence of folic acid, played a major role in sustaining curcumin release. *In vitro* studies with MDA-MB-231 and MDA-MB-468 cells revealed that the particles without curcumin exhibited low cytotoxicity up to 2 mg/mL in both cells lines. However, in the presence of curcumin, toxicity to MDA-MB-468 cells was observed. In addition, folic acid functionalized particles showed enhanced uptake in MDA-MB-468 cells, which express elevated levels of the folic acid receptor, in comparison to non-targeted particles, suggesting the possibility of selective delivery towards cancer cells.

Keywords

targeted cancer treatment, drug delivery, curcumin, folate receptor, magnetic nanoparticles, controlled drug release

Co-Authorship Statement

This thesis is an integration of two articles. Chapter two was written based on a published review paper, and chapter three is a research article in preparation for submission.

Chapter 2: Curcumin, a promising anti-cancer therapeutic: a review of its chemical properties, bioactivity and approaches to cancer cell delivery, published in RSC Advances in 2014 (DOI:10.1039/c3ra46396f).

The published review paper was written with Dr. Sohrab Rohani, and Dr. Elizabeth Gillies. My contributions included research and extracting information from literature, along with writing of the review paper. Dr. Elizabeth Gillies also contributed to the writing of the review paper, and all authors contributed to the review process before publication.

Chapter 3: Synthesis, characterization, and *in vitro* activity of curcumin-loaded folic acid-conjugated magnetic nanoaggregates – in preparation for submission.

My contributions to this work included data preparation and experimentation, results analysis and validation, and manuscript preparation. This work was performed under the supervision of Dr. Sohrab Rohani and Dr. Elizabeth Gillies, and collaboration with Dr. Allison Allan. Cell studies were carried out under the supervision of Dr. Allan and conducted by the post-doctoral fellow in Dr. Allan's lab, Dr. Ying Xia, and the experimental methods for the cell work were written by her. All authors will contribute to the manuscript preparation and review.

Acknowledgments

First, I would like to thank my supervisors, Dr. Sohrab Rohani and Dr. Elizabeth Gillies, for giving me the opportunity to gain from their experience and knowledge, as well as for their support and confidence in me. Dr. Rohani always encouraged me to explore new ideas and never failed to offer support and advice in times where I felt uncertain. Dr. Gillies always made time to answer my questions, edit my papers, and offer support and advice despite being very busy, especially since she was on sabbatical during the last year of my period of study. In addition to academic knowledge, both Dr. Rohani and Dr. Gillies taught me to maintain a positive attitude and passion for science and research.

I would like to sincerely acknowledge Dr. Allison Allan for her collaboration on this project, and Dr. Ying Xia for putting endless time and effort into ensuring the accuracy and validity of the cell study results. Additionally, I would like to acknowledge my advisory committee members, Dr. Wankei Wan and Dr. Kibret Mequanint, for their insight and feedback and Dr. Jose Herrera for his general advice and support.

Additionally, I would like to thank all my labmates, with special thanks to Dr. Doaa Ragab, Dr. Mahmoud Moustafa, Dr. John Trant, Andrew Wong, and Trevor McIntosh for their support with data interpretation and the operation of different equipment.

Lastly, I would like to acknowledge Somiraa Said for her inspiring ideas and endless support, and my family, with a very special thanks to my mother who has always inspired me to follow my dreams and stayed by my side during my journey.

Table of Contents

Abstract.....	ii
Co-Authorship Statement.....	iii
Acknowledgments.....	iv
Table of Contents.....	v
List of Tables.....	viii
List of Figures.....	ix
List of Appendices.....	xi
List of Abbreviations.....	xii
Chapter 1.....	1
1 Introduction.....	1
1.1 Motivation and Cancer Treatment Overview.....	1
1.2 Drug Delivery Systems (DDS) for Cancer Treatment.....	1
1.2.1 Liposomes, Micelles, and Exosomes.....	2
1.2.2 Hydrogels.....	2
1.2.3 Dendrimers.....	3
1.2.4 Nanoparticles.....	3
1.3 History of Metallic Compounds for Medical Treatments.....	4
1.3.1 Magnetic Iron Oxide Nanoparticles.....	5
1.4 Thesis Objectives and Hypothesis.....	7
1.5 Thesis Outline.....	7
1.6 Bibliography.....	9
Chapter 2.....	11
2 Curcumin, a Promising Anti-cancer Therapeutic.....	11
2.1 Introduction.....	11

2.2 Physicochemical Properties	12
2.2.1 Effect of pH.....	13
2.2.2 Effect of Temperature	14
2.2.3 Degradation Products of Curcumin	17
2.3 Effect of Curcumin on Cancer Cells.....	19
2.4 Clinical Studies	27
2.5 Enhancement of Curcumin Solubility and Bioavailability	28
2.5.1 Preparation of Curcumin Co-crystals.....	29
2.5.2 Delivery Systems for Curcumin.....	30
2.6 Conclusions and Future Prospects	38
2.7 Bibliography	40
Chapter 3.....	47
3 Synthesis, Characterization, and <i>in vitro</i> Activity of Curcumin-Loaded Folic Acid- Conjugated Magnetic Nanoaggregates	47
3.1 Introduction.....	47
3.2 Materials	50
3.3 Synthesis Procedures	51
3.3.1 Preparation of PPG-NH ₂ /β-CD Coated Nanoaggregates Sample S4 and Representative Procedure for the Preparation of Samples S1 – S3	52
3.3.2 Functionalization of PPG-NH ₂ /β-CD-Coated Nanoaggregates Samples with Folic Acid	53
3.3.3 β-CD/curcumin Complex Synthesis and Curcumin Loading of Nanoaggregates.....	53
3.3.4 Preparation of FITC-labeled Particles	54
3.4 Characterization of Synthesized Nanoaggregates.....	54
3.4.1 Particle Morphology	54
3.4.2 Particle Size Analysis	55

3.4.3	X-ray Diffraction (XRD) Analysis	55
3.4.4	Fourier Transform Infrared (FTIR) Spectroscopy	55
3.4.5	Vibrating Sample Magnetometer (VSM) Measurements	55
3.5	<i>In vitro</i> Studies Experimental Procedures.....	56
3.5.1	Curcumin Release	56
3.5.2	<i>In vitro</i> Cytotoxicity Assays	56
3.5.3	Flow Cytometry Analysis	56
3.6	Results and Discussion	57
3.6.1	Nanoaggregate Synthesis	57
3.6.2	Nanoaggregate Characterization.....	58
3.6.3	Curcumin Loading and <i>in vitro</i> Release	64
3.6.4	<i>In vitro</i> Cell Studies	67
3.7	Conclusion	72
3.8	Bibliography	74
Chapter 4	76
4	Conclusions and Future Prospects	76
Appendix	78
Copyright Permissions	84
Curriculum Vitae	87

List of Tables

Table 1.1: Common synthesis methods for iron oxide nanoparticles	6
Table 2.1: Comparison of incidences and deaths in India and United States for common cancers showing cases per 1 million persons.....	20
Table 3.1: Polymer compositions, and folic acid and curcumin content of synthesized samples	52
Table 3.2: Individual particle size and aggregate size of synthesized samples	59
Table 3.3: Diffusional exponent and diffusion mechanism for non-swellable systems of different geometries	67

List of Figures

Figure 2.1: Tautomeric forms of curcumin.....	13
Figure 2.2: Proposed structure of curcumin in (a) acidic, (b) neutral, and (c) basic environments	14
Figure 2.3: ThT assay results, showing that the ability of curcumin to inhibit the amyloid fibrillation of HEWL (inhibition is detected as a decrease in fluorescence intensity). Reprinted from reference 12 with permission from Elsevier	16
Figure 2.4: Proposed degradation products of curcumin.....	17
Figure 2.5: Proposed mechanism for the autoxidation of curcumin.....	19
Figure 2.6: Structural features of curcumin involved in binding to protein targets.....	21
Figure 2.7: Common cofomers used with curcumin to produce cocrystals	29
Figure 2.8: Curcumin-loaded drug delivery systems.....	30
Figure 2.9: Schematic of the collection and loading of exosomes	31
Figure 2.10: Schematic of a hydrogel with encapsulated curcumin	36
Figure 2.11: Schematic of the synthesis of a curcumin-conjugated dendrimer.....	37
Figure 3.1: Schematic of a folic acid-conjugated curcumin-loaded magnetic nanoparticle.....	50
Figure 3.2: Chemical scheme of synthesis process.....	51
Figure 3.3: Nucleation and growth schematic	58
Figure 3.4: TEM images of A) uncoated nanoaggregates, and B) sample S2.....	60
Figure 3.5: a) XRD spectra of synthesized samples, and b) standard XRD pattern of magnetite	61

Figure 3.6: a) Magnetization curves of uncoated nanoaggregates and sample S2 and b) their corresponding magnetic properties.	62
Figure 3.7: FTIR spectra of (a) uncoated nanoaggregates, (b) β -CD, (c) PPG-NH ₂ , (d) folic acid, (e) sample S2, and (f) sample S2FA	63
Figure 3.8: Encapsulation efficiency trends for samples S1c and S2c	65
Figure 3.9: In vitro curcumin release profiles for (a) S1c, (b) S1FAc, (c) S2c, and (d) S2FAc...	66
Figure 3.10: Folate receptor expression in MDA-MB-231 and MDA-MB-468 cells	68
Figure 3.11: Uptake of samples S2 and S2FA by MDA-MB-231 and MDA-MB-468 cells	69
Figure 3.12: Free curcumin dose response curve.....	70
Figure 3.13: Cytotoxicity of curcumin-loaded nanoaggregates on breast cancer cells	71
Figure 3.14: Cytotoxicity of samples S2 and S2FA	72

List of Appendices

Appendix 1: Standard XRD pattern for magnetite corresponding to ICCD card number 00-019-0629.....	78
Appendix 2: ^1H NMR spectra of curcumin and β -cyclodextrin	80
Appendix 3: ^1H NMR of β -CD/curcumin Complex in Water	82
Appendix 4: ^1H NMR of β -CD/curcumin Complex in Acetone.....	83

List of Abbreviations

β -CD	β -cyclodextrin
DIPEA	<i>N,N</i> -Diisopropylethylamine
DLS	Dynamic light scattering
DMSO	Dimethyl sulfoxide
EDC	1-Ethyl-3-(3-dimethylaminopropyl) carbodiimide
FA	Folic acid
FBS	Fetal bovine serum
FITC	Fluorescein isothiocyanate
FTIR	Fourier transform infrared spectroscopy
^1H NMR	Proton nuclear magnetic resonance
MNP	Magnetic nanoparticles
PPG-NH ₂	poly (propylene glycol) bis (2-aminopropyl ether)
RES	Reticuloendothelial system
TEM	Transmission electron microscopy
VSM	Vibrating sample magnetometer

XRD X-ray diffraction

231 MDA-MB-231 cells

468 MDA-MB-468 cells

Chapter 1

1 Introduction

1.1 Motivation and Cancer Treatment Overview

For years researchers have been seeking a means of solving one of the toughest puzzles in the world; cancer. In 2013, there were approximately 1.6 million cases of cancer with 580,350 deaths occurring in the United States,¹ and 187,600 cases of cancers in Canada, of which 75,500 cases resulted in death.² Traditional treatment methods including one of, or a combination of, surgery, radiation therapy, and chemotherapy have been enhanced overtime which is evident by the high incidences of cured individuals. However, these treatment methods are still not flawless. Surgery is invasive, bearing many risks to the patient before and after the procedure. Radiation therapy involves both early side effects such as skin erythema, nausea, dryness, and itchiness, and late effects which include long term conditions such as vascular or neural damage, atrophy, and radiation-induced fibrosis.³ Both early and late side effects associated with radiation therapy are local, being manifested in the tissue that was irradiated. This outlines the main difference between radiation therapy and chemotherapy, as the latter causes systemic side effects (throughout the entire human body). The anti-cancer agents used in chemotherapy destroy rapidly dividing cells, whether cancerous or healthy. Therefore, there is a strong need for a technology that can direct chemotherapeutic agents to the tumour site once administered, thereby rendering healthy tissue unharmed.

1.2 Drug Delivery Systems (DDS) for Cancer Treatment

Today, many cancer awareness societies quote targeted therapy as one of the options of cancer treatment. Indeed, there has been a plethora of research aimed at the development of drug delivery systems (DDS) that can transport chemotherapeutics to the site of interest, thereby localizing the drug and decreasing or potentially eliminating side effects. Common drug delivery systems include liposomes, exosomes, micelles, dendrimers or different polymeric networks, and nanoparticles, which encompass a wide variety of different systems.⁴

1.2.1 Liposomes, Micelles, and Exosomes

Lipid-based systems such as liposomes and micelles have been used for drug delivery and cell targeting due to their biocompatibility and ability to increase the bioavailability of many drugs.⁵ Sardan *et al.* synthesized peptide amphiphile (PA)-incorporating liposomes for cell targeting.⁶ Liposomes containing PA were made using a 7:8:1 ratio of 1, 2-dioleoyl-*sn*-glycero-3-[phosphor-*rac*-(1-glycerol)] (DOPG), cholesterol (CHOL), and PA respectively using a curvature tuned preparation method. The amphiphilic nature of the system allowed for the incorporation of Rhodamine B and Nile red as model hydrophilic and hydrophobic drugs, respectively.

In other work, reduction-sensitive, shell-sheddable micelles synthesized using poly(ethylene glycol)-poly(ϵ -caprolactone) (PEG-PCL) copolymers were used to encapsulate doxorubicin for targeting of tumour cell nuclei.⁷ The authors reported more efficient release of doxorubicin when using reduction-sensitive *versus* non-reduction-sensitive micelles. Exosomes—endocytotic membrane vesicles excreted by many cells—are also used for drug encapsulation. Tian *et al.* focused on the delivery of doxorubicin, but using exosomes as delivery vehicles.⁸ Exosomes were obtained from immature dendritic cells (imDCs) of mice in order to reduce immunogenicity and toxicity, and then functionalized to express a common exosomal membrane protein (Lamp2b) conjugated to α v integrin iRGD peptide for tumour targeting.

1.2.2 Hydrogels

There has been extensive research involving hydrogels—materials composed of polymer chain networks—for targeted cancer treatment and other biomedical applications,⁹⁻¹¹ with recent emphasis on “smart” hydrogels which are capable of changing their properties in response to certain stimuli such as temperature and pH.¹² Thermoresponsive poloxamer hydrogels conjugated with linoleic acid-coupled Pluronic-F127 (Plu-CLA) were synthesized and loaded with docetaxel for the treatment of metastatic gastric cancer.¹³ The hydrogels remained in solution at room temperature for intraperitoneal injection, upon which gelation occurred at body temperature. The gelation along with the coupled Plu-CLA was noted to achieve more sustained release of docetaxel, with higher cancer cell destruction was reported for hydrogel-loaded docetaxel than docetaxel alone.

1.2.3 Dendrimers

Dendrimers may be one of the oldest known drug delivery systems, dating back to the late 1970's, although their application as drug delivery vehicles or “host-guest” systems was not described at the time.¹⁴ However, for the past decade there has been a strong focus on the use of dendrimers as drug delivery systems for cancer treatment.¹⁵ Because dendrimers can be synthesized to incorporate a wide variety of anti-cancer agents, and functionalized to include various ligands capable of targeting cancer cell surface receptors, they make promising drug delivery vehicles. Modi *et al.* synthesized fluorescein-labeled generation 5 (G5) PAMAM dendrimers conjugated with FSH33 which is the binding domain of follicle stimulating hormone (FSH).¹⁶ Due to the high affinity of FSH33 to the FSH receptor (FSHR) present on the surface of ovarian cancer cells, the functionalized dendrimers showed significant uptake by ovarian cancer cells resulting in the down-regulation of survivin (an anti-apoptotic protein) meanwhile rendering normal non-FSHR expressing ovarian cells unharmed.

1.2.4 Nanoparticles

Several types of nanoparticles have been developed using a wide variety of different materials for the delivery of therapeutic agents. By definition, nanomaterials are materials or aggregates of materials in the size range of 1 – 100 nm.¹⁷ Li *et al.* proposed fluorescent theranostic silica nanoprobe for cancer cell imaging and growth inhibition.¹⁸ The nanoprobe was synthesized using a reverse emulsion method and functionalized to incorporate a cell targeting moiety (AS1411 aptamer) and 2'-O-methyl-modified miRNA-21 molecular beacon (miR-21-MB) to particularly recognize miRNA-21 present in breast cancer cells. The authors reported monodisperse nanoprobe with an approximate size of 50 nm which demonstrated the ability to specifically target cancer cells and inhibit cell growth while simultaneously allowing for cancer cell and intracellular miRNA-21 imaging.

In other work, Deng *et al.* co-encapsulated MiR-34a—an endogenous tumour suppressor molecule present in breast cancer cells –and doxorubicin into hyaluronic acid-chitosan nanoparticles, synthesized using an ionotropic gelation method in water, for breast cancer therapy.¹⁹ The size of nanoparticles containing both MiR-34a and doxorubicin increased as the amount of hyaluronic acid used in the formulation was increased, and the authors reported

sustained release of both components in the delivery system for up to 10 days. Furthermore, the study revealed that the co-delivery of MiR-34a and doxorubicin resulted in the enhancement of doxorubicin anti-tumour activity, in addition to suppression of cancer cell migration by targeting the Notch-1 signaling pathway.

Rouhani *et al.* considered cancer treatment through oxidation therapy—the use of reactive oxygen species (ROS) as oxidant or anti-oxidant inhibitors to cause apoptosis or necrosis.²⁰ The authors investigated poly(lactic-co-glycolic acid) (PLGA) nanoparticles loaded with zinc protoporphyrin (ZnPP) as a heme oxygenase (HO)—an anti-oxidant enzyme known to play a role in cell growth and proliferation—inhibitor. The average size of the synthesized nanoparticles was precisely reported to be 100.12 ± 5.345 nm with a smooth, spherical morphology, and showed potent cytotoxic effects as well as high cellular uptake in PC3 human prostate cancer cells.

1.3 History of Metallic Compounds for Medical Treatments

Among the various nanoparticles that have been investigated for therapeutic purposes are magnetic nanoparticles. Although there has been intensive research involving their use for diagnostic and therapeutic purposes in the last decade, the use of nanoparticles dates hundreds of years back. Daniel and Astruc described a detailed history of nanoparticles, specifically gold nanoparticles, as this was one of few metals present in ancient times.²¹ The authors make reference to a book written by Francisci Antonii in 1618 on colloidal gold, which is considered the first book on colloidal gold. The book gives detailed information regarding colloidal gold sols and their medical uses. He also went further to describe the appearance of a “soluble gold” in ancient Egypt and China, stating that the “curable powers” of this gold were appreciated until the Middle Ages. Also, it is noted that in 1676 a book published by Johann Kunckels mentions a drinkable light pink solution that contains metallic gold capable of curing several diseases.

Although there was little evidence in past civilizations that these metallic compounds in fact cured diseases, today there is extensive research on the use of nanoparticles for the use in biomedical applications. For medical applications, a balance between biocompatibility and large magnetic moments must be achieved, which is why iron-based nanoparticles (such as iron

oxides) are ideal candidates for medical applications compared to others which are composed of toxic metals.²²

1.3.1 Magnetic Iron Oxide Nanoparticles

Theoretically, magnetic iron oxide nanoparticles can be guided via an external magnetic field to the site of interest. Among many examples, Carenza *et al.* evaluated the guidance of magnetic iron oxide nanoparticles to the brain using an external magnet for neurorepair therapy.¹³ To date, these nanovectors have widely been explored for use as contrast agents for imaging modalities such as computed tomography (CT), positron emission tomography (PET), and magnetic resonance imaging (MRI) as they present increased sensitivity and short acquisition time, allowing for the production of high resolution images.²³⁻²⁵ In fact, Ferumoxytol (an FDA-approved magnetite-based product used to treat iron deficient patients) has been clinically tested for its use as an MRI contrast agent for imaging of the liver.²⁶

Of the many iron oxides available, magnetite (Fe_3O_4) has received considerable attention for biomedical applications due to its biocompatibility and biodegradability.²⁷ Many reviews have been published in literature outlining various synthesis methods, coatings, and applications of magnetic nanoparticles.²⁷⁻²⁹ Several methods have been developed to synthesize Fe_3O_4 nanoparticles. These synthesis methods can be categorized into physical methods, wet chemical methods, and microbial methods.²⁷ Table 1.1 lists common examples of synthesis techniques for each category, and the advantages and disadvantages outlined by each.

Table 1.1: Common synthesis methods for iron oxide nanoparticles^{27, 29}

Category	Techniques	Advantages	Disadvantages
Physical	Electron beam lithography	Easily change/optimize patterns using CAD software	Poor control of particle size down to the nm scale
	Gas-phase deposition	Results in 1-dimensional iron oxide nanostructures	
Wet chemical	Chemical co-precipitation	Mild reaction conditions, very simple, cheap chemicals	Difficult to control size and oxidation
	Hydrothermal reaction	Narrow size distribution, tunable magnetism, controllable shape and crystallinity	High temperature, and toxic organic compounds required
	Thermal deposition	Tunable magnetism and size, good crystallinity	High temperature and pressure required
Microbial	Microbial Processes	High yield, good reproducibility, required low temperature and energy	Process takes from several days up to 3 weeks

Also, for biomedical applications, it is desirable to coat the nanoparticle surface in order to produce biocompatible nanoparticles with chemically reactive groups for additional functionalization.²⁵ Nanoparticles can be coated with an organic coating using biocompatible polymers and functionalized through hydrophobic interactions or covalent bonds such as amides. Inorganic coatings such as silica can also be used to surround the nanoparticle core in a core-shell structure. In fact, these surface coatings play a crucial role in the toxicity and *in vivo* fate of the iron oxide nanoparticles as reported by Feng *et al.*³⁰ Uncoated iron oxide nanoparticles caused hepatic, renal, and splenic disturbances, specifically in terms of renal toxicity, compared to coated nanoparticles. However, these disturbances can be reversed, particularly in coated nanoparticles after excretion, which was attributed to the recovery process observed 48 hours after administration. Furthermore, uncoated iron oxide nanoparticles tend to gather in biological fluids resulting in their rapid clearance from the body.³¹ In comparison, coated iron oxide nanoparticles, specifically 10 – 100 nm in size, offer a long circulation time in the body. In addition, the surface chemistry of the particles plays an important role in their uptake by the liver and spleen. Feng *et al.* studied the fate of dextran-coated iron oxide nanoparticles and found that 70% of the dextran was found in the urine within 24 hours of administration, and 30% was

retained over a period of a few days.³⁰ Eventually, these particles are eliminated through the excretory system.

1.4 Thesis Objectives and Hypothesis

The objective of this thesis project was to develop coated magnetic iron oxide nanoparticles for the targeted and sustained delivery of curcumin to cancerous cells. In addition, the development of folate-labeled magnetic nanoparticles for their selective uptake by cancer cells was investigated. The central hypothesis of this thesis is that coated magnetic nanoparticles will increase the bioavailability of curcumin to cancer cells, and sustained release will be achieved depending on the amounts and ratios of molecules used to coat the magnetic core. Furthermore, folate-labeling will enhance the uptake of nanoparticles by cancer cells. The magnetic properties of the iron oxide core, along with the selective targeting of the folate ligand is intended to serve as a dual targeting system to destroy cancer cells, meanwhile rendering healthy tissue unharmed.

1.5 Thesis Outline

We proposed a dual targeting drug delivery system for the sustained delivery of curcumin to cancer cells. Magnetite (Fe_3O_4) nanoparticles were synthesized via a simple precipitation method using only one iron salt, and simultaneously coated with β -cyclodextrin (β -CD) and poly(propylene glycol) bis(2-aminopropyl ether) (PPG-NH₂) during the synthesis process. β -CD is an FDA approved cyclic molecule composed of seven sugar units, which was used for curcumin encapsulation. PPG-NH₂ is a poly(propylene glycol) with functional amines on both ends of the molecule. This poly(propylene glycol) derivative was chosen due to its hydrophobic properties allowing it to be trapped within the β -CD core.^{32,33} Folic acid will be attached to PPG-NH₂ through an amide bond in order to selectively target the folate receptor which is overexpressed on the surface of cancer cells. With the magnetic properties of iron oxide potentially allowing magnet-induced guidance to tumour sites, along with the selective targeting of the folate ligand, this dual targeting system was designed for the destruction of cancer cells without affecting healthy tissue. Synthesized magnetite nanoparticles containing different ratios of β -CD:PPG-NH₂ were characterized using different techniques and tested for their ability to sustain curcumin release. Chapter 2 gives a detailed description of the chemical properties of curcumin, along with

its bioactivity for cancer treatment, and previous delivery approaches. The research results of this thesis are described in detail in Chapter 3.

1.6 Bibliography

1. R. Siegel, D. Naishadham and A. Jemal, *CA: A Cancer Journal for Clinicians*, 2013, **63**, 11-30.
2. C.C.S.s.A.C.o.C. Statistics, *Canadian Cancer Statistics 2013*. 2013, Canadian Cancer Society: Toronto, ON.
3. S.M. Bentzen, *Nature Reviews Cancer*, 2006, **6**, 702-713.
4. M. Salem, S. Rohani and E.R. Gillies, *RSC Advances*, 2014, **4**, 10815-10829.
5. D.D. Lasic and D. Needham, *Chemical Reviews*, 1995, **95**, 2601-2628.
6. M. Sardan, M. Kilinc, R. Genc, A.B. Tekinay and M.O. Guler, *Faraday Discussions*, 2013, **166**, 269-283.
7. Y. Zhong, W. Yang, H. Sun, R. Cheng, F. Meng, C. Deng and Z. Zhong, *Biomacromolecules*, 2013, **14**, 3723-3730.
8. Y. Tian, S. Li, J. Song, T. Ji, M. Zhu, G.J. Anderson, J. Wei and G. Nie, *Biomaterials*, 2014, **35**, 2383-2390.
9. Y. Li, J. Rodrigues and H. Tomas, *Chemical Society Reviews*, 2012, **41**, 2193-2221.
10. R. Tian, J. Chen and R. Niu, *Nanoscale*, 2014.
11. A. Vashist, A. Vashist, Y.K. Gupta and S. Ahmad, *Journal of Materials Chemistry B*, 2014, **2**, 147-166.
12. H.L. Lim, Y. Hwang, M. Kar and S. Varghese, *Biomaterials Science*, 2014.
13. W.K. Bae, M.S. Park, J.H. Lee, J.E. Hwang, H.J. Shim, S.H. Cho, D.-E. Kim, H.M. Ko, C.-S. Cho, I.-K. Park and I.-J. Chung, *Biomaterials*, 2013, **34**, 1433-1441.
14. A.W. Bosman, H.M. Janssen and E.W. Meijer, *Chemical Reviews*, 1999, **99**, 1665-1688.
15. Y. Cheng, L. Zhao, Y. Li and T. Xu, *Chemical Society Reviews*, 2011, **40**, 2673-2703.
16. D.A. Modi, S. Sunoqrot, J. Bugno, D.D. Lantvit, S. Hong and J.E. Burdette, *Nanoscale*, 2014, **6**, 2812-2820.
17. L. Calzolari, D. Gilliland and F. Rossi, *Food Addit Contam Part A Chem Anal Control Expo Risk Assess*, 2012, **29**, 1183-93.
18. H. Li, Y. Mu, J. Lu, W. Wei, Y. Wan and S. Liu, *Anal Chem*, 2014.
19. X. Deng, M. Cao, J. Zhang, K. Hu, Z. Yin, Z. Zhou, X. Xiao, Y. Yang, W. Sheng, Y. Wu and Y. Zeng, *Biomaterials*, 2014, **35**, 4333-4344.

20. H. Rouhani, N. Sepehri, H. Montazeri, M.R. Khoshayand, M.H. Ghahremani, S.N. Ostad, F. Atyabi and R. Dinarvand, *Pharm Res*, 2014.
21. M.C. Daniel and D. Astruc, *Chem Rev*, 2004, **104**, 293-346.
22. A. Sandhu, H. Handa and M. Abe, *Nanotechnology*, 2010, **21**, 442001.
23. M.H. Publico-Lansigan, S.F. Situ and A.C.S. Samia, *Nanoscale*, 2013, **5**, 4040-4055.
24. H. Shokrollahi, *Materials Science and Engineering: C*, 2013, **33**, 4485-4497.
25. J. Gallo, N.J. Long and E.O. Aboagye, *Chemical Society Reviews*, 2013, **42**, 7816-7833.
26. B.J. McCullough, O. Kolokythas, J.H. Maki and D.E. Green, *J Magn Reson Imaging*, 2013, **37**, 1476-9.
27. L.H. Reddy, J.L. Arias, J. Nicolas and P. Couvreur, *Chem Rev*, 2012, **112**, 5818-78.
28. M. Colombo, S. Carregal-Romero, M.F. Casula, L. Gutierrez, M.P. Morales, I.B. Bohm, J.T. Heverhagen, D. Prospero and W.J. Parak, *Chemical Society Reviews*, 2012, **41**, 4306-4334.
29. K. Yan, P. Li, H. Zhu, Y. Zhou, J. Ding, J. Shen, Z. Li, Z. Xu and P.K. Chu, *RSC Advances*, 2013, **3**, 10598-10618.
30. J. Feng, H. Liu, K.K. Bhakoo, L. Lu and Z. Chen, *Biomaterials*, 2011, **32**, 6558-6569.
31. A.K. Gupta and M. Gupta, *Biomaterials*, 2005, **26**, 3995-4021.
32. A. Harada, M. Okada, J. Li and M. Kamachi, *Macromolecules*, 1995, **28**, 8406-8411.
33. Y. Liu, Y.-W. Yang, Y. Chen and H.-X. Zou, *Macromolecules*, 2005, **38**, 5838-5840.

Chapter 2

2 Curcumin, a Promising Anti-cancer Therapeutic

2.1 Introduction

For the past few decades there has been rapid growth in the interest of using natural products for therapeutic applications. Although this idea seems recent, our ancestors frequently used natural compounds to combat illness. The development of synthetic pharmaceuticals revolutionized modern medicine over the last century, but the undesirable properties and side effects of these drugs has inspired a search for natural approaches to disease prevention and treatment with the hope that naturally occurring compounds may be better tolerated than their synthetic counterparts. Of particular interest is curcumin, the principal active ingredient in the traditional dietary spice turmeric, responsible for its colour, taste, and most of its chemical and biological properties. Curcumin is derived from *Curcuma longa*, a plant of the ginger family. The other two curcuminoids present in turmeric in lower concentrations are demethoxycurcumin, and *bis*-demethoxycurcumin.

While curcumin gained immense attention as a medicinal drug in modern medical applications only a few decades ago, it has been used for hundreds of years in some areas of the world. In Asia, specifically India and China, turmeric has been used as a drug for more than two thousand years.¹ Ayurveda, an ancient medicinal system practiced in India, incorporated the use of natural herbs to treat various illnesses. Amongst the commonly used herbs, turmeric was used most abundantly due to the medical effects of curcumin. In the traditional Ayurvedic approach, turmeric was crushed into a paste for the treatment of eye infections, burns, bug bites, and any skin related diseases. Furthermore, new mothers in India are given a drink containing turmeric paste, honey, ginger, and milk to drink daily following child birth.¹ Turmeric is also used in different forms to cure cough and respiratory complications, along with dental diseases, flatulence, and indigestion. Curcumin was also used as a medicine in ancient Polynesian culture. It has been noted in historical documents that the Polynesian people carried turmeric with them during long voyages to Hawaii.² Today, Hawaiians utilize curcumin for various medicinal purposes. It is known to them as Olena.

Curcumin was not introduced to Western cultures until the 14th century when European explorers were introduced to Asian countries. In particular, Marco Polo was introduced to curcumin during his visit to the Asian continent in 1280 AD.^{2, 3} It was noted in his writings that the native people of India and China used a vegetable that contained all the properties of saffron, but this spice was not quite saffron. In addition, the Portuguese sailor, Vasco de Gama, sailed to India approximately 500 years ago specifically in search of spices for their medicinal use.⁴ It was not until his return to Europe that curcumin was truly introduced into Western cultures. Despite curcumin's extensive history, scientists were not able to isolate the curcumin molecule until the 1800s. In 1870, scientists obtained the crystalline form of curcumin, and elucidated its overall structure in 1910.³ Its chemical structure is responsible for its unique physicochemical and biological properties.

2.2 Physicochemical Properties

Curcumin, 1,7-*bis*(4-hydroxy-3-methoxyphenyl)-1,6-heptadiene-3,5-dione, is a hydrophobic polyphenol. It is a golden-yellow solid, with a molecular weight of 368 g/mol and a melting point of 183 °C. It is often used as a dye owing to its vibrant colour. As shown in Figure 2.1, curcumin can exist in different tautomeric forms. The aromatic rings are functionalized with methoxy and hydroxy groups in an *ortho* position with respect to one another. The aromatic rings are connected to one another via a seven-carbon spacer that contains two α,β -unsaturated carbonyl groups. As a result of this structure, a beta-diketone and equilibrating keto-enol tautomeric forms of curcumin are possible.⁵

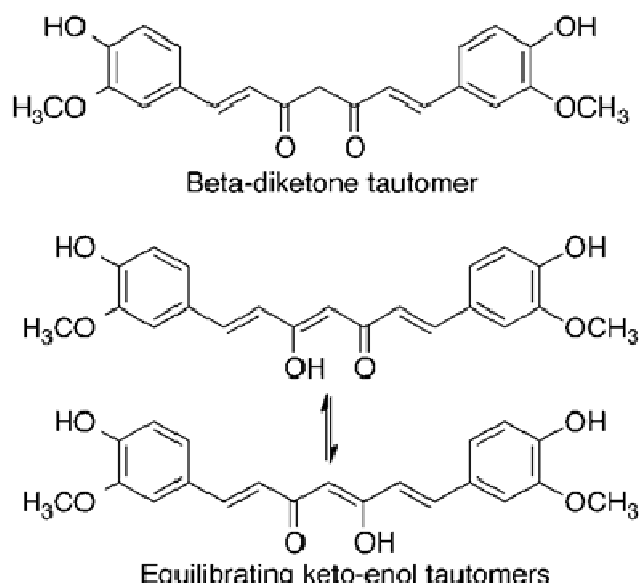


Figure 2.1: Tautomeric forms of curcumin

2.2.1 Effect of pH

Among the factors that affect the properties of curcumin is pH. Although curcumin has been shown by X-ray diffraction analysis to exist in the keto-enol form in the solid state,⁶ there has been controversy concerning whether curcumin exists in its beta-diketo or keto-enol form at neutral and slightly acidic pH.⁵ For example, Jovanovic *et al.* have proposed that the beta-diketone form of curcumin predominates in mildly acidic aqueous solution and in cell membranes.⁷ They have also suggested that the central methylene group of the diketone form can act as a potent hydrogen atom donor in radical reactions, potentially mediating its biological activity. However, Payton *et al.* have recently performed detailed NMR studies supporting that curcumin exists as keto-enol tautomers in a range of hydrophobic and hydrophilic solvents, over a pH range from 3-9.⁵ These results are in agreement with density functional theory calculations by Shen and Li,⁸ which correlated the calculated absorption wavelength and oscillator strength of curcumin with the experimental values, supporting the predominance of the keto-enol tautomers. The keto-enol form was calculated to be more stable than the diketone form by 7.75 kcal/mol. This was attributed to the planar structure of the enol form, allowing for resonance stabilization to occur, while that of the ketone form was twisted.

As shown in Figure 2.2, at pH less than 1, a protonated form of curcumin is observed and the molecule can adopt a fully conjugated protonated form.⁹ Figure 2.2 also illustrates the proposed deprotonated forms of curcumin that can occur as the pH is increased.⁹ As a consequence of deprotonation, curcumin exhibits increased aqueous solubility in alkaline solutions while it is practically insoluble in water at acidic and neutral pH. However, curcumin has been demonstrated to undergo degradation under alkaline conditions, as demonstrated by Tonnesen *et al.* and Wang *et al.*^{9, 10}

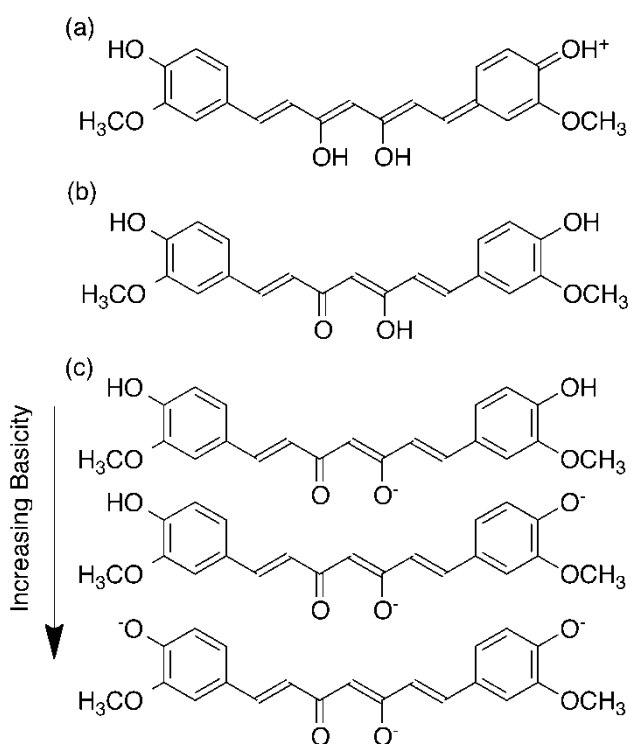


Figure 2.2: Proposed structure of curcumin in (a) acidic, (b) neutral, and (c) basic environments

2.2.2 Effect of Temperature

Solid curcumin is generally stored at -20°C , though there is no evidence that curcumin is not stable at somewhat higher temperatures. Wang *et al.* studied the stability of curcumin at body temperature.¹⁰ In this study, curcumin was incubated under various physiological conditions at 37°C to measure its stability. Curcumin was incubated in 0.1 M phosphate buffer solution, culture medium, culture medium with 10% serum, and human blood. Samples were analyzed by

high performance liquid chromatography (HPLC) after one, four, and eight hours of incubation. It was noted that the rate of curcumin degradation was dependent on the conditions. When no serum was present, curcumin underwent degradation more rapidly than in the medium with serum or in human blood. This difference was accounted for by the stabilization of curcumin by the serum and it was suggested that care must be taken in the manipulation of curcumin under serum-free conditions, particularly in the interpretation of the results of biological studies, where the presence of degradation products such as vanillin should be taken into account.

In another study, Gopinath *et al.* investigated curcumin incorporated collagen films (CICFs) for dermal wound healing.¹¹ CICFs were prepared by dissolving a weighed amount of curcumin in ethanol, and mixing this solution with 50 mL of collagen/acetic acid solution at 4°C for 24 hours. Micro-shrinkage temperature measurements were carried out on both CICF and pure collagen. It was found that without curcumin, the shrinkage temperature of collagen was 55°C, which was increased to 78°C when curcumin was incorporated in the collagen. It was concluded from this finding that curcumin increases the thermal stability of collagen. This group previously reported that quercetin also increased the thermal stability of collagen, allowing them to draw the conclusion that polyphenols are generally capable of enhancing the temperature stability of collagen and matrices of different types.

Previous studies have demonstrated that natural phenolic compounds suffer from biodegradation, change of structure, and loss of biological activity when heated. Based on this, Liu *et al.* set out to investigate the thermal stability of curcumin.¹² Specifically, the relationship between the pre-incubation temperature of curcumin and its inhibitory effect on amyloid fibrillation of hen egg-white lysozyme (HEWL) was studied. Unmodified HEWL was used as a control agent, along with HEWL modified with curcumin pre-incubated at 10, 25, 40, 55, and 70°C for 329 hours. The result of the Thioflavin T (ThT) fluorescence assay is shown in Figure 3, where a decrease in fluorescence corresponds to a decrease in amyloids.

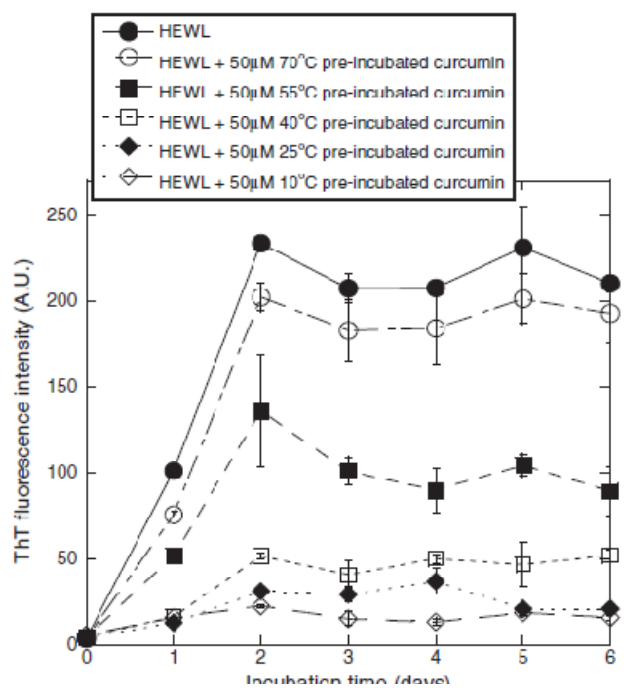


Figure 2.3: ThT assay results, showing that the ability of curcumin to inhibit the amyloid fibrillation of HEWL (inhibition is detected as a decrease in fluorescence intensity). Reprinted from reference 12 with permission from Elsevier

As shown in Figure 2.3, the unmodified HEWL exhibited the highest amyloid content, and the HEWL sample modified with curcumin pre-incubated at 70°C provided similar results. This can be attributed to the lack of biologically active curcumin following incubation at this temperature. However, at a pre-incubation temperature of 55°C, it was evident that not all of the curcumin degraded, as the fluorescence decreased by approximately 50%. Therefore, a clear dependence of curcumin stability on temperature was observed. This trend was further verified using transmission electron microscopy (TEM), where the images clearly illustrated the presence of high amounts of amyloid fibrils in the unmodified HEWL, and that modified with curcumin pre-incubated at 70°C. However, the samples containing curcumin pre-incubated at lower temperatures exhibited fewer amyloid fibrils, with the amount decreasing with decreasing pre-incubation temperature. Similar results were obtained in the cell viability study, leading the authors to conclude that curcumin is most stable in the temperature range of 10-55°C and degraded almost completely at 70°C within 24 hours.

Thus, it can be generally concluded that curcumin is most stable at low temperatures; however, its stability is still maintained at room temperature and physiological temperature, allowing it to be used in medical applications. At very high temperatures however, curcumin degrades into different products, which will be discussed briefly below.

2.2.3 Degradation Products of Curcumin

Under certain conditions curcumin becomes unstable, as previously discussed, and degrades, yielding other compounds. The three degradation products often found are vanillin, ferulic acid, and feruloylmethane.¹³ In the previously described study by Wang *et al.* it was noted that when curcumin degraded in different media, the resulting degradation products were characterized by HPLC-mass spectrometry to be vanillin, ferulic acid, and feruloylmethane.¹⁰ However, in this study there was also an unknown product present in larger amounts. It was hypothesized that this product was *trans*-6-(4'-hydroxy-3'-methoxyphenyl)-2, 4-dioxo-5-hexenal.

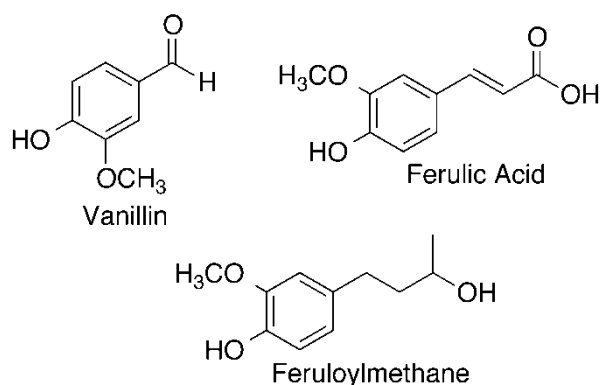


Figure 2.4: Proposed degradation products of curcumin

A study conducted by Schieffer investigated the degradation products of curcumin obtained after exposure to light.¹⁴ Curcumin is extremely sensitive to light and undergoes degradation in its presence. The study concluded that curcumin underwent photolytic degradation to produce several products with the most abundant being *p*-hydroxybenzaldehyde, vanillic acid, vanillin, and ferulic acid. The difference in some of the products proposed in this study versus those obtained by Wang *et al.* suggests that the thermal and photochemical degradation pathways of curcumin may be different, though it is generally agreed that the degradation of curcumin is much more rapid in the presence of light.

Singh *et al.* explored the photodegradation of curcumin in the presence of a TiO₂ catalyst.¹⁵ It was reported that curcumin formed a complex with TiO₂, which was evidenced by the presence of a broad, red-shifted absorption band. Photodegradation was carried out in two solvent media, water-methanol and water-acetonitrile, and the degradation products were evaluated using gas chromatography. The results were similar for both media, with the predominant degradation product being vanillin, along with minimal amounts of CO₂, 4-hydroxybenzaldehyde, and methoxyvanillin.

It is widely proposed that vanillin and ferulic acid are the major degradation products and in fact contribute to the therapeutic effects of curcumin. In fact, there is a variety of work concerning the therapeutic effects of vanillin.^{13, 16-18} Despite the potential therapeutic effects of vanillin, the recent work of Wang *et al.* outlined above,¹⁰ casts doubt on the proposition that vanillin is in fact a major degradation product of curcumin. In the case of this study, vanillin and ferulic acid were only minor degradation products, and there existed a major degradation product with currently unconfirmed identity.

Gordon and Schneider, and Griesser *et al.* also performed similar degradation reactions in order to challenge the belief that vanillin, ferulic acid, and feruloylmethane are the major degradation products of curcumin.^{19, 20} The results obtained using HPLC suggested the presence of one major product, while vanillin, ferulic acid, and feruloylmethane were close to undetectable. Further analysis revealed a molecular weight of 400 g/mol, indicating insertion of oxygen to curcumin. Based on 1D and 2D homo- and heteronuclear NMR experiments, the unknown compound was identified as a bicyclopentadione form of curcumin.¹⁹ Figure 2.5 illustrates the proposed autoxidation mechanism leading to this product. It was proposed that this degradation mechanism accounts for curcumin's antioxidant properties, and not the alternative degradation products.

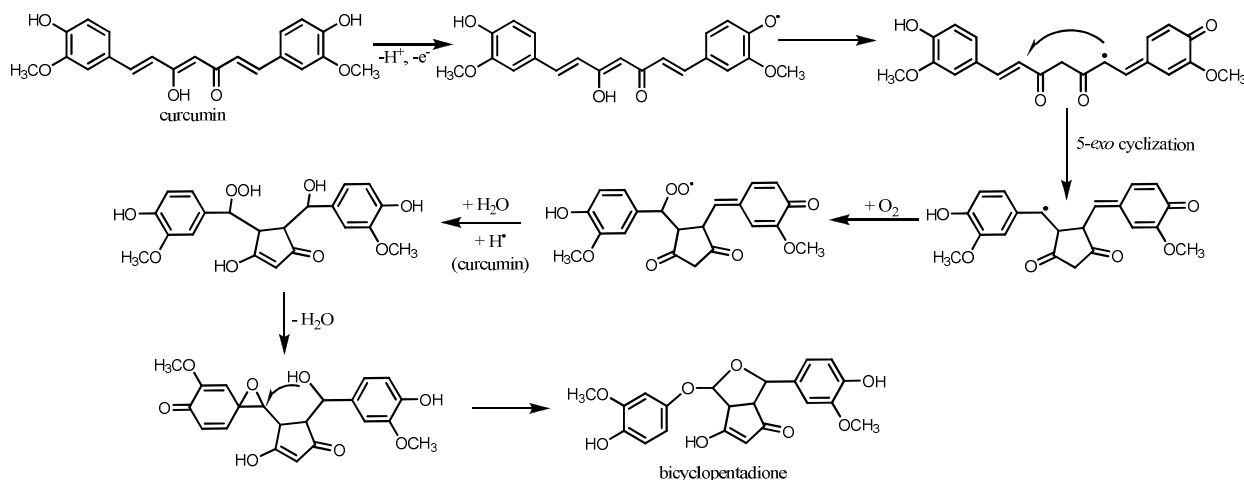


Figure 2.5: Proposed mechanism for the autoxidation of curcumin¹⁹

Ketron *et al.* also investigated the oxidative properties of the bicyclopentadione form of curcumin, exploring its effects on human type II topoisomerases.²¹ A series of experiments were performed to evaluate the effect of the bicyclopentadione form of curcumin, stable curcumin, vanillin, ferulic acid, and feruloylmethane on the human enzymes. The results revealed that the bicyclopentadione form of curcumin poisons human topoisomerases, in contrast to curcumin and its three fragmentation products, which did not reveal a significant effect. Thus, while vanillin, ferulic acid, and feruloylmethane may exhibit therapeutic effects, it still remains to be confirmed which therapeutic effects of curcumin arise from the parent molecule, and which arise from the various possible degradation products.

2.3 Effect of Curcumin on Cancer Cells

Although curcumin has been used as a traditional medicine to treat several conditions including inflammation, respiratory infection, and blood clogging, there is rapidly growing interest in its effects on cancer. The motivation for the use of curcumin arises not only from its potential therapeutic effects, but also from the knowledge that it may be better tolerated by patients, in comparison with most chemotherapeutic drugs that suffer from numerous harmful side effects such as nausea and vomiting, diarrhea, hair loss,²² and more serious long term conditions such as liver failure.²³ Several studies comparing the incidences of cancer and cancer related deaths in India and the West revealed lower risk of cancer in India (Table 2.1).²⁴ It is proposed that one of

the major reasons for the drastic difference in cancer occurrences in these regions is the increased intake of dietary agents such as curcumin, and other plant derivatives in Asia.

Table 2.1: Comparison of incidences and deaths in India and United States for common cancers showing cases per 1 million persons²⁴

Cancer	USA		India	
	Cases	Deaths	Cases	Deaths
Lung	660	580	38	37
Breast	660	160	79	41
Prostate	690	130	20	9
Colon/rectum	530	220	30	18
Bladder	202	43	15	11
Thyroid	55	5	12	3
Leukemia	100	70	19	17

Why does curcumin possess anti-cancer properties? Generally, cancer with its diverse origins has several molecular markers involved in its onset and progression. Curcumin is capable of interfering with several biochemical pathways involved in the proliferation and survival of cancer cells by directly and indirectly binding to different targets. Curcumin has been shown to interact with various targets including transcription factors, growth factors, DNA, RNA, and several proteins that are involved in cell signal transduction pathways.^{25, 26} There are several features of curcumin's chemical structure that make it a favourable and versatile binding partner for a wide variety of molecular targets (Figure 2.6). For example, curcumin possesses two hydrophobic phenyl groups connected by a relatively flexible linker. This allows the molecule to assume different conformations that can maximize π - π and van der Waals interactions with aromatic and other hydrophobic amino acid residues of proteins. The phenolic hydroxyl and methoxy groups, as well as the ketone and enol groups present on the ends and in the middle of the molecule respectively can participate in strong and directed hydrogen-bonding interactions. The possibility for keto-enol tautomerism introduces additional functionality, with the possibility to arrange donor and acceptor groups for hydrogen bonding in multiple ways. Furthermore, the

α,β -unsaturated ketone moiety can serve as a Michael acceptor for nucleophilic attack by the thiol moieties of cysteine residues or the Se⁻ moieties of selenocysteine. The proposed pathways by which curcumin exhibits anti-cancer properties have been described in detail in several recent reviews²⁵⁻²⁹ and some of these mechanisms are described below.

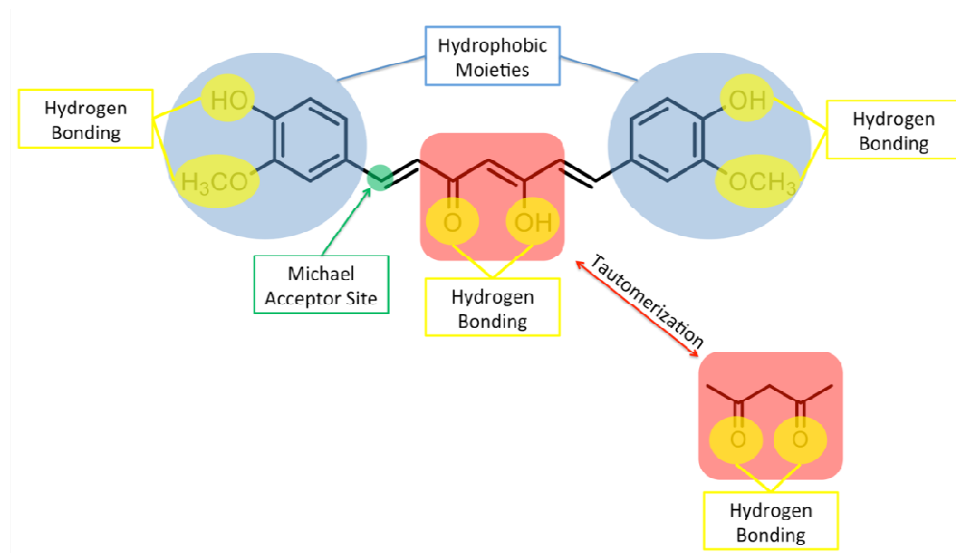


Figure 2.6: Structural features of curcumin involved in binding to protein targets

Curcumin's mechanism of action can occur both intrinsically (mitochondrial) and extrinsically (mediated via cell surface transmembrane death receptors).³⁰ The intrinsic pathway is generally initiated by activation of tumour suppressor p53 (p53), which is a cell cycle regulator, as well as through members of the B-cell lymphoma 2 (Bcl-2) family. Up-regulation of p53 activates Bcl-2 homologous antagonist killer (Bak) and Bcl-2 associated X protein (Bax), which are pro-apoptotic members of the Bcl-2 family. Bak and Bax promote apoptosis by forming pores in the mitochondrial membrane releasing cytochrome c into the cytoplasm, thereby activating a caspase cascade.³⁰ Curcumin is capable of inhibiting Bcl-2 and B-cell lymphoma extra large (Bcl-x_L) which is another pro-survival protein of the Bcl-2 family. Luthra *et al.* showed using molecular docking studies that curcumin may inhibit Bcl-2 by directly binding to cavity 2 of the protein through interactions with multiple amino acids.³¹ Guo *et al.* showed that curcumin significantly inhibited growth of human colorectal carcinoma LoVo cells.³² Nuclear and annexin V/PI staining confirmed that curcumin induced apoptosis in LoVo cells, in addition to decreasing

the mitochondrial membrane potential and activating caspase-3 and -9 at concentrations of 0 – 30 μ M.

Nuclear factor (erythroid-derived 2)-like 2 (Nrf2) is a transcription factor involved in the primary defense pathway against the effects of oxidative stress.³³⁻³⁵ Under normal conditions, Nrf2 is located in the cytoplasm with its activity suppressed by the chaperon protein Kelch like-ECH-associated protein 1 (Keap1). Under conditions of oxidative stress, which alter the thiol groups on Keap 1, the Nrf2-Keap1 interaction is disturbed, causing Nrf2 to be transported to the nucleus where it binds to the anti-oxidative response element (ARE) and activates the transcription of genes encoding for detoxifying enzymes such as hemeoxygenase-1 (HO-1), which protect against various forms of stress.³⁶ It has been proposed that Michael addition of curcumin to thiols on Keap1 may result in a conformational change that disrupts the Nrf2-Keap1 complex, promoting Nrf2 binding to AREs, but this still requires structural verification.²⁸

Another transcription factor commonly studied as a target for cancer treatment is nuclear factor kappa-light-chain-enhancer of activated B cells (NF- κ B). This transcription factor is involved in cell response to free radicals, cytokines, ultraviolet radiation, and viral or bacterial antigens. Because NF- κ B is present in the cytoplasm in an inactive form until stimulated, it is considered a first responder transcription factor as it does not require synthesis for activation. Upon stimulation, NF- κ B is translocated to the nucleus triggering the expression of certain genes that suppress apoptosis and promote proliferation and metastasis.

In the work of Youns *et al.* the effects of curcumin were studied on human pancreatic cell lines expressing different levels of cyclooxygenase-2 (COX-2), an enzyme that plays an important role in response to inflammation.³⁷ Curcumin was capable of inhibiting proliferation and inducing apoptosis through the extrinsic pathway mediated through tumour necrosis factor (TNF) receptor activation. The TNF pathway triggers caspase-8 and -3 activation, which are pro-apoptotic, but also induces NF- κ B, which regulates the expression of the COX-2 gene. Curcumin also resulted in down-regulation of COX-2, suggesting the suppression of NF- κ B activation. Using molecular docking studies, curcumin has been shown to bind to TNF- α through various van der Waals and hydrogen bonding interactions, which may inhibit the binding of TNF- α to its receptor, thus preventing the activation of NF- κ B.³⁸

In another study, curcumin's ability to chemosensitize breast cancer cells to 5-fluorouracil was investigated.³⁹ 5-Fluorouracil has been noted to up-regulate the NF- κ B pathway inducing the expression of its regulated genes, leading to chemoresistance. I κ B kinase (IKK) is a signal-induced enzyme, which phosphorylates I κ B α , an NF- κ B inhibitory protein. Upon phosphorylation, I κ B α is detached from NF- κ B, leaving NF- κ B free to translocate to the nucleus and induce the expression of different genes. The authors showed that curcumin inhibited the phosphorylation of I κ B α by IKK, preventing the dissociation of I κ B α from NF- κ B, keeping NF- κ B dormant. As a result, chemoresistance towards 5-fluorouracil treatment was significantly decreased.

Activated protein-1 (AP-1), composed of Jun, FOS, and ATF protein dimers,⁴⁰ is another transcription factor commonly used as a target for cancer treatment as it is responsible for differentiation, proliferation, apoptosis, and oncogenic transformations.⁴¹ Activation of AP-1 by stimuli such as growth factors, bacterial/viral infections, cytokines, stress signals, or oncogenic factors promotes the binding of AP-1 to the TPA responsive element (TRE) causing the expression of several genes such as cyclin-D1, MMP, VEGF, and uPA, some of which mirror genes activated by NF- κ B and are involved in the angiogenesis and growth of cancer cells.²⁴ Curcumin has been proposed to inhibit this pathway via direct interaction with the AP-1 DNA-binding site.⁴² Spectroscopic evidence has shown that curcumin can in general bind to DNA through O2 of thymine in the minor groove, N7 of guanine and adenine in the major groove and to the backbone phosphate moieties with a binding constant of $4.3 \times 10^4 \text{ M}^{-1}$.⁴³

Curcumin was shown to suppress binding of AP-1 to DNA in human leukemia cells,⁴⁴ and transformed keratinocytes.⁴⁵ Furthermore, curcumin possesses cytotoxic activities towards human papillomavirus (HPV)-16 and HPV-18 infected cells associated with the development of cervical cancer, in addition to promotion of cervical cancer cell apoptosis, and inhibition of AP-1-DNA binding, thereby preventing HPV gene expression.⁴⁶ The down regulation of AP-1 by curcumin has also been reported for prostate cancer.^{47,48} It was reported that exogenous hydrogen peroxide induces prostate cancer LNCaP cell proliferation via activation of AP-1 and consequent stimulation of heparin affinity regulatory peptide (HARP) gene.⁴⁹ This cascade is halted by curcumin inhibition of the hydrogen peroxide induced HARP expression.

The Janus kinase/signal transducer and activator of transcription (JAK/STAT) signaling pathway is another cascade noted to be involved in the progression of cancer.⁵⁰ JAK belongs to the non-protein receptor tyrosine kinase family, and STATs are latent cytoplasmic transcription factors. The JAK/STAT pathway plays a role in immune response, mediating interactions of cytokines, hormones, and growth factors and their respective receptors. Upon binding of a ligand to its receptor, JAK is activated and the increased kinase activity induces phosphorylation of tyrosine residues on the receptor. Tyrosine phosphorylation creates phosphotyrosine sites on the receptor, which STATs are capable of binding to. The STATs recruited to these binding sites are themselves phosphorylated, creating phosphotyrosine sites for other STATs, thereby creating dimers. STAT dimers accumulate in the nucleus and activate their target genes. Kroon *et al.* studied the effect of this pathway on prostate cancer cells, specifically with respect to STAT3 which of the seven known STAT proteins has been reported to be closely associated to a variety of human cancers.⁵¹

Yang *et al.* investigated the effect of curcumin on the JAK/STAT signaling pathway in small lung cancer cells.⁵² The authors reported that curcumin was capable of suppressing cell proliferation and migration through inhibition of STAT3 phosphorylation, thus suppressing downstream target genes. To further ensure the role of this cascade on the cancer cells, the authors showed that activation of STAT3 induced by interleukin-6 (IL-6), a pro-inflammatory cytokine, lead to increased proliferation and cell survival. These results supported the conclusion that this pathway can be a potential target for cancer treatment with curcumin. Comparable results were demonstrated earlier on glioblastomas by Weissenberger *et al.* in 2010.⁵³

In addition to the above, other molecular signaling pathways reported to be associated with cancer cell proliferation have also been studied in the context of curcumin. The effect of curcumin on both the phosphoinositide 3-kinase (PI3K)/protein kinase B (AKT)/mammalian target of rapamycin (mTOR) pathway and the mitogen-activated protein kinases (MAPK) pathway has been investigated by Ono *et al.*⁵⁴ PI3K, a family of enzymes involved in cell growth, survival, and proliferation, are activated via ligand/receptor interactions where they are recruited to the inner cell membrane. PI3K activates AKT, which in turn activates mTOR through direct phosphorylation, promoting cell survival.⁵⁵ MAPK are activated by a series of phosphorylation cycles in response to a variety of stimuli. The authors were able to demonstrate

that curcumin inhibited the phosphorylation of mTOR by AKT, suppressing its downstream targets and inducing apoptosis. Interestingly, curcumin enhanced MAPK activity. Specifically, ERK1/2, a subgroup of MAPK, activation by curcumin promoted apoptosis in colorectal carcinoma cells. As determined by Western blotting, both pathways were associated with G₂/M phase arrest, and poly (ADP-ribose) polymerase (PARP) cleavage, which is characteristic of cells undergoing apoptosis.

The exportin 1 (CRM1)-dependent nuclear export pathway is a less commonly investigated cascade. CRM-1 facilitates the transport of large molecules across the nuclear membrane to the cytoplasm.⁵⁶ Furthermore, the structure of CRM1 allows the binding of Ran protein bound to GTP promoting the binding of different cargo proteins to CRM1 in response to a nuclear export signal (NES). Nui *et al.* showed that curcumin targets CRM1 through the Michael addition reaction of the α,β -unsaturated carbonyl of curcumin and the nucleophilic Cys⁵²⁸ of CRM1.⁵⁷ Mass spectrometry revealed that curcumin bound directly to a CRM1-derived peptide containing the Cys⁵²⁸ moiety, making it capable of arresting this cascade. Furthermore, the authors investigated the effect of curcumin on cargo proteins, as many cancer-promoting proteins are trafficked by CRM1. It was found that curcumin treatment caused the up-regulation of tumour suppressor cargo proteins p73 and p27, and a down-regulation of the pro-survival COX-2 and Cyclin D1.

In other work, the TNF-related apoptosis-inducing ligand (TRAIL) pathway and its enhancement by curcumin has been investigated.⁵⁸ TRAIL is a protein that acts as a ligand, binding to death receptor (DR)-4 and -5, to activate caspase-8. Caspase-8 cascade activates procaspase-3, -6, and -7 downstream to induce apoptosis. It was reported that breast cancer cells pre-incubated with curcumin became sensitized to TRAIL, promoting cell death.⁵⁸ However, the enhancement of TRAIL sensitization was cell-type dependent, with the extent of sensitization differing from one breast cancer cell line to another.

Steroid receptors such as estrogen receptors (ER), progesterone receptors (PR), and androgen receptors (AR) function as transcription factors, regulating their respective target genes. Abnormal expression of steroid receptors' transcription coregulators causes the deviation away from their normal functions, thereby participating in the onset and progression of cancers.⁵⁹ For

this reason, anti-steroid receptor compounds are used clinically to treat cancer due to their apoptosis-inducing properties.

Curcumin analogues were shown to behave as androgen receptor antagonists in human prostate cancer as studied by Ohtsu *et al.*⁶⁰ Curcumin was identified as a binding ligand for the nuclear vitamin D receptor (VDR) correlated with human colon cancer, playing a role in cancer chemoprevention.⁶¹ In particular, curcumin was capable of competing with 1,25-dihydroxyvitamin D₃ (1,25D) for the direct binding to VDR. Occupation of the VDR binding site by curcumin caused conformational changes to the receptor, transforming it to its transcriptionally active form, thereby inducing the expression of tumour suppressor genes. Moreover, the use of curcumin in breast cancer treatment showed that it can interact with breast cell lines expressing varying cellular receptor phenotypes involved in breast cancer, thus inducing anti-proliferative effects.^{62,63}

In addition to anti-proliferative and apoptotic effects, curcumin possess chemosensitizing,^{64, 65} radiosensitizing,^{64, 66} and radioprotective effects.^{66, 67} Furthermore, the effect of curcumin on newly identified pathways associated with microRNA, stem cells, and autophagy have been studied.²⁶ MicroRNA are small, noncoding RNAs that negatively regulate the expression of genes by binding to the 3' region of the untranslated target mRNA, thereby inhibiting translation or inducing mRNA degradation. Because microRNA possess both oncogenic and tumour suppressing properties, anti-cancer effects were achieved upon treatment with curcumin, through the up- and down-regulation of certain microRNA.⁶⁸⁻⁷⁰ Cancer stem cells—undifferentiated cancer cells that can generate tumours by self-renewal—have been shown to drive and sustain human cancers, and treatment with curcumin has been demonstrated to interfere with the self-renewal of cancer stem cells.⁷¹⁻⁷³ Moreover, autophagy is the catabolic or “self-eating” mechanism involving the sequestration of unnecessary, dysfunctional components or organelles into autophagosomes and their degradation in lysosomes.⁷⁴ This process is altered in cancer cells, promoting cell survival. Curcumin was shown to trigger autophagy in pleural mesothelioma,⁷⁵ oral cell carcinoma,⁷⁶ and glioma cells.^{77, 78} With the many molecular targets of curcumin, indeed it can serve as a potential therapeutic for the destruction of cancer cells.

2.4 Clinical Studies

Thus far, more than 20 clinical trials with curcumin for various cancers including colorectal, pancreatic, breast, prostate, multiple myeloma, lung, head and neck, and cancer lesions have been completed. The results of these studies have been summarized in recent review articles,^{25,26,79} so we describe here only a few recent noteworthy examples.

At a dose of 360 mg, three times per day, curcumin was found to increase body weight, increase the number of apoptotic cells, and enhance the expression of p53 in colorectal cancer patients after diagnosis and before surgery.⁸⁰ However, the health improvement related to increase p53 expression still needs to be studied. Curcumin was also shown to reduce the formation of aberrant crypt foci (ACF), the precursor of colorectal polyps, in smokers at a dose of 4 g/day, suggesting a potential cancer chemopreventive role for curcumin.⁸¹ A recent study demonstrated that following doses of 2.35 g/day for 14 days prior to biopsy or colonic resection, curcuminoids were detectable in colonic tissue, mucosa and urine of most patients, with minimal side effects observed.⁸² The efficacy of curcumin in combination with gemcitabine against advanced pancreatic cancer was also recently evaluated in two different trials.^{83,84} Kanai *et al.* found that curcumin at a 8 g/day in combination with gemcitabine was safe and well-tolerated.⁸⁴ However, Epelbaum and coworkers found that some patients experienced abdominal pain at this dose, and did not obtain a highly promising therapeutic response.⁸³ Curcumin in combination with docetaxel in patients with advanced and metastatic breast cancer was also recently studied in a Phase 1 trial.⁸⁵ It was found that the maximum tolerable dose of curcumin was 8 g/day and in combination with the standard dose of docetaxel, the recommended dose was 6 g/day for seven consecutive days every three weeks. The safety, tolerability, and efficacy of curcumin in patients with asymptomatic, relapsed, or plateau phase multiple myeloma has also evaluated by Vadhan-Raj *et al.*⁸⁶ At doses of 4 to 8 g/day for a year, curcumin was found to down-regulate the activation of NF- κ B and STAT3, and suppress COX-2 expression, but further studies are required to demonstrate efficacy against multiple myeloma. In patients with familial adenomatous polyposis, curcumin was reported to provide improvements in patients with precancerous lesions at a dose of 12 g/day (0.5% curcumin).⁸⁷

Based on a search of www.clinicaltrials.gov, there are currently more than 15 clinical trials ongoing for the treatment of various cancers with curcumin. Curcumin is approved by the United States Food and Drug Administration as being generally regarded as safe (GRAS). It is marketed in various forms as a dietary supplement in many countries. However, there is not yet an approved drug license for curcumin. This can likely be attributed in part to the multi-targeting property of curcumin.⁸⁸ It also results from the extremely poor solubility in aqueous media and very low bioavailability of curcumin.^{89, 90} The next section of the review discusses potential means of increasing the solubility and bioavailability of curcumin in order for the drug to make the transition from the lab into clinical use.

2.5 Enhancement of Curcumin Solubility and Bioavailability

Curcumin has been reported to be safe at doses up to 12 g/day.⁹¹⁻⁹³ However, because curcumin undergoes rapid metabolism and clearance when administered, it has very poor bioavailability.⁹⁴ A study demonstrated that when curcumin was administered orally to rats at a dose of 500 mg/kg, a peak concentration of 1.8 ng/mL was detected in the plasma, while curcumin given intravenously showed no trace of the drug in plasma within 1 hour of administration.⁹⁵ In another study, an intraperitoneal injection of 0.1 g/kg in mice showed a plasma concentration of 2.25 µg/mL after 15 minutes of administration, with concentrations of 177.04, 26.06, 26.9, and 7.51 µg/mL in the intestines, spleen, liver, and kidneys, respectively.⁹⁶ A human study revealed that a total oral dose of 3.6 g/day of curcumin resulted in nanomolar amounts of curcumin in plasma samples on day one at the 1 hour mark, with similar amounts on day 2, 8, and 29.⁹⁷ How can the bioavailability of curcumin be enhanced knowing that concentrations of at least 10^{-5} – 10^{-4} M are required for the drug to have any therapeutic impact?⁹⁵ One approach can involve the co-administration of adjuvants that can block the metabolic processing of curcumin. For example, the co-administration of curcumin and piperine, a known inhibitor of intestinal and hepatic glucuronidase, involved in curcumin glucuronidation, was shown to increase the bioavailability of curcumin by 2000%.⁹⁸ There has also been ongoing research on drug delivery systems that may be used to transport curcumin to the desired site, or simply enhance its solubility.

2.5.1 Preparation of Curcumin Co-crystals

A promising approach to solubility enhancement is the development of co-crystals. Co-crystals are a class of solid drugs formed using an active pharmaceutical ingredient (API), and a solubilizing agent.⁹⁹ The resulting co-crystals generally possess enhanced physicochemical properties such as solubility and stability, due to increased hydrogen bonds in the system.⁹³

Sanphui and coworkers studied co-crystals synthesized using curcumin as the API with two different solubilizing agents, resorcinol and pyrogallol (Figure 2.7), by a liquid-assisted grinding method.⁹³ The melting point of the co-crystals was reported to be between that of pure curcumin and the solubilizing agent, with curcumin-pyrogallol having a lower melting point than curcumin-resorcinol. Curcumin-resorcinol co-crystals exhibited a dissolution rate 5-fold that of curcumin alone, while curcumin-pyrogallol co-crystals had a dissolution rate 12-fold higher than that of curcumin.

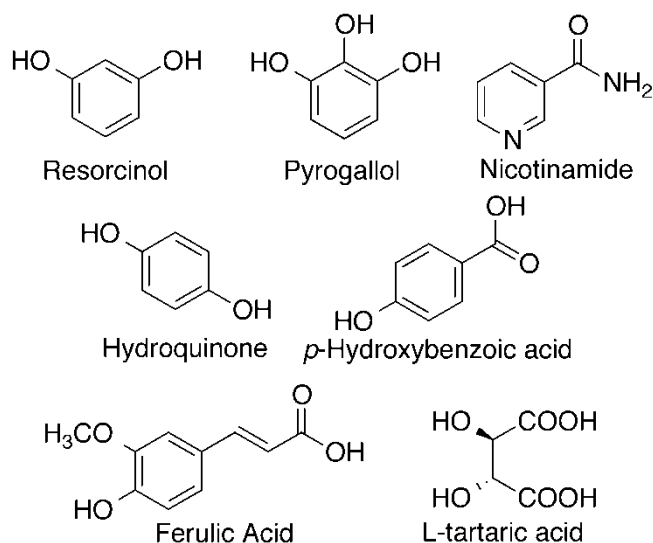


Figure 2.7: Common coformers used with curcumin to produce cocrystals

In another study, curcumin co-crystals were synthesized with five different coformers including nicotinamide, ferulic acid, hydroquinone, *p*-hydroxybenzoic acid, and L-tartaric acid (Figure 2.7).⁹⁰ All five co-crystal solids were noted to be eutectic, having lower melting points than both constituents alone, and dissolved faster than pure curcumin, with curcumin-nicotinamide having the fastest dissolution rate. Undoubtedly, curcumin co-crystals can serve as a solution to increase

the bioavailability of curcumin when administered orally. With the wide variety of cofomers such as therapeutic drugs, salts, or even natural spices, that can be used, curcumin co-crystals can potentially be synthesized to treat several conditions.

2.5.2 Delivery Systems for Curcumin

Alternative to co-crystals, which simply enhance the dissolution rate of the drug, methods have been developed to transport curcumin throughout the body to the desired sites for therapeutic applications. A variety of nano-vehicles including liposomes, exosomes, micelles, nanoparticles, and dendrimers have been used to encapsulate and deliver curcumin, resulting in enhanced water solubility, stability and bioactivity (Figure 2.8).

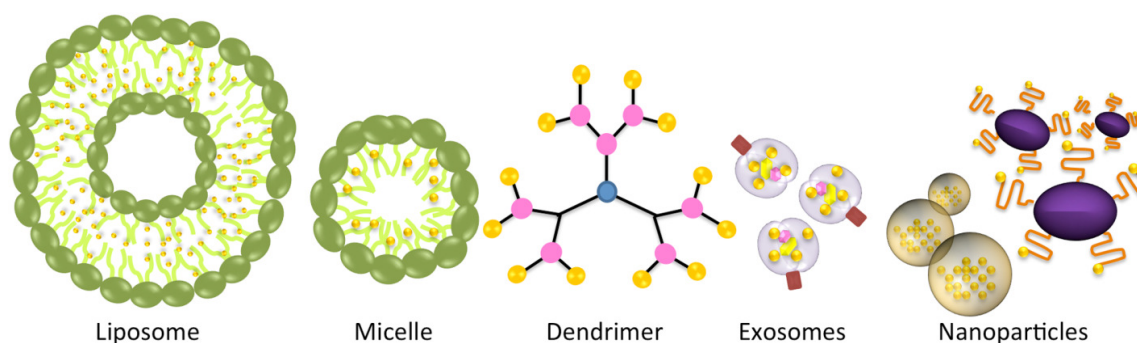


Figure 2.8: Curcumin-loaded drug delivery systems

2.5.2.1 Liposomes

Liposomes can be described as phospholipid bilayers surrounding an aqueous core, and have been investigated for the delivery of a wide variety of different pharmaceutical agents.¹⁰⁰ In fact, lipid-based drug delivery systems are available in the clinic. One such product is Doxil, which is a PEGylated liposomal doxorubicin.¹⁰¹ Li *et al.* have studied the *in vitro* and *in vivo* effects of liposome-encapsulated curcumin on human pancreatic carcinoma cells.¹⁰² The liposomes were prepared from a 10:1 weight ratio of lipid (1,2-dimyristoyl-sn-glycero-3-phosphocholine (DMPC) and/or 1,2-dimyristoyl-sn-glycero-3-phosphor-rac-(1-glycerol) sodium salt (DMPG)) to curcumin. It was demonstrated that liposomal curcumin was capable of down-regulating NF- κ B machinery, resulting in suppressed growth and increased apoptosis of various human pancreatic cancer cell lines *in vitro*. In addition, tumour suppressive and anti-angiogenic effects

were observed for both BxPC-3 and MiaPaCa2 cell lines in murine models. In a recent study, Saengkrit *et al.* investigated the cellular uptake of curcumin-loaded didecyldimethylammonium bromide (DDAB)-modified liposomes compared to non-modified liposomes on cervical cancer cells.¹⁰³ Liposomes were prepared using various ratios of soybean lecithin, non-ionic surfactant, cholesterol and DDAB by means of the conventional thin film hydration method. The authors reported that cell uptake was enhanced with DDAB-containing liposomes, however the cytotoxicity of these cationic liposomes was high and more work is required to optimize this. Furthermore, *in vitro* release studies showed that curcumin was released faster from DDAB-containing liposomes, which the authors hypothesized to be a consequence of reduced interaction forces between lipid chains due to the cationic charges of DDAB.

2.5.2.2 Exosomes

An alternative to synthetic phospholipid vesicles is the naturally occurring analogue, referred to as exosomes. Exosomes are small, endocytic membrane vesicles that are excreted by many cells. They are generally formed by budding from the membrane of multivesicular endosomes found in different cell types, and thus contain different protein families (Figure 2.9). Exosomes are usually 30 – 100 nm in diameter and are capable of floating on sucrose gradients making them easy to separate from other contaminants.¹⁰⁴ Due to their small size and biocompatibility these vesicles can potentially be used for the delivery of pharmaceuticals.

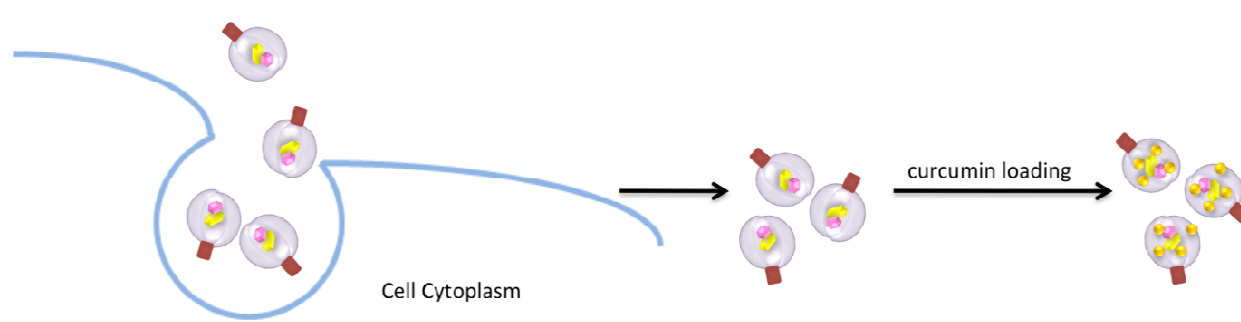


Figure 2.9: Schematic of the collection and loading of exosomes

Sun *et al.* studied the anti-inflammatory effects of curcumin when encapsulated in exosomes.¹⁰⁵ Curcumin was mixed at 22 °C with exosomes derived from EL-4 cells, and the mixture was purified by sucrose gradient separation. A loading capacity of 2.9 g curcumin per 1 g exosomes

was reported and the solubility of curcumin was five-fold higher with exosome-entrapment in comparison to free curcumin. Furthermore, a stability study was conducted and it was found that in phosphate buffered saline at 37 °C, in the absence of exosomes, 75% of curcumin was degraded over 2.5 hours, while only 20% degradation was observed for exosome-encapsulated curcumin. An *in vivo* study was carried out on mice with a dose of 100 mg/kg of curcumin administered orally or intraperitoneally. Exosomal curcumin was present in peripheral blood at concentrations five to ten-fold higher than free curcumin, with no detectable amount of free curcumin circulating in the blood. The *in vivo* anti-inflammatory effects of curcumin were also evaluated, using a lipopolysaccharide-induced septic shock model. A significant survival advantage and lower cytokine levels were demonstrated for mice treated with exosomal curcumin in comparison with free curcumin or curcumin-free exosome and saline controls.

2.5.2.3 Micelles

Mohanty *et al.* proposed a polymeric micelle as a drug delivery system for curcumin encapsulation to be used for cancer therapy.¹⁰⁶ Curcumin-containing micelles were synthesized using a methoxy poly(ethylene glycol) (mPEG)/poly- ϵ -caprolactone (PCL) formulation. The micelles were loaded with curcumin via a dialysis method at room temperature. The micellar solution was then freeze dried to obtain a dry solid form of curcumin-containing micelles. The authors reported a curcumin encapsulation efficiency of 60%, with a micelle size of 110 nm. The loaded micelles showed sustained release of curcumin lasting for one week. Furthermore, curcumin uptake was investigated on PANC-1 pancreatic cancer cell line using both curcumin-loaded micelles, and unmodified curcumin for comparison. Curcumin concentrations of 10, 20, and 30 μ M were studied. The authors observed that cell uptake of curcumin-loaded micelles at a concentration of 10 μ M was ~3-folds higher than that of unmodified curcumin. However, at the highest curcumin concentration (30 μ M), the micellar uptake was only ~2-folds higher than unmodified curcumin. This led the authors to conclude that cell uptake is more efficient at lower concentrations, rationalizing that at higher concentrations of curcumin-loaded micelles, saturation may occur, causing decreased entry of micelles into the cells.

In another study, Podaralla *et al.* investigated a micellar formulation of curcumin prepared from mPEG conjugated to zein, a hydrophobic plant protein.¹⁰⁷ Curcumin was encapsulated in mPEG-zein micelles by dissolving mPEG-zein and curcumin (100:2 wt/wt) in 90% ethanol, followed by

dialysis to remove the remaining ethanol and free curcumin. The authors reported a micelle size range of 95 – 125 nm, and release of curcumin over a period of ~24 hours *in vitro*. The micellar system resulted in 1000-2000-fold enhancement in curcumin water solubility and a ~6-fold increase in stability, as evaluated by UV-visible spectroscopy. The uptake of curcumin-loaded micelles by ovarian cancer cells was 2-3-fold higher than free curcumin, leading the authors to conclude that this delivery system is highly promising for the delivery of anti-cancer drugs. They also suggested that the core or shell could potentially be modified by cross-linking in order to further sustain the release.

Gao *et al.* studied biodegradable mPEG-poly(lactide) copolymer (mPEG-PLA) micelles for curcumin delivery in colon cancer therapy.¹⁰⁸ The micelles were prepared by a self-assembly method, and were reported to have a narrow size distribution with an average diameter of 30 nm. *In vitro* release studies carried out in PBS containing 0.5% w/w Tween-80 at physiological temperature showed that free curcumin was rapidly released reaching maximum release (83%) within 12 hours. However, curcumin-loaded micelles showed more sustained release, reaching approximately 60% curcumin release in the same time period. The authors also reported enhanced uptake and apoptosis of colon cancer cells demonstrated by curcumin-loaded micelles compared to free curcumin alone.

2.5.2.4 Nanoparticles

Nanoparticle vehicles for the encapsulation and transportation of curcumin have also been developed. For example, in the formulation THERACURMIN®, curcumin powder and glycerin was added to a solution of polysaccharides from ghatti trees, then the mixture was processed by wet grinding and high-pressure homogenization to produce a stable colloidal dispersion of nanoparticles with diameters of 190 nm.¹⁰⁹ In clinical trials, the area under the blood concentration-time curve was found to be 27-fold higher for this formulation than for curcumin powder.¹⁰⁹ In addition, in pancreatic or biliary tract cancer patients receiving gemcitabine no increase in adverse effects was observed for THERACURMIN® at a curcumin dose of 200 or 400 mg/day.¹¹⁰

O'Toole *et al.* have used chitosan-based particles to encapsulate curcumin.¹¹¹ The authors used a spray drying method to encapsulate curcumin inside chitosan/Tween 20 particles where the ratio

of chitosan/Tween 20 was varied. The particle size was noted to be 285 ± 30 nm, with a curcumin encapsulation efficiency of nearly 100%. In release experiments, a burst release profile was observed with all of the curcumin released over a period of 2 hours. While suitable for applications in which a rapid release of curcumin is desired, additional work may be required to prolong the curcumin release for some applications.

Misra and Sahoo have co-encapsulated curcumin with doxorubicin in poly(D,L-lactide-co-glycolide) nanoparticles.¹¹² Doxorubicin is used to treat a variety of cancers, including leukemia; however, a number of cancer cells, including the chronic myeloid leukemia blasts such as K562 cells are resistant to doxorubicin due to its sequestration into cytoplasmic vesicles and the induction of multi-drug resistance (MDR). Along with its other anti-cancer properties, as curcumin has been demonstrated to down-regulate MDR transporters, it was of particular interest to investigate the potential beneficial effects of incorporating both drugs into a single nanoparticle. The particles were prepared by a single emulsion, solvent evaporation technique, which resulted in particles with diameters of ~ 250 nm. Incorporation of the drugs into the nanoparticles resulted in ~ 8 -fold higher uptake than for the free drugs in solution. The dual drug nanoparticle formulation also resulted in increased nuclear retention of doxorubicin. This was found to correspond to lower levels of expression of resistance genes MDR1 and BCL-2 in K562 cells, attributed to curcumin inhibition. Combined, these properties resulted in increased *in vitro* cytotoxicity for the dual drug nanoparticles in comparison to doxorubicin nanoparticles or the dual drugs in solution.

Curcumin was also encapsulated in another nanoparticle system developed by Mohanty and Sahoo.¹¹³ Curcumin was loaded in glycerol monooleate (GMO)/Pluronic F-127 particles using an emulsification technique upon the addition of 0.5% w/v polyvinyl alcohol. The nanoparticles displayed an average diameter of 192 ± 7 nm and had a spherical morphology. HPLC studies revealed an encapsulation efficiency of $90 \pm 3\%$, and *in vitro* release experiments demonstrated an initial burst of 46% of drug released in 24 hours, after which the remaining drug was released over a period of 10 days. Similar to the cell uptake of curcumin-loaded micelles investigated by Mohanty *et al.*, the authors found that cell uptake was concentration dependent, with lower concentrations of curcumin-loaded nanoparticles exhibiting better cell uptake than unmodified curcumin, in addition to more effective anti-proliferative activity.

Sindhu *et al.* synthesized spherical gold nanoparticles using curcumin alone as a reducing agent.¹¹⁴ The particles were spherical, with an average size of 58 nm and a zeta potential of -23 mV. The authors reported that the particles were stable at room temperature for up to 6 months, and that they were non-toxic *in vitro*. Mesoporous silica nanoparticles (MSN) (type MCM-41) have also been used to encapsulate curcumin within the pores of the nanoparticles in order to enhance its solubility.¹¹⁵ The authors demonstrated that the solubility of curcumin encapsulated in the silica nanoparticles (0.53 $\mu\text{g/mL}$) was increased by 71% compared to that of curcumin alone (0.31 $\mu\text{g/mL}$) and curcumin-MSN physical mixture (0.36 $\mu\text{g/mL}$). The authors noted that *in vitro* curcumin release was much more rapid when encapsulated in the MSN, reaching 29% over 72 hours due to the formation of curcumin nano-aggregates in the pores, compared to 8.9% and 9.0% as demonstrated by curcumin and curcumin-MSN physical mixture, respectively. This resulted in enhanced cytotoxic effects for curcumin-MSN on human breast cancer cells compared to free curcumin and curcumin-MSN physical mixture.

2.5.2.5 Hydrogels

Though not formally nanomaterials in their simplest form, hydrogels, composed of networks of polymer chains, are high water-content materials that can possess strength and flexibility similar to human tissue (Figure 2.10).¹¹⁶ Because there exists a large array of water-soluble polymers that can be used for the preparation of hydrogels having a wide variety of physical morphologies (eg. particles, slabs, and films) and properties, hydrogels can potentially be used for many different biomedical applications including drug delivery. Curcumin-encapsulating hydrogels containing 0.5, 1, or 2 wt% of a 20 amino acid peptide referred to as MAX8, have been synthesized via a self-assembly method upon the addition of salt solution buffered to pH 7.4 or cell culture medium at the same pH, where curcumin-encapsulation and hydrogel formation occurs concurrently.¹¹⁷ Hydrogels containing curcumin displayed solid-like properties even after shear thinning, where they were capable of re-healing quickly according to the oscillatory rheology and shear stiffness study conducted. This suggested their potential as injectable materials for localized curcumin delivery. The release of curcumin occurred over a period of 14 days and could be modulated to some extent as a function of the MAX8 peptide concentration. In addition, through *in vitro* experiments, it was demonstrated that the presence of curcumin in the

hydrogels inhibited the growth of human medulloblastoma cells on the hydrogel. The bioactivity of the released curcumin was also confirmed by its ability to inhibit growth of the same cell line.

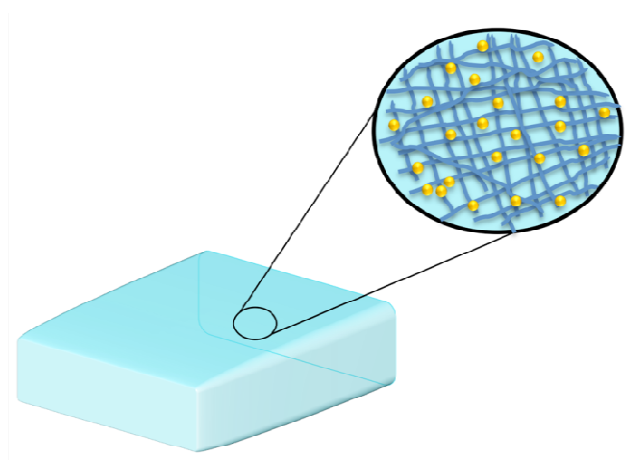


Figure 2.10: Schematic of a hydrogel with encapsulated curcumin

An emerging field of hydrogels, called “smart” hydrogels, has gained immense interest. Smart hydrogels are capable of dramatically changing their properties in response to stimuli such as temperature, pH, and chemicals.¹¹⁸ Chen *et al.* reported a curcumin-loaded thermosensitive hydrogel for brain targeting applications through intranasal administration.¹¹⁹ Hydrogels were synthesized using Pluronic F127 and Poloxamer 188. The curcumin-loaded hydrogels underwent sol-gel transition in the temperature range 32-35 °C, therefore undergoing gelation at physiological temperatures. *In vitro* release studies revealed that 80% of curcumin was released within 6 hours, and *in vivo* studies showed that curcumin-loaded hydrogels took approximately one hour to pass from the nasal cavity of rats to their oropharynx. In addition, brain tissue distribution analyses showed the presence of curcumin in the cerebellum, cerebrum, hippocampus, olfactory bulb, and plasma after the administration of 250 µg/kg of the nasal hydrogel. This suggests the application of these curcumin hydrogels for targeting of brain tumours.

2.5.2.6 Dendrimers and Proteins

In addition to assemblies of phospholipids and polymers into which curcumin can be physically encapsulated, dendrimers have also been widely studied for drug delivery and have often been used for the preparation of covalent drug conjugates.¹²⁰ Dendrimers are highly branched

polymers with precise architectures that result from their step-wise synthesis.¹²¹ Because these structures are prepared on a generation-by-generation basis, they can be tailored for use in many applications. Shi *et al.* used dendrimers for the enhancement of curcumin's bioavailability and its effects in the dissolution of amyloid fibrils.¹²² The group produced monofunctional derivatives of curcumin where one of the phenolic groups of curcumin was modified with azide, alkyne, or carboxylic acid. These monofunctional derivatives of curcumin were then used to produce other forms of curcumin, among them a polyamidoamine (PAMAM) dendrimer-curcumin conjugate (Figure 2.11). The PAMAM-curcumin conjugate was synthesized using a fourth generation PAMAM dendrimer with a cystamine core and amine surface groups. Curcumin monocarboxylic acid was coupled to the amine termini using 1,3-dicyclohexyl-carbodiimide, *N*-hydroxysuccinimide, and triethanolamine. The biological activity of curcumin was not disrupted by its chemical modification as reported; In fact the chemical properties of curcumin were enhanced. The water-soluble PAMAM-curcumin conjugate was able to stain and dissolve amyloid fibrils *in vitro*. The enhanced water solubility of curcumin by attachment to dendrimers suggests promising therapeutic applications.

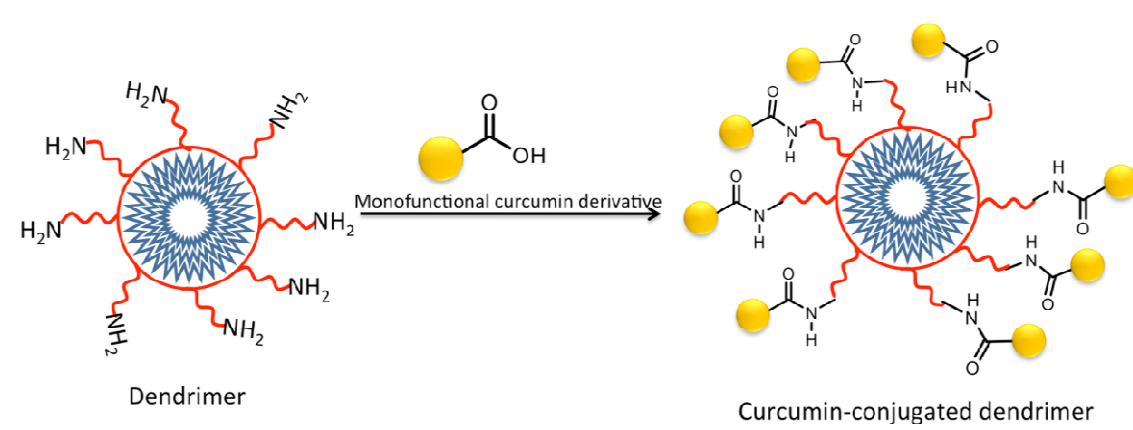


Figure 2.11: Schematic of the synthesis of a curcumin-conjugated dendrimer

In another study, with the aim of understanding curcumin's wound healing properties despite its rapid degradation in aqueous solution, the stabilization of curcumin by four different plasma proteins, human serum albumin (HSA), fibrinogen, immunoglobulin G (IgG), and transferrin was investigated.¹²³ It was reported that curcumin degradation was suppressed with a yield of $94.2 \pm 13.9\%$ when stabilized with HSA, and $93.6 \pm 14.0\%$ with fibrinogen. Transferrin did not

suppress curcumin degradation as efficiently ($47.8 \pm 14.1\%$), and IgG had no effect on degradation. The impressive degradation suppression of HSA and fibrinogen were attributed to the hydrophobic interactions between the proteins and curcumin, where binding of curcumin takes place in the hydrophobic pocket in the protein. This eliminates interactions with surrounding water molecules inhibiting curcumin degradation by hydrolysis.

2.6 Conclusions and Future Prospects

With the potential application of the wide range of above vehicles as drug delivery systems come several challenges. Vesicles often require complex preparation procedures, and are often too large for drug delivery applications. The large size (> 200 nm) results in clearance by the reticuloendothelial system (RES) thereby eliminating the drug from the circulatory system.¹²⁴ Nanoparticles are also often too large to exhibit long circulation times *in vivo*, frequently having diameters > 200 nm. In addition, they have some tendency to exhibit an undesirable "burst" release of the drug. Micelles on the other hand are smaller, and can sometimes exhibit long circulation times *in vivo*. However, as they are prepared by self-assembly approaches, their behaviour *in vivo* in the presence of membranes and hydrophobic serum proteins, will not always be the same as their *in vitro* behaviour in simpler model systems. In addition, the metabolic fate of these carriers is often difficult to determine, and some may not be biodegradable. Nevertheless, the work this far has demonstrated the great potential of drug delivery systems to overcome some of curcumin's problematic properties such as its extremely low aqueous solubility, stability, and bioavailability.

Although there is still much to be investigated with respect to curcumin and its therapeutic properties, it has great potential in cancer therapy and prevention. Curcumin is proposed to exert its anti-cancer effects through a variety of mechanisms including the down-regulation of NF- κ B, the suppression of AP-1 activity, various effects on STAT proteins, as well as other mechanisms. The controversy regarding curcumin's chemical structure in aqueous solution at neutral pH appears to be solved, with the dominance of the keto-enol form well supported by NMR spectroscopy as well as theoretical studies. However, there is still debate as to whether it is curcumin itself or its degradation products that provide the observed biological activities. This issue highlights one of the main challenges in working with curcumin - its susceptibility to rapid

degradation in a wide range of environments and its sensitivity to pH and light. Other major challenges include curcumin's extremely low aqueous solubility and bioavailability. While curcumin has been safely administered at high doses in many clinical trials, has achieved the status of GRAS, and is marketed as a dietary supplement in many countries, it has yet to be licensed as a drug, likely due to the above-mentioned limitations as well as its multi-target property.

To address the solubility and bioavailability limitations, a variety of approaches have been explored to improve its solubility and to deliver it to cancer cells. The formation of co-crystals with a variety of molecules has resulted in significant enhancements in the curcumin dissolution rate. Liposomes, micelles, nanoparticles, and other delivery systems have generally led to enhanced curcumin solubility, stability, cell uptake, and improved biological activities, and are starting to be evaluated in clinical trials.

Despite the immense progress made on the study and application of curcumin over the last couple of decades, many questions and challenges still exist. For example, it will be critical to determine whether the biological properties of curcumin indeed result from the parent compound or from its degradation products. This is important not only for the fundamental understanding of this drug but also because the drug delivery systems tend to stabilize curcumin, an advantage that only persists if this is the bioactive molecule. It will also be important to continue the development of viable drug delivery systems for curcumin. Here, the critical aspects will involve the enhancement of curcumin solubility and bioavailability, as well as approaches for selectively targeting these delivery systems to the disease sites. With this promising progression, the use of curcumin for the treatment of cancer and other diseases can be envisioned in the near future.

2.7 Bibliography

1. H. Hatcher, R. Planalp, J. Cho, F.M. Torti and S.V. Torti, *Cell Mol. Life Sci.*, 2008, **65**, 1631.
2. B.K. Tiwari and G.P. Agrawal, *World J. Pharm. Pharm. Sci.*, 2012, **1**, 161.
3. B.B. Aggarwal, C. Sundaram, N. Malani and H. Ichikawa, *Adv. Exp. Med. Biol.*, 2007, **595**, 1.
4. B.B. Aggarwal and S. Shishodia, *Ann. N. Y. Acad. Sci.*, 2004, **1030**, 434.
5. F. Payton, P. Sandusky and W.L. Alworth, *J. Nat. Prod.*, 2007, **70**, 143.
6. H.H. Tonnesen, J. Karlsen and A. Mostad, *Acta Chem. Scand., Ser. B*, 1982, **36**, 475.
7. S.V. Jovanovic, S. Steenken, C.W. Boone and M.G. Simic, *J. Am. Chem. Soc.*, 1999, **121**, 9677.
8. L. Shen and H.F. Ji, *Spectrochim. Acta, A Mol. Biomol. Spectrosc.*, 2007, **67**, 619.
9. H.H. Tonnesen and J. Karlsen, *Z. Lebensm. Unters. Forsch.*, 1985, **180**, 402.
10. Y.J. Wang, M.H. Pan, A.L. Cheng, L.I. Lin, Y.S. Ho, C.Y. Hsieh and J.K. Lin, *J. Pharm. Biomed. Anal.*, 1997, **15**, 1867.
11. D. Gopinath, M.R. Ahmed, K. Gomathi, K. Chitra, P.K. Sehgal and R. Jayakumar, *Biomaterials*, 2004, **25**, 1911.
12. K.N. Liu, C.M. Lai, Y.T. Lee, S.N. Wang, R.P. Chen, J.S. Jan, H.S. Liu and S.S. Wang, *Biochim. Biophys. Acta*, 2012, **1820**, 1774.
13. L. Shen and H.F. Ji, *Trends Mol. Med.*, 2012, **18**, 138.
14. G.W. Schieffer, *J. Liq. Chromatogr. Rel. Technol.*, 2002, **25**, 3033.
15. U. Singh, S. Verma, H.N. Ghosh, M.C. Rath, K.I. Priyadarsini, A. Sharma, K.K. Pushpa, S.K. Sarkar and T. Mukherjee, *J. Mol. Catal. A: Chem.*, 2010, **318**, 106.
16. K. Lirdprapamongkol, H. Sakurai, S. Suzuki, K. Koizumi, O. Prangsaengtong, A. Viriyaroj, S. Ruchirawat, J. Svasti and I. Saiki, *In Vivo*, 2010, **24**, 501.
17. S.L. Wu, J.C. Chen, C.C. Li, H.Y. Lo, T.Y. Ho and C.Y. Hsiang, *J. Pharmacol. Exp. Ther.*, 2009, **330**, 370.
18. C. Zhang, X. Li, L. Lian, Q. Chen, O. Abdulmalik, V. Vassilev, C.S. Lai and T. Asakura, *Br. J. Haematol.*, 2004, **125**, 788.
19. O.N. Gordon and C. Schneider, *Trends Mol. Med.*, 2012, **18**, 361-3; author reply 363-4.

20. M. Griesser, V. Pistis, T. Suzuki, N. Tejera, D.A. Pratt and C. Schneider, *J. Biol. Chem.*, 2011, **286**, 1114.
21. A.C. Ketron, O.N. Gordon, C. Schneider and N. Osheroff, *Biochemistry*, 2013, **52**, 221.
22. T.G. Burish and R.A. Jenkins, *Health Psychol.*, 1992, **11**, 17.
23. W.M. Lee, *N. Eng. J. Med.*, 1993, **329**, 1862.
24. T. Dorai and B.B. Aggarwal, *Cancer Lett.*, 2004, **215**, 129.
25. A. Shehzad, J. Lee and Y.S. Lee, *Biofactors*, 2013, **39**, 56.
26. S.C. Gupta, G. Kismali and B.B. Aggarwal, *Biofactors*, 2013, **39**, 2.
27. J. Epstein, I.R. Sanderson and T.T. Macdonald, *Br. J. Nutr.*, 2010, **103**, 1545.
28. S.C. Gupta, S. Prasad, J.H. Kim, S. Patchva, L.J. Webb, I.K. Priyadarsini and B.B. Aggarwal, *Nat. Prod. Rep.*, 2011, **28**, 1937.
29. A.B. Kunnumakkara, P. Anand and B.B. Aggarwal, *Cancer Lett.*, 2008, **269**, 199.
30. A. Shehzad and Y.S. Lee, *Biofactors*, 2013, **39**, 27.
31. P.M. Luthra, R. Kumar and A. Prakash, *Biochem. Biophys. Res. Commun.*, 2009, **384**, 420.
32. L.D. Guo, X.J. Chen, Y.H. Hu, Z.J. Yu, D. Wang and J.Z. Liu, *Phytother. Res.*, 2013, **27**, 422.
33. J.W. Kaspar, S.K. Niture and A.K. Jaiswal, *Free Radical Biol. Med.*, 2009, **47**, 1304.
34. S.K. Niture, J.W. Kaspar, J. Shen and A.K. Jaiswal, *Toxicol. Appl. Pharmacol.*, 2010, **244**, 37.
35. A.M. Pickering, R.A. Linder, H. Zhang, H.J. Forman and K.J. Davies, *J. Biol. Chem.*, 2012, **287**, 10021.
36. S. Shishodia, *Biofactors*, 2013, **39**, 37.
37. M. Youns and G.M. Fathy, *J. Cell. Biochem.*, 2013, **114**, 2654.
38. S.T. Wua, J.-C. Sun, K.-J. Lee and Y.-M. Sun, *Int. J. Eng. Sci. Technol.*, 2010, **2**, 4263.
39. B.S. Vinod, J. Antony, H.H. Nair, V.T. Puliappadamba, M. Saikia, S.S. Narayanan, A. Bevin and R.J. Anto, *Cell Death Dis.*, 2013, **4**, e505.
40. J. Hess, P. Angel and M. Schorpp-Kistner, *J. Cell. Sci.*, 2004, **117**, 5965.
41. E.F. Wagner, *Ann. Rheum. Dis.*, 2002, **61 Suppl 2**, ii40-2.
42. A. Bierhaus, Y. Zhang, P. Quehenberger, T. Luther, M. Haase, M. Muller, N. Mackman, R. Ziegler and P.P. Nawroth, *Thromb. Haemost.*, 1997, **77**, 772.

43. S. Nafisi, M. Adelzadeh, Z. Norouzi and M.N. Sarbolouki, *DNA Cell Biol.*, 2009, **28**, 201.
44. S.S. Han, Y.S. Keum, H.J. Seo and Y.J. Surh, *J. Biochem. Mol. Biol.*, 2002, **35**, 337.
45. S. Balasubramanian and R.L. Eckert, *J. Biol. Chem.*, 2007, **282**, 6707.
46. C.S. Divya and M.R. Pillai, *Mol. Carcinog.*, 2006, **45**, 320.
47. K. Nakamura, Y. Yasunaga, T. Segawa, D. Ko, J.W. Moul, S. Srivastava and J.S. Rhim, *Int. J. Oncol.*, 2002, **21**, 825.
48. M.H. Teiten, F. Gaascht, S. Eifes, M. Dicato and M. Diederich, *Genes Nutr.*, 2010, **5**, 61.
49. C. Polytarchou, M. Hatziapostolou and E. Papadimitriou, *J. Biol. Chem.*, 2005, **280**, 40428.
50. T. Decker, *Jak-Stat Signaling: From Basics to Disease*. Springer: Vienna, 2012.
51. P. Kroon, P.A. Berry, M.J. Stower, G. Rodrigues, V.M. Mann, M. Simms, D. Bhasin, S. Chettiar, C. Li, P.K. Li, N.J. Maitland and A.T. Collins, *Cancer Res.*, 2013, **73**, 5288.
52. C.L. Yang, Y.Y. Liu, Y.G. Ma, Y.X. Xue, D.G. Liu, Y. Ren, X.B. Liu, Y. Li and Z. Li, *PLoS One*, 2012, **7**, e37960.
53. J. Weissenberger, M. Priester, C. Bernreuther, S. Rakel, M. Glatzel, V. Seifert and D. Kogel, *Clin. Cancer Res.*, 2010, **16**, 5781.
54. M. Ono, T. Higuchi, M. Takeshima, C. Chen and S. Nakano, *Anticancer Res.*, 2013, **33**, 1861.
55. J. Rodon, R. Dienstmann, V. Serra and J. Tabernero, *Nat. Rev. Clin. Oncol.*, 2013, **10**, 143.
56. K.T. Nguyen, M.P. Holloway and R.A. Altura, *Int. J. Biochem. Mol. Biol.*, 2012, **3**, 137.
57. M. Niu, S. Wu, L. Mao and Y. Yang, *Traffic*, 2013, **14**, 1042.
58. S. Park, D.H. Cho, L. Andera, N. Suh and I. Kim, *Mol. Cell. Biochem.*, 2013, **383**, 39.
59. X. Gao, B.W. Loggie and Z. Nawaz, *Mol. Cancer*, 2002, **1**, 7.
60. H. Ohtsu, Z. Xiao, J. Ishida, M. Nagai, H.K. Wang, H. Itokawa, C.Y. Su, C. Shih, T. Chiang, E. Chang, Y. Lee, M.Y. Tsai, C. Chang and K.H. Lee, *J. Med. Chem.*, 2002, **45**, 5037.
61. L. Bartik, G.K. Whitfield, M. Kaczmarska, C.L. Lowmiller, E.W. Moffet, J.K. Furnick, Z. Hernandez, C.A. Haussler, M.R. Haussler and P.W. Jurutka, *J. Nutr. Biochem.*, 2010, **21**, 1153.

62. J.D. Altenburg, A.A. Bieberich, C. Terry, K.A. Harvey, J.F. Vanhorn, Z. Xu, V. Jo Davisson and R.A. Siddiqui, *BMC Cancer*, 2011, **11**, 149.
63. M.A. Tessel, N.L. Krett and S.T. Rosen, *Curr. Opin. Oncol.*, 2010, **22**, 592.
64. A.K. Garg, T.A. Buchholz and B.B. Aggarwal, *Antioxid. Redox Signal.*, 2005, **7**, 1630.
65. P. Limtrakul, *Adv. Exp. Med. Biol.*, 2007, **595**, 269.
66. G.C. Jagetia, *Adv. Exp. Med. Biol.*, 2007, **595**, 301.
67. N. Sebastià, A. Montoro, A. Montoro, M. Almonacid, J.I. Villaescusa, J. Cervera, E. Such, M.A. Silla and J.M. Soriano, *Radiat. Meas.*, 2011, **46**, 962.
68. M. Sun, Z. Estrov, Y. Ji, K.R. Coombes, D.H. Harris and R. Kurzrock, *Mol. Cancer Ther.*, 2008, **7**, 464.
69. S. Ali, A. Ahmad, A. Aboukameel, B. Bao, S. Padhye, P.A. Philip and F.H. Sarkar, *Cancer Lett.*, 2012, **319**, 173.
70. S. Ali, A. Ahmad, S. Banerjee, S. Padhye, K. Dominiak, J.M. Schaffert, Z. Wang, P.A. Philip and F.H. Sarkar, *Cancer Res.*, 2010, **70**, 3606.
71. M. Kakarala, D.E. Brenner, H. Korkaya, C. Cheng, K. Tazi, C. Ginestier, S. Liu, G. Dontu and M.S. Wicha, *Breast Cancer Res. Treat.*, 2010, **122**, 777.
72. K.J. Lim, S. Bisht, E.E. Bar, A. Maitra and C.G. Eberhart, *Cancer Biol. Ther.*, 2011, **11**, 464.
73. L. Lin, Y. Liu, H. Li, P.K. Li, J. Fuchs, H. Shibata, Y. Iwabuchi and J. Lin, *Br. J. Cancer.*, 2011, **105**, 212.
74. Y. Ohsumi, *Nat. Rev. Mol. Cell. Biol.*, 2001, **2**, 211.
75. Y. Yamauchi, Y. Izumi, K. Asakura, Y. Hayashi and H. Nomori, *Phytother. Res.*, 2012, **26**, 1779.
76. J.Y. Kim, T.J. Cho, B.H. Woo, K.U. Choi, C.H. Lee, M.H. Ryu and H.R. Park, *Arch. Oral Biol.*, 2012, **57**, 1018.
77. H. Aoki, Y. Takada, S. Kondo, R. Sawaya, B.B. Aggarwal and Y. Kondo, *Mol. Pharmacol.*, 2007, **72**, 29.
78. W. Zhuang, L. Long, B. Zheng, W. Ji, N. Yang, Q. Zhang and Z. Liang, *Cancer Sci.*, 2012, **103**, 684.
79. S.C. Gupta, S. Patchva and B.B. Aggarwal, *AAPS J.*, 2013, **15**, 195.

80. Z.-Y. He, C.-B. Shi, H. Wen, F.-L. Li, B.-L. Wang and J. Wang, *Cancer Invest.*, 2011, **29**, 208.
81. R.E. Carroll, R.V. Benya, D.K. Turgeon, S. Vareed, M. Neuman, L. Rodriguez, M. Kakarala, P.M. Carpenter, C. McLaren, F.L. Meyskens, Jr. and D.E. Brenner, *Cancer Prev. Res.*, 2011, **4**, 354.
82. G.R. Irving, L.M. Howells, S. Sale, I. Kralj-Hans, W.S. Atkin, S.K. Clark, R.G. Britton, D.J. Jones, E.N. Scott, D.P. Berry, D. Hemingway, A.S. Miller, K. Brown, A.J. Gescher and W.P. Steward, *Cancer Prev. Res.*, 2013, **6**, 119.
83. R. Epelbaum, M. Schaffer, B. Vizel, V. Badmaev and G. Bar-Sela, *Nutr. Cancer*, 2010, **62**, 1137.
84. M. Kanai, K. Yoshimura, M. Asada, A. Imaizumi, C. Suzuki, S. Matsumoto, T. Nishimura, Y. Mori, T. Masui, Y. Kawaguchi, K. Yanagihara, S. Yazumi, T. Chiba, S. Guha and B. Aggarwal, *Cancer Chemother. Pharmacol.*, 2011, **68**, 157.
85. M. Bayet-Robert, F. Kwiatkowski, M. Leheurteur, F. Gachon, E. Planchat, C. Abrial, M.A. Mouret-Reynier, X. Durando, C. Barthomeuf and P. Chollet, *Cancer Biol. Ther.*, 2010, **9**, 8.
86. S. Vadhan-Raj, D. Weber, M. Wang, S. Giralt, R. Alexanian, S. Thomas, X. Zhou, P. Patel, C. Bueso-Ramos, R. Newman and B. Aggarwal, *Blood*, 2007, **110**, 357a.
87. A. Shehzad, F. Wahid and Y.S. Lee, *Arch. Pharm.*, 2010, **343**, 489.
88. G. Liang, *Curr. Pharm. Des.*, 2013, **19**, 1965.
89. Y. Gao, Z. Li, M. Sun, C. Guo, A. Yu, Y. Xi, J. Cui, H. Lou and G. Zhai, *Drug Deliv.*, 2011, **18**, 131.
90. N.R. Goud, K. Suresh, P. Sanphui and A. Nangia, *Int. J. Pharm.*, 2012, **439**, 63.
91. P. Anand, A.B. Kunnumakkara, R.A. Newman and B.B. Aggarwal, *Mol. Pharm.*, 2007, **4**, 807.
92. P. Basnet and N. Skalko-Basnet, *Molecules*, 2011, **16**, 4567.
93. P. Sanphui, N.R. Goud, U.B.R. Khandavilli and A. Nangia, *Cryst. Growth Des.*, 2011, **11**, 4135.
94. S.K. Vareed, M. Kakarala, M.T. Ruffin, J.A. Crowell, D.P. Normolle, Z. Djuric and D.E. Brenner, *Cancer Epidemiol. Biomarkers Prev.*, 2008, **17**, 1411.

95. C. Ireson, S. Orr, D.J. Jones, R. Verschoyle, C.K. Lim, J.L. Luo, L. Howells, S. Plummer, R. Jukes, M. Williams, W.P. Steward and A. Gescher, *Cancer Res.*, 2001, **61**, 1058.
96. M.H. Pan, T.M. Huang and J.K. Lin, *Drug Metab. Dispos.*, 1999, **27**, 486.
97. R.A. Sharma, S.A. Euden, S.L. Platton, D.N. Cooke, A. Shafayat, H.R. Hewitt, T.H. Marczylo, B. Morgan, D. Hemingway, S.M. Plummer, M. Pirmohamed, A.J. Gescher and W.P. Steward, *Clin. Cancer Res.*, 2004, **10**, 6847.
98. G. Shoba, D. Joy, T. Joseph, M. Majeed, R. Rajendran and P.S.S.R. Srinivas, *Planta Med.*, 1998, **64**, 353.
99. J. Lu and S. Rohani, *J. Pharm. Sci.*, 2010, **99**, 4042.
100. D.D. Lasic and D. Needham, *Chem. Rev.*, 1995, **95**, 2601.
101. T.M. Allen and P.R. Cullis, *Science*, 2004, **303**, 1818.
102. L. Li, F.S. Braiteh and R. Kurzrock, *Cancer*, 2005, **104**, 1322.
103. N. Saengkrit, S. Saesoo, W. Srinuanchai, S. Phunpee and U.R. Ruktanonchai, *Colloids Surf., B*, 2014, **114**, 349.
104. C. Théry, L. Zitvogel and S. Amigorena, *Nat. Rev. Immunol.*, 2002, **2**, 569.
105. D. Sun, X. Zhuang, X. Xiang, Y. Liu, S. Zhang, C. Liu, S. Barnes, W. Grizzle, D. Miller and H.G. Zhang, *Mol. Ther.*, 2010, **18**, 1606.
106. C. Mohanty, S. Acharya, A.K. Mohanty, F. Dilnawaz and S.K. Sahoo, *Nanomedicine*, 2010, **5**, 433.
107. S. Podaralla, R. Averineni, M. Alqahtani and O. Perumal, *Mol. Pharm.*, 2012, **9**, 2778.
108. X. Gao, F. Zheng, G. Guo, X. Liu, R. Fan, Z.-y. Qian, N. Huang and Y.-q. Wei, *J. Mater. Chem. B*, 2013, **1**, 5778.
109. H. Sasaki, Y. Sunagawa, K. Takahashi, A. Imaizumi, H. Fukuda, T. Hashimoto, H. Wada, Y. Katanasaka, H. Kakeya, M. Fujita, K. Hasegawa and T. Morimoto, *Biol. Pharm. Bull.*, 2011, **34**, 660.
110. M. Kanai, Y. Otsuka, K. Otsuka, M. Sato, T. Nishimura, Y. Mori, M. Kawaguchi, E. Hatano, Y. Kodama, S. Matsumoto, Y. Murakami, A. Imaizumi, T. Chiba, J. Nishihira and H. Shibata, *Cancer Chemother. Pharmacol.*, 2013, **71**, 1521.
111. M.G. O'Toole, R.M. Henderson, P.A. Soucy, B.H. Fasciotto, P.J. Hoblitzell, R.S. Keynton, W.D. Ehringer and A.S. Gobin, *Biomacromolecules*, 2012, **13**, 2309.
112. R. Misra and S.K. Sahoo, *Mol. Pharmaceutics*, 2011, **8**, 852.

113. C. Mohanty and S.K. Sahoo, *Biomaterials*, 2010, **31**, 6597.
114. K. Sindhu, A. Rajaram, K.J. Sreeram and R. Rajaram, *RSC Adv.*, 2014, **4**, 1.
115. S. Jambhrunkar, S. Karmakar, A. Popat, M. Yu and C. Yu, *RSC Adv.*, 2014, **4**, 709.
116. T.R. Hoare and D.S. Kohane, *Polymer*, 2008, **49**, 1993.
117. A. Altunbas, S.J. Lee, S.A. Rajasekaran, J.P. Schneider and D.J. Pochan, *Biomaterials*, 2011, **32**, 5906.
118. L.-W. Xia, R. Xie, X.-J. Ju, W. Wang, Q. Chen and L.-Y. Chu, *Nat. Commun.*, 2013, **4**, 3226/1.
119. X. Chen, F. Zhi, X. Jia, X. Zhang, R. Ambardekar, Z. Meng, A.R. Paradkar, Y. Hu and Y. Yang, *J. Pharm. Pharmacol.*, 2013, **65**, 807.
120. S. Svenson, *Eur. J. Pharm. Biopharm.*, 2009, **71**, 445.
121. J.M.J. Fréchet and D.A. Tomalia, *Dendrimers and Other Dendritic Polymers*. Wiley and Sons, Chichester and New York, 2001.
122. W. Shi, S. Dolai, S. Rizk, A. Hussain, H. Tariq, S. Averick, W. L'Amoreaux, A. El Idrissi, P. Banerjee and K. Raja, *Org. Lett.*, 2007, **9**, 5461.
123. M.H.M. Leung and T.W. Kee, *Langmuir*, 2009, **25**, 5773.
124. B. Wang, X. He, Z. Zhang, Y. Zhao and W. Feng, *Acc. Chem. Res.*, 2012, **46**, 761.

Chapter 3

3 Synthesis, Characterization, and *in vitro* Activity of Curcumin-Loaded Folic Acid-Conjugated Magnetic Nanoaggregates

3.1 Introduction

For many years cancer has been, and still remains, one of the most difficult diseases to treat. Despite the sophisticated cancer treatment methods available today compared to when cancer was first discovered, there remain several drawbacks to the available options. With surgery being too invasive in many cases, and chemotherapy presenting many adverse side effects such as vomiting and nausea, hair loss, and liver damage, there has been a drift away from synthetic pharmaceuticals towards the use of natural medicines. One such medicine is curcumin—a natural polyphenol derived from turmeric—which has been shown to inhibit cancer cell survival by inducing apoptosis, and arresting different phases of the cancer cell cycle.¹ Due to curcumin's poor solubility, there is a strong need for a technology that not only enhances the solubility of curcumin, but can also transport it to the site of interest in order to avoid its clearance from the body, and decrease the required dose for treatment.

Of particular interest are magnetic nanoparticles (MNP) due to their small size, biocompatibility, high stability and surface area, and magnetic properties.² Because these nanovehicles can be tailored in terms of size, morphology, and surface chemistry, they have been identified as a promising technology for virus detection,³ the promotion of human fibroblast growth,⁴ and most importantly as contrast agents for diagnosis of cancer using magnetic resonance imaging (MRI).⁵ Their use as contrast agents for cancer diagnosis has also inspired interest in their use as drug delivery systems for the potential treatment of cancer.⁶ Of the available MNP, magnetite (Fe_3O_4) has been found in the teeth of chitons, honey bees, homing pigeons and magnetotactic bacteria and algae, and is generally used as a navigation device.⁷ Therefore, it is interesting to investigate this navigational system in humans. Common synthesis methods of iron oxide nanoparticles include precipitation, thermal decomposition, and hydrothermal/solvothermal synthesis.⁸

In order to enhance the stability of curcumin and increase its bioavailability for cancer treatment it is possible to incorporate it onto magnetite. This can potentially decrease the amount of time it is left in the circulatory system, thereby avoiding first pass clearance by the reticuloendothelial system (RES), and it can also decrease the dose required for treatment. Yallapu and coworkers have explored the potential of curcumin as an anticancer agent,⁹ and have worked on its incorporation into magnetite delivery systems. In 2011, Yallapu *et al.* synthesized β -cyclodextrin/pluronic F127 coated magnetite nanoparticles through the co-precipitation of Fe^{2+} and Fe^{3+} iron salts in the presence of ammonia.¹⁰ This water dispersible system was tested for hyperthermia, MRI, and drug delivery applications, and showed superior activity for all three applications compared to pure iron oxide, and β -cyclodextrin-coated iron oxide. In 2012, the same group synthesized β -cyclodextrin/pluronic F68 coated magnetite nanoparticles using the same co-precipitation method, and the nanoparticles were then loaded with curcumin.¹¹ The drug-loaded nanoparticles had an average aggregate size of 123 nm and showed controlled curcumin release for up to 28 days. Furthermore, the authors reported good cellular uptake and toxicity in MDA-MB-231 breast cancer cells. Curcumin loaded nanoparticles developed by Yallapu *et al.* were also tested *in vitro* in two human pancreatic cell lines, and *in vivo* in mouse models.¹² The nanoparticles inhibited the growth of pancreatic cancer cells, and improved survival of mice by delaying tumour growth. Furthermore, the bioavailability of curcumin in mice increased 2.5-fold when using drug loaded iron oxide nanoparticles, as compared to free curcumin.

Several other researchers have worked to incorporate curcumin into magnetite-based nanovehicles for cancer treatment. For example, Wang *et al.* developed a core-shell drug delivery system consisting of a commercial amine modified iron oxide core covalently bound to a poly(ethylene oxide)-poly(propylene oxide)-poly(ethylene oxide) block copolymer shell.¹³ These nanoparticles were reported to have a diameter of 113 nm as measured by DLS, and magnetite cores of 15 nm as measured by TEM. *In vitro* release studies showed 70% curcumin release over a period of 4 hours, which may need to be optimized for biomedical applications. Devkota *et al.* reported the development of a curcumin-loaded alginate/magnetite nanoconjugate for inductive heating and detection, which can be employed in hyperthermia, biodetection, and drug delivery applications.¹⁴ Nanoparticles were synthesized using the traditional co-precipitation method, and were approximately 120 nm as measured by DLS. The authors also

reported a decreased saturation magnetization of the curcumin-loaded nanoconjugates (35 emu/g) as compared to uncoated magnetite (60 emu/g); however, nanoconjugates showed a promising inductive heating capacity and high detection sensitivity, which is beneficial for hyperthermia and detection applications. Paulino *et al.* developed hydrogels from different natural polymeric networks loaded with 50 nm magnetite particles for controlled curcumin release.¹⁵ The authors demonstrated decreased hydrogel swelling in the presence of magnetite nanoparticles, in addition to magnetic field-induced curcumin release when the magnetite is stimulated using a magnetic field.

With the promising results obtained by other researchers on the anti-cancer potential of curcumin-containing magnetite nanoparticles, we propose for the first time to the best of our knowledge a dual targeting curcumin delivery system for cancer treatment (Figure 3.1). Magnetite nanoaggregates, synthesized through the precipitation of a single iron salt, are coated with an amino functionalized poly(propylene glycol) (PPG-NH₂), which is used to couple folic acid at its carboxylic acid. Magnetite nanoaggregates were also simultaneously coated with β -cyclodextrin (β -CD) for curcumin encapsulation. Poly(propylene glycols) have been demonstrated to form complexes with β -CD, where the poly(propylene glycol) is weaved through the β -CD cavity.^{16, 17} The magnetic properties of the iron oxide core can allow the nanovehicle to be guided to the target site, while the folic acid acts as a ligand to selectively target the folate receptor, which is overexpressed on the cell surface of some cancer cells.^{18, 19} This dual targeting system will allow for the destruction of cancerous cells meanwhile rendering the surrounding healthy tissue unharmed.

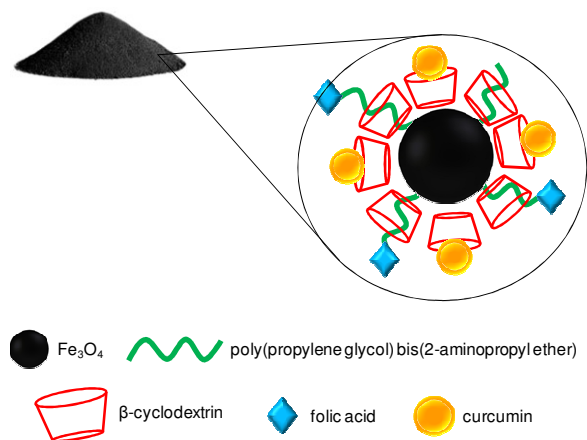


Figure 3.1: Schematic of a folic acid-conjugated curcumin-loaded magnetic nanoparticle

3.2 Materials

The iron precursor ferrous sulphate heptahydrate ($\text{FeSO}_4 \cdot 7\text{H}_2\text{O}$) was purchased from VWR International. β -cyclodextrin (β -CD) (MW: 1135 g/mol) was purchased from Sigma-Aldrich along with poly(propylene glycol) bis(2-aminopropyl ether) (PPG-NH₂) (MW: 2000 g/mol), curcumin (MW: 368 g/mol), and *N, N*-diisopropylethylamine (DIPEA) (MW: 129.25 g/mol). Folic acid (FA) (441 g/mol) and fluorescein isothiocyanate (FITC) (389 g/mol) were purchased from Alfa Aesar. 1-Ethyl-3-(3-dimethylaminopropyl) carbodiimide (EDC) (MW: 155.24 g/mol) was purchased from Advanced ChemTech, and ammonium hydroxide (NH₄OH) and dimethylsulfoxide (DMSO) were obtained from VWR.

For the cell studies, MDA-MB-231 cells were obtained from American Type Culture Collection (Manassas, VA) and maintained in DMEM/F12 + 10% fetal bovine serum (FBS). MDA-MB-468 cells were obtained from Dr. Janet Price (MD Anderson Cancer Center, Houston, TX) and maintained in α MEM + 10% FBS. All growth media and supplements were obtained from Invitrogen (Carlsbad, CA). FBS was obtained from Sigma-Aldrich (St. Louis, MO). All plastics were from Nunc™ (Thermo Fisher Scientific, Ottawa, ON). All cells were incubated at 37°C under a 5% CO₂ atmosphere.

3.3 Synthesis Procedures

Figure 3.2 shows the overall synthesis process, and the contents of each sample synthesized is summarized in Table 3.1.

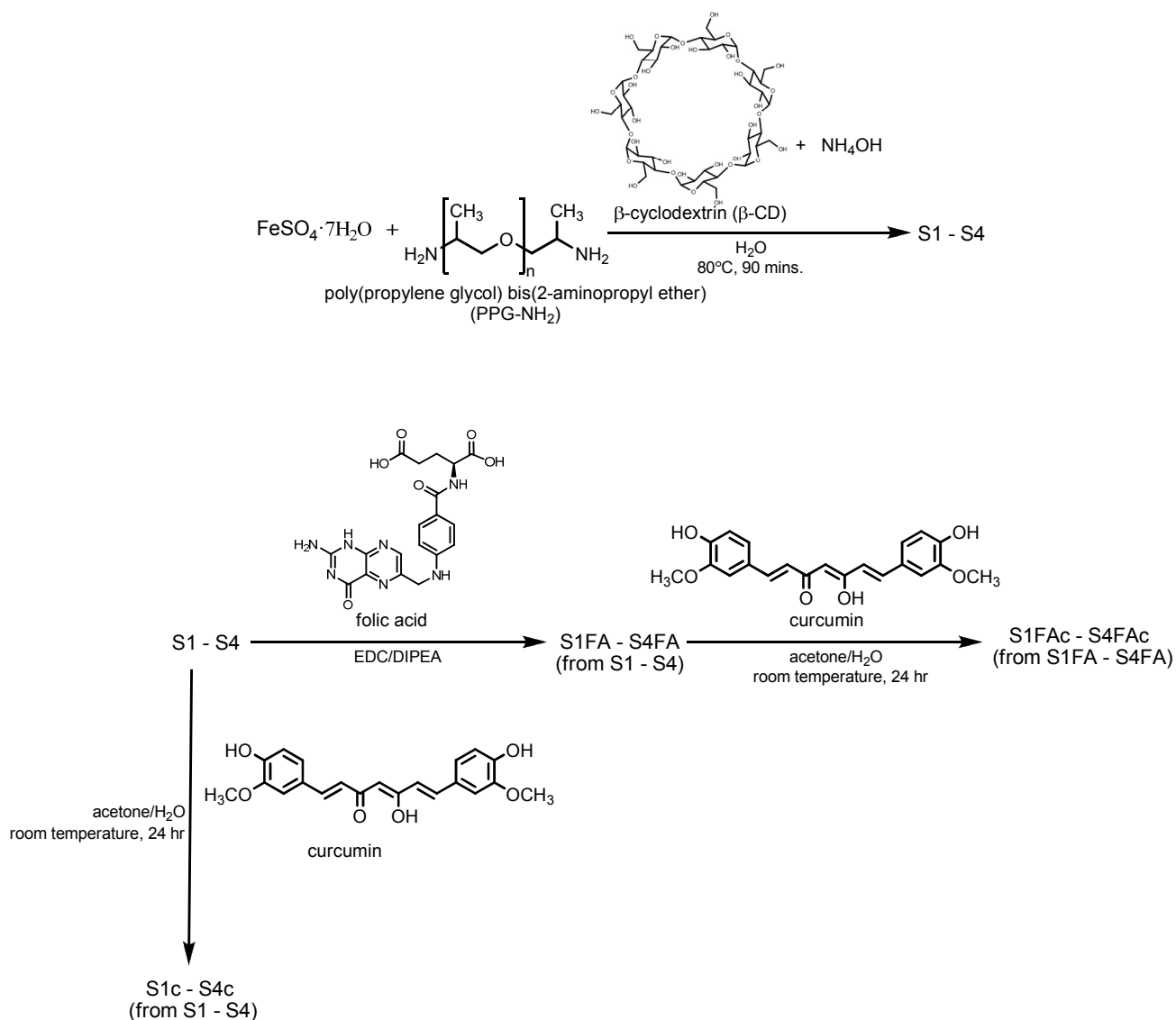


Figure 3.2: Chemical scheme of synthesis process

Table 3.1: Polymer compositions, and folic acid and curcumin content of synthesized samples

Sample	mmol PPG-NH ₂ : mmol β-CD (FeSO ₄ ·7H ₂ O is constant at 5 mmol)	Folic Acid	Curcumin
S1	0.25 : 1.0	-	-
S2	0.50 : 1.0	-	-
S3	1.0 : 0.50	-	-
S4	1.0 : 1.0	-	-
S1c	0.25 : 1.0	-	+
S2c	0.50 : 1.0	-	+
S3c	1.0 : 0.50	-	+
S4c	1.0 : 1.0	-	+
S1FA	0.25 : 1.0	+	-
S2FA	0.50 : 1.0	+	-
S3FA	1.0 : 0.50	+	-
S4FA	1.0 : 1.0	+	-
S1FAc	0.25 : 1.0	+	+
S2FAc	0.50 : 1.0	+	+
S3FAc	1.0 : 0.50	+	+
S4FAc	1.0 : 1.0	+	+

3.3.1 Preparation of PPG-NH₂/β-CD Coated Nanoaggregates Sample S4 and Representative Procedure for the Preparation of Samples S1 – S3

Magnetic nanoaggregates were synthesized based on a modified method reported by Ragab *et al.*²⁰ 1.40g (5 mmol) of the iron precursor FeSO₄·7H₂O were dissolved in 50 mL distilled water, and 2 mL (1 mmol) of PPG-NH₂ was added to the dissolved precursor under stirring (400 rpm) and left until a colour change was noticed (green to orange/yellow). 1.20 g (1 mmol) of β-CD dissolved in 20 mL of ammonium hydroxide (NH₄OH) was gradually added to this mixture, at which point stirring was immediately increased to 1200 rpm and the temperature was increased to 80°C. The mixture was covered and left for 90 minutes under stirring. The prepared sample (S4) was separated from the supernatant using a magnet and the supernatant was removed using a pipette. The particles were then redispersed in distilled water. The sample was then recollected

using the magnet and the distilled water was removed before the sample was redispersed in ethanol. The sample was washed 3 times in ethanol using this procedure, and then dried at 60°C. Samples S1 – S3 were prepared in the same manner, but the absolute amounts of PPG-NH₂ and β-CD were reduced according to Table 3.1.

3.3.2 Functionalization of PPG-NH₂/β-CD-Coated Nanoaggregates Samples with Folic Acid

Samples S1 – S4 were functionalized with folic acid using the following method. 20 mg (46 μmol) of folic acid were dissolved in 10 mL of DMSO containing 20 μL (92 μmol) of DIPEA in a nitrogen atmosphere. This solution was added to 20 mg of dry polymer-coated nanoaggregates (S1 – S4), after which 10 mL of DMSO containing 7 mg (46 μmol) of EDC was added under nitrogen. The samples were left shaking in a water bath for 2 days, initially at room temperature for the first 3 hours, after which the temperature was increased to 35°C. After removal of the samples from the water bath, the aggregates were left on a magnetic plate to settle completely before the folic acid content in the supernatant was analyzed using UV-visible spectroscopy to quantify the amount of folic acid attached. The folic acid functionalized nanoaggregates (S1FA – S4FA) were then separated using a magnet, the supernatant was removed, and the samples were redispersed in ethanol for washing. The samples were recollected with a magnet, the ethanol supernatant removed, and the samples were dispersed again in ethanol. This washing procedure was carried out 3 times, and the samples were dried at 50°C.

3.3.3 β-CD/curcumin Complex Synthesis and Curcumin Loading of Nanoaggregates

β-CD/curcumin complex was synthesized by adding a solution containing 36 mg () of curcumin in 1.5 mL of acetone to a solution of 120 mg () of β-CD in 24 mL distilled water under stirring (400 rpm). The mixture was left for 24 hours before the supernatant was collected by centrifugation and freeze dried for 24 hours to obtain a dry β-CD/curcumin complex solid. The synthesized complex, along with β-CD, and curcumin were analyzed using proton nuclear magnetic resonance (¹H NMR).

Nanoaggregate samples were loaded with curcumin via a modified method reported by Yallapu *et al.* to produce curcumin loaded samples.¹¹ 10 mg of nanoaggregates were dispersed in 2.8 mL

of distilled water under stirring at 400 rpm. Curcumin (1.0, 1.5, 2.0, 3.0, or 5.0 mg) was dissolved in 200 μ L of acetone and added dropwise to the nanoaggregate suspension. The mixture was stirred for 24 hours at room temperature. The resulting curcumin-loaded nanoaggregates (S1c – S4c and S1FAC – S4FAC) were thoroughly washed with distilled water by magnetically collecting the samples, removing the supernatant, and re-adding distilled water. The washing process was carried out 6 times. Samples were then freeze dried to obtain dry nanoaggregates. To determine the loading efficiency, 5.0 mg of curcumin loaded nanoaggregates were suspended in 10 mL of ethanol. The samples were left shaking in a water bath at 25 °C for 24 hours, after which samples were removed from the water bath and placed on a magnetic plate to allow the nanoaggregates to settle. The supernatant was collected using a pipette and the curcumin content was measured using UV-visible spectroscopy at 427 nm.

3.3.4 Preparation of FITC-labeled Particles

1.0 mg FITC were dissolved in 3 mL acetone/water (0.3/2.7 v/v) mixture and added to a dispersion of magnetic nanoaggregates (10 mg) in 10 mL of PBS. The reaction was left stirring at 1000 rpm in the dark for 24 hours at room temperature. The resulting FITC-labeled samples were washed with PBS and stored at 4°C. Similar fluorescence of FITC-labeled samples was obtained, as measured by a Photon Technology International (PTI) fluorometer. 1 mg of FITC-labeled nanoaggregates was suspended in 1 mL of PBS and measured at an emission range of 450 – 650 nm, an excitation wavelength of 494 nm, a length of 200 nm, step size of 0.5 nm, and integration of 0.1 seconds.

3.4 Characterization of Synthesized Nanoaggregates

3.4.1 Particle Morphology

The general morphology of the synthesized nanoaggregates was examined using a Philips CM 10 transmission electron microscope operating at 80 kV. Samples were prepared on Formvar carbon-coated-100-mesh copper grids. One drop of a 0.50 mg/mL nanoaggregate suspension was used to cover the grid surface. Excess water was removed using fine filter paper, and the grid was left for approximately 30 minutes to dry in air prior to examination.

3.4.2 Particle Size Analysis

The mean diameter of the individual particles and the polydispersity indices were determined using a Malvern Instruments Ltd. Zetasizer 3000 HS_A particle sizer. The size analysis was performed at a scattering angle of 90° and room temperature. Nanoparticle suspensions (1.0 mg/mL) were prepared and diluted by a factor of 45 to obtain homogeneous suspensions of nanoparticles. Three runs were carried out per sample in order to obtain a standard deviation.

The aggregate size was determined using a Malvern Instruments Ltd. Zetasizer Nano ZS. Samples were prepared at concentrations of 0.50 mg/mL and analyzed at a measurement angle of 173° at room temperature. Samples were run three times each in order to obtain a standard deviation value.

3.4.3 X-ray Diffraction (XRD) Analysis

The crystal structures of the samples were analyzed using a Rigaku-Miniflex X-ray diffractometer (The Woodlands, TX). The samples were exposed to radiation (CuK α (30 kV, 15 mA)) at a wavelength of 1.54 Å, and scanned over a 2 θ range of 5 - 90° with a step size of 0.05°.

3.4.4 Fourier Transform Infrared (FTIR) Spectroscopy

A Bruker-Tensor 27 (Germany) spectrophotometer was used to obtain the FTIR spectra of the samples in the solid state. Samples were mixed with potassium bromide in a 1.0:10 w/w ratio and pressed into a disc prior to examination. Samples were scanned between 4000 – 600 cm⁻¹ at a scanning speed of 4 cm⁻¹.

3.4.5 Vibrating Sample Magnetometer (VSM) Measurements

A model 74035 VSM was used to explore the magnetic properties of the samples. Approximately 15 mg of sample were added in the sample holder, after which the samples were exposed to a magnetic field at a field range of ± 10000 G.

3.5 *In vitro* Studies Experimental Procedures

3.5.1 Curcumin Release

In vitro curcumin release was carried out at 37°C in a water bath under constant shaking. Briefly, 1.0 mg of curcumin-loaded nanoaggregates was dispersed in 10 mL of PBS containing 0.10% Tween 80. At predetermined intervals, the supernatant was collected and fresh buffer/Tween solution was replaced in the sample vials. The collected supernatant was measured using UV-visible spectroscopy at 427 nm.

3.5.2 *In vitro* Cytotoxicity Assays

MDA-MB-231 and MDA-MB-468 cells were plated in 100 µL of culture medium at a density of 2.5×10^4 cells/well in 96-well plates. After 24 hours, various treatments (sample S2, sample S2c, sample S2FA, sample S2FAc [up to 2000 µg/mL of particles], or free curcumin [up to 260 µg/mL] (Sigma-Aldrich, St. Louis MO)) were added to the cells and incubated for 48 hours. Cell viability was determined using the Alamar Blue Assay (Life Technologies, Inc., Burlington, ON).

3.5.3 Flow Cytometry Analysis

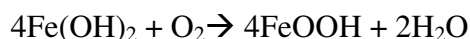
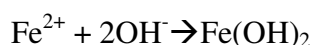
For assessment of folate receptor expression, human breast cancer cells were harvested and stained with a mouse anti-human folate receptor antibody (LK26, AbcamInc, Cambridge MA) for 30 min at 4 °C. After removal of excess antibody by PBS washing, cells were incubated with AlexaFluor488-conjugated goat anti-mouse IgG (Life Technologies) for another 30 min at 4 °C, washed with PBS, and analyzed by flow cytometry using a Beckman Coulter EPICS XL-MCL flow cytometer.

For assessment of nanoparticle uptake, human breast cancer cells were seeded into 60mm culture dishes and grown until 80% confluent. FITC-labeled sample S2or S2FA (2000 µg/mL) were added to the cells. After 4 hours incubation at 37 °C, particles that were not internalized were washed away using PBS and cells were harvested. Extracellular FITC was quenched by incubating with 200 µg/mL Trypan Blue (Sigma-Aldrich) for 10 min at room temperature. Cells were washed using PBS and analyzed by flow cytometry.

3.6 Results and Discussion

3.6.1 Nanoaggregate Synthesis

Magnetic nanoaggregate samples were synthesized using a precipitation method involving one iron salt, as compared to the traditional co-precipitation method where Fe^{2+} and Fe^{3+} salts must be used with the iron cations having a precise 1:2 molar ratio. The traditional method involves the need for strict oxidation control in order to avoid the formation of $\gamma\text{-Fe}_2\text{O}_3$ instead of Fe_3O_4 , which requires a complicated experimental setup in order to run the reaction under a nitrogen atmosphere. Therefore, the method employed here is advantageous due to its simplicity and is carried out based on the following reactions:



Nanoaggregates were synthesized by the addition of $\beta\text{-CD}$ to a mixture of ferrous sulphate and PPG-NH₂ under alkaline conditions (Figure 3.2), as a high pH promotes small particle formation,²¹ which is desirable for biomedical applications. Another factor that was employed to control the particle size was the addition of PPG-NH₂, as this polymer can act as a stabilizer by adsorbing on the crystal structure surface.²¹ The resulting reduction in surface tension causes a reduction in the Gibbs free energy and consequently an increase in nucleation rate, resulting in smaller particle size. In solution, the metal component of the precursor forms *seeds* which allow the growth of metal ions or metal-stabilizer complexes (*monomers*) on the surface, forming crystals.^{21, 22} Therefore, with fast nucleation more seeds are present to consume *monomers* on their surfaces, yielding smaller particles (Figure 3.3). However, under conditions of slow nucleation, few *seeds* are produced, which consume a larger amount of the produced *monomers* on their surface.

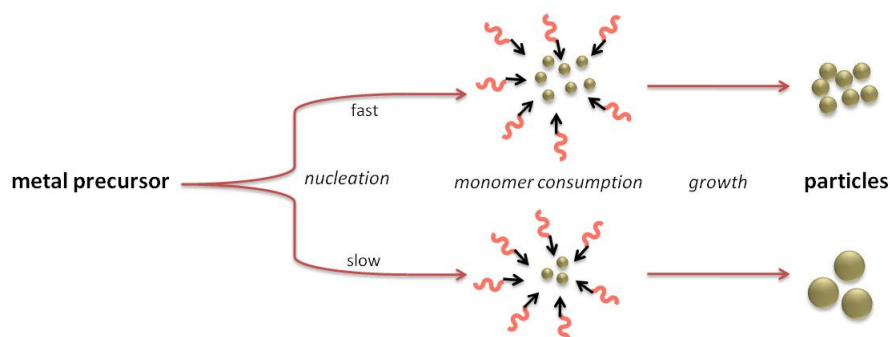


Figure 3.3: Nucleation and growth schematic

Figure 3.2 briefly outlines the synthesis process. PPG-NH₂ and β -CD were added in different amounts as shown in Table 3 to obtain samples with varying PPG-NH₂/ β -CD ratios (S1 – S4), which were then used to produce folic acid functionalized samples (S1FA – S4FA). Samples with and without folic acid were then loaded with curcumin to obtain both folate positive, and folate negative drug loaded samples for future experiments (Table 3.1).

3.6.2 Nanoaggregate Characterization

The size of drug delivery vehicles is one of the most important parameters to be considered for biomedical applications. Particle size analysis was carried out to determine the size of both the individual particles, as well as the aggregates formed (Table 3.2). Generally, there was a slight decrease in the average individual particle size when the amount of PPG-NH₂ in the system was higher than the amount of β -CD, as demonstrated by the results for samples S1, S2, S3, and S4. This may be attributed to the interference of the polymer with the growth of the crystals upon adsorption on the crystal surfaces.^{21, 23} The desired size range of individual nanoparticles was 10 – 20 nm. The sizes of the individual particles were measured by DLS following sonication for 5 seconds followed by dispersion using a vortex and then immediate dilutions until a clear light yellow, homogeneous solution was obtained. Sample diameters were in the expected size range. Aggregates were also measured by DLS following dispersion using a vortex and allowing the sample to reach an equilibrium aggregation state. Aggregates grow to decrease surface energy, and aggregation is generally dependant on particle-particle interactions.²¹ In general, samples formed smaller aggregates with increasing ratio of PPG-NH₂: β -CD suggesting that PPG-NH₂ helps stabilize the particles, thereby decreasing particle-particle interactions. However, S2 did

not follow this trend completely. The specific ratio of PPG-NH₂ to β -CD present in S2 may be ideal for decreasing particle-particle interactions which may explain why the aggregate size is less than the other samples.

Table 3.2: Individual particle size and aggregate size of synthesized samples

Sample	S1	S2	S3	S4
Aggregate Diameter (nm)	1000 \pm 75	223 \pm 10	443 \pm 9	355 \pm 5
Polydispersity index	0.35 \pm 0.09	0.30 \pm 0.06	0.31 \pm 0.06	0.43 \pm 0.02
Individual Particle Diameter (nm)	13 \pm 5.6	10 \pm 6	9.1 \pm 3.4	11 \pm 6.5
Polydispersity index	0.20 \pm 0.1	0.24 \pm 0.07	0.28 \pm 0.07	0.27 \pm 0.1

Samples were chosen for transmission electron microscopy (TEM) analysis in order to study the morphologies of the nanoaggregates. Uncoated nanoaggregates and sample S2 were chosen as representative samples for comparison (Figure 3.4). Images confirmed that the nanoparticles have spherical, uniform morphologies that form aggregates. However, this aggregation is reversible, meaning that certain techniques can be employed to obtain individual nanoparticles. One such technique is the use of surfactants or surface coatings at specific pH values to create a surface charge on the iron oxide nanoparticles.^{21, 24} Such surface charges can create repulsive forces, promoting deaggregation. This is demonstrated on iron oxide nanoparticles upon polymer coating, when compared to uncoated samples (Figure 3.4).

In other work, Stuyven *et al.* showed that deaggregation of Ludox[®] silica sol samples in a KNO₃ solution depended on the presence of a magnetic field (0.31 T), and the type of flow.²⁵ The authors showed that in the presence of a magnetic field, under turbulent flow conditions, particle size decreased (deaggregation) and a narrow size distribution was established. However, under laminar flow conditions (such as that seen in blood flow) aggregation was the dominant condition even with the presence of a magnetic field. This was attributed to the movement of charged particles to the channel wall where velocity is low. Based on this study, it would be interesting to employ a similar experiment on the current iron oxide samples—as they show

better magnetic properties than silica—by increasing the magnetic field gradually under laminar flow conditions and recording the aggregation behaviour.

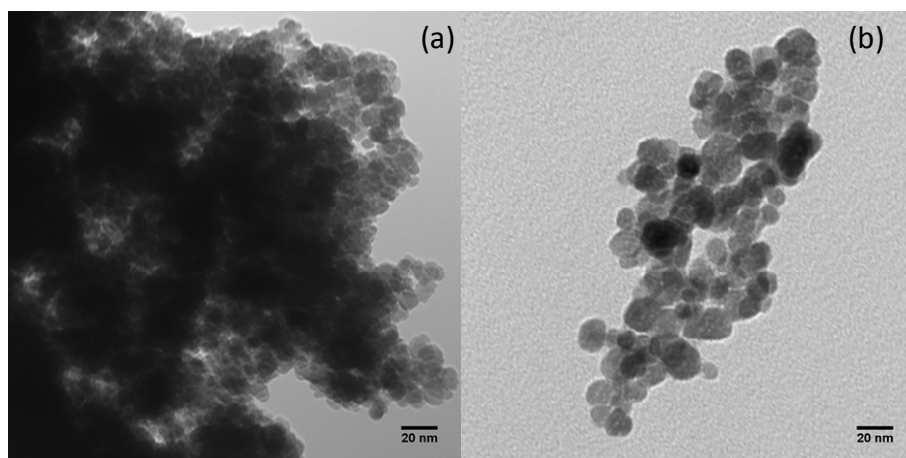


Figure 3.4: TEM images of A) uncoated nanoaggregates, and B) sample S2

For biomedical applications, it is not only important to optimize the surface properties of the delivery system, but also the amount of drug loaded. In order to maximize the amount of curcumin in the system, it is beneficial to have more β -CD than PPG-NH₂ in the nanoparticle system. For this reason, samples S1 and S2, along with their folic acid conjugated counterparts (S1FA and S2FA), were chosen for future experiments. Also, samples S2 and S2FA were chosen as representative samples for the remainder of the characterization studies used.

X-ray diffractometry (XRD) was used to analyze the crystallinity of the iron oxide samples. XRD was carried out on uncoated nanoaggregates, and samples S2 and S2FA to ensure that the samples produced are in fact magnetite, and that their crystal structure remained unchanged after polymer coating, and folic acid functionalization. The five characteristic peaks noted for each sample are at 2θ angles of approximately 30° , 35° , 43° , 57° , and 62° (Figure 3.5a) with the same relative intensities, indicating a retained crystal structure of nanoparticles as peak shifting was not observed. Furthermore, the peak positions along with the relative peak intensities of each sample were compared with the standard XRD pattern for magnetite corresponding to ICCD card number 00-019-0629 obtained using the PDF-4+ software (Figure 3.5b). The full standard magnetite XRD pattern corresponding to ICCD card number 00-019-0629 is presented in Appendix 1. It was verified that the synthesized nanoparticles are magnetite based on the peak

position and intensities of the standard XRD pattern, which matched those obtained by the synthesized samples. Magnetite has the chemical formula Fe_3O_4 where the iron component consists of both Fe^{II} and Fe^{III} . Magnetite has an inverse spinel structure where the Fe^{II} ions are all in octahedral sites and the Fe^{III} ions occupy both tetrahedral and octahedral sites.²⁶ In addition, the oxygen atoms have a face centred cubic close packed alignment along [111].

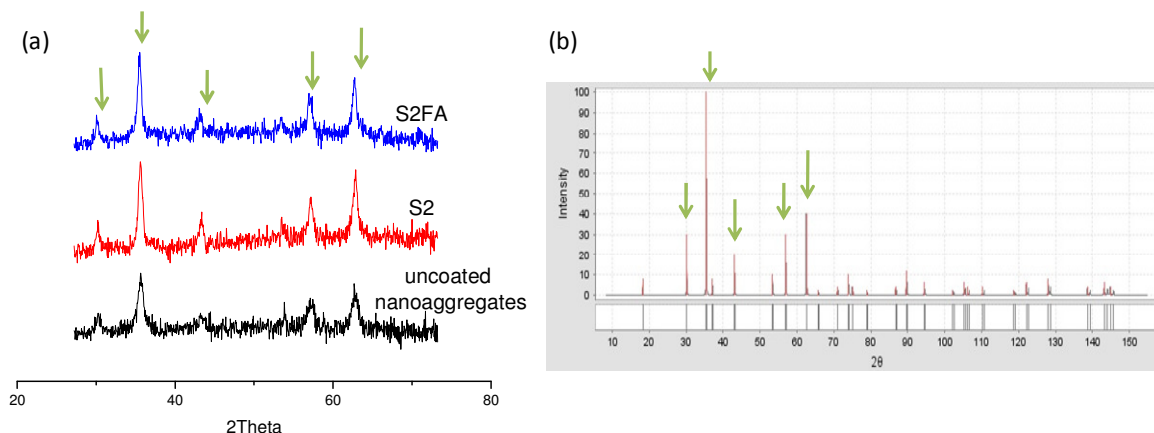


Figure 3.5: a) XRD spectra of synthesized samples, and b) standard XRD pattern of magnetite (See Appendix 1).

The magnetic properties of uncoated nanoaggregates, and sample S2 were studied to determine how the magnetic properties of Fe_3O_4 are affected by the presence of surface coatings (Figure 3.6a). Magnetite is ferrimagnetic at room temperature due to the presence of at least two sublattices composed of the two different cationic sites in the structure (tetrahedral site of Fe^{3+} and octahedral site of both Fe^{3+} and Fe^{2+}).²⁷ However, magnetite shows super-paramagnetic behaviour as the size of the particles decreases ($\sim \leq 20$ nm),^{27, 28} and as a result of the easy magnetization along the crystallographic axis [111] present in the structure.²⁶ This is evident by the low coercivity of each sample (Figure 3.6b) which is characteristic of super-paramagnetic materials. Surface modification of the nanoparticles decreased the saturation magnetization (M_s) and the corresponding magnetic properties, but not significantly, which is beneficial for the desired application.

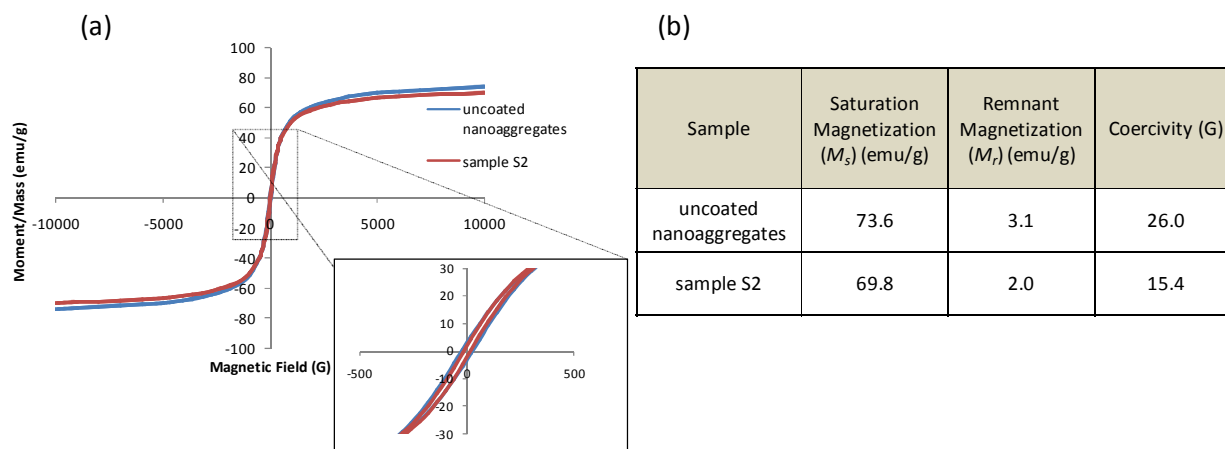


Figure 3.6: a) Magnetization curves of uncoated nanoaggregates and sample S2 and b) their corresponding magnetic properties.

Because nuclear magnetic resonance (NMR) could not be used to verify the presence of certain functional groups due to the magnetic properties of the aggregates, FTIR spectra of uncoated nanoaggregates, β -CD, PPG-NH₂, and samples S2 and S2FA were obtained in order to ensure the successful synthesis of nanoparticles, and coupling of folic acid on the amino terminus of the PPG-NH₂. FTIR spectra are presented in Figure 3.7, and the major peaks at wavenumbers higher than 1500 cm⁻¹ are indicated. A peak is observed on uncoated magnetite nanoaggregates at approximately 3450 cm⁻¹ due to O-H stretching vibrations (Figure 3.7a), in addition to the peak present at 1630 cm⁻¹ corresponding to H-O-H stretching vibrations of residual water in the sample.²⁹ As shown in Figure 3.7b for β -CD, the broad stretch between 3000 cm⁻¹ and 3500 cm⁻¹ corresponds to the presence of O-H groups of β -CD and the peak at 1630 cm⁻¹ is characteristic of H-O-H stretching vibrations.³⁰ β -CD also has a characteristic peak at 2900 cm⁻¹ caused by C-H stretching vibrations of CH₂. The infrared spectrum of PPG-NH₂ (Figure 3.7c) contains a strong peak between 2800 cm⁻¹ and 3000 cm⁻¹ corresponding to C-H stretching. For S2, as shown in Figure 3.7e, a combination of these peaks corresponding to the magnetite, β -CD, and PPG-NH₂ were observed. Sample S2FA (Figure 3.7f) also includes these characteristic peaks, however the C-H stretch intensity between 2800 cm⁻¹ and 3000 cm⁻¹ is decreased and the peak in the region of 3000 – 3500 cm⁻¹ is broadened, suggesting the possible presence of an N-H stretch from the amide bond that is formed upon conjugation. Two peaks were also observed in the region of

1600 – 1650 cm^{-1} , suggesting the presence of a C=O stretch from the amide bond, adjacent to the H-O-H stretch.

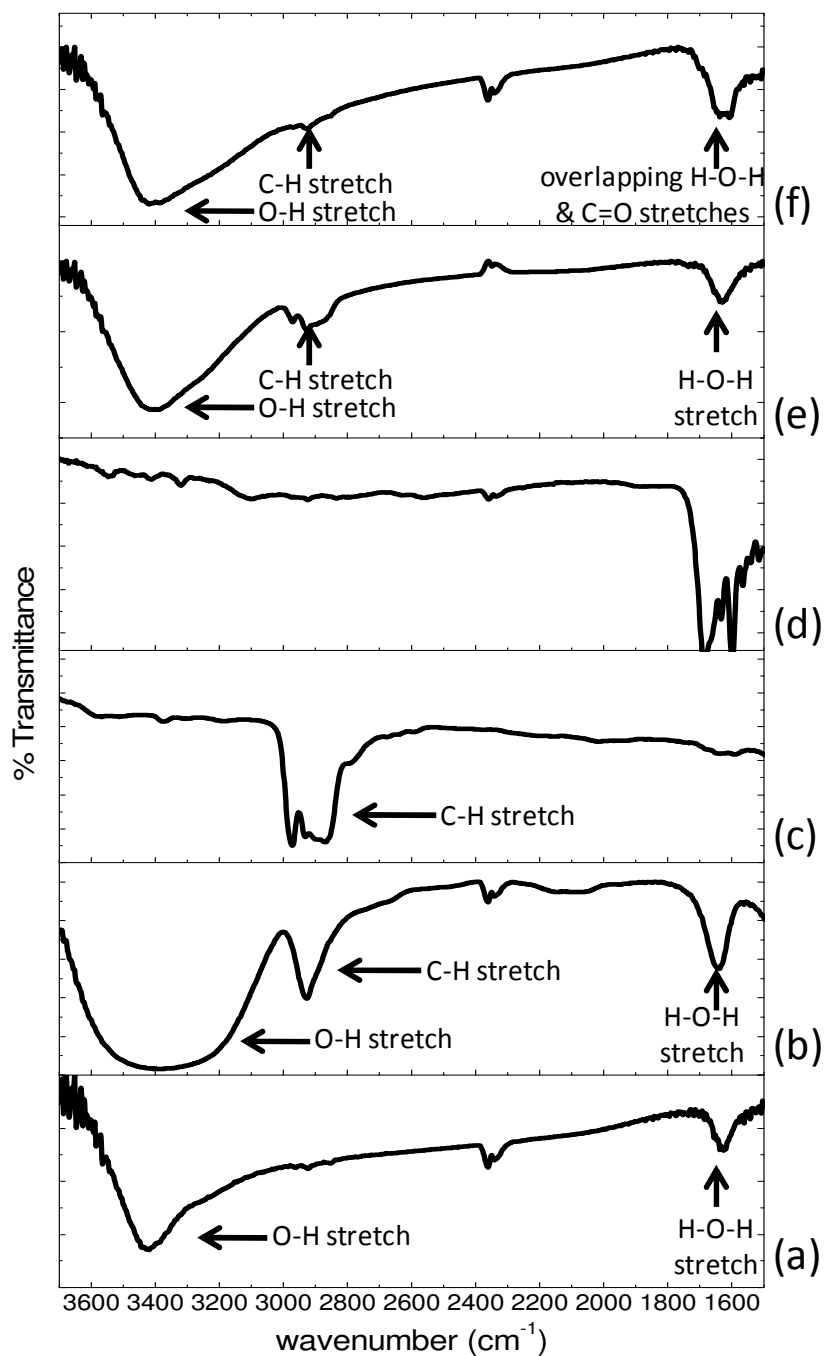


Figure 3.7: FTIR spectra of (a) uncoated nanoaggregates, (b) β -CD, (c) PPG-NH₂, (d) folic acid, (e) sample S2, and (f) sample S2FA

The amount of folic acid attached was quantified to further ensure its presence on nanostructures. The amount of folic acid to nanoaggregates was selected through the modification of a method reported by Sun *et al.*³¹ The presence of folic acid conjugated to the amino terminals was measured to be 27±9% and 23±6% for samples S1FA and S2FA, respectively. This was calculated based on the folic acid content remaining in the supernatant (as measured by UV-visible spectroscopy) following the coupling process using the following equation:

$$\%Conjugation = \frac{W_i - W_s}{W_i} \times 100\% \quad (1)$$

where, w_i is the weight of folic acid used in the coupling reaction, and w_s is the weight of folic acid remaining in the supernatant. Despite S2 having more PPG-NH₂ in the system, the amount of FA conjugated to S1 and S2 were statistically equivalent to one another.

3.6.3 Curcumin Loading and *in vitro* Release

To ensure curcumin's presence within the β -CD cavities, a β -CD/curcumin complex was synthesized and studied using nuclear magnetic resonance (NMR). The characteristic chemical shifts of β -CD and curcumin were first determined (Appendix 2) and then used for comparison with the NMR spectrum of the synthesized complex. An NMR spectrum of the complex was obtained in deuterated water (Appendix 3) and only the chemical shifts of β -CD were observed. However, when an NMR spectrum of the complex was obtained in deuterated acetone (Appendix 4) chemical shifts of both β -CD and curcumin are observed. Because curcumin is soluble in acetone, it acted to extract the curcumin from the β -CD cavities.

In order to optimize the loading of curcumin, curcumin was added in varying amounts to samples S1 and S2 to obtain samples S1c and S2c, and the corresponding encapsulation efficiencies were obtained (Figure 3.8). The resulting trend revealed that the encapsulation efficiencies increased up to 0.3 mg/mg of MNP, then decreased at the highest curcumin amount of 0.5 mg/mg of MNP. Therefore, based on the results shown in Figure 3.8, the optimal amount of curcumin was chosen to be 0.3 mg/mg of MNP. At this loading ratio, encapsulation efficiencies of 73±4% and 86±5% were obtained for S1c and S2c, respectively, corresponding to drug contents of 23±1 % w/w and 26±2 % w/w. Because S1 forms large aggregates as stated previously, the high aggregation may

hinder the ability of curcumin to enter the β -CD cavity. This can explain why sample S2c has higher encapsulation efficiency compared to S1c. When samples containing folic acid (S1FA and S2FA) were loaded at 0.3 mg/mg of MNP to obtain samples S1FAc and S2FAc, considerably lower encapsulation efficiencies of $41\pm 4\%$ and $31\pm 2\%$ were obtained, corresponding to drug contents of $12\pm 1\%$ and $9.0\pm 0.40\%$, respectively. This significant decrease in drug loading is attributed to the presence of folic acid, preventing the diffusion of curcumin into the β -CD cavity.

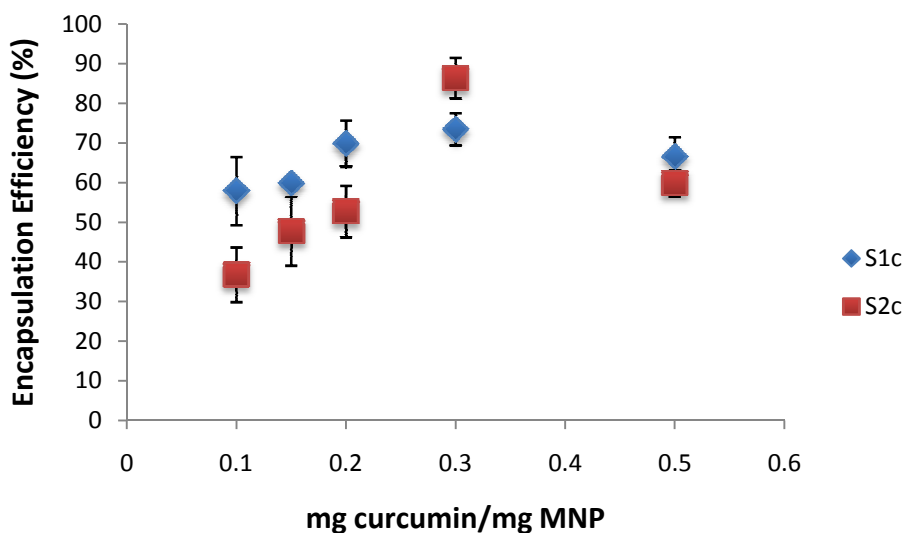


Figure 3.8: Encapsulation efficiency trends for samples S1c and S2c

The *in vitro* curcumin release profiles of samples S1c, S2c, S1FAc, and S2FAc were obtained to study the type of drug release demonstrated by each system (Figure 3.9). Generally, the four samples demonstrated a sustained release profile, but over varying time periods. Comparing S1c and S2c, sample S2c shows more sustained release of curcumin, which might be attributed to the presence of higher amounts of PPG-NH₂. The presence of higher amounts of PPG-NH₂ likely increases the hydrophobic interactions with curcumin which must be disrupted in order for the drug to diffuse. Samples S1c and S1FAc show similar release behaviours, however samples S2c and S2FAc show quite different trends. The time of sustained release decreased from 11 days as demonstrated by sample S2c, to 3 days corresponding to S2FAc. This is likely due to the presence of the bulky folic acid molecules attached to the PPG-NH₂ terminals. Because curcumin is loaded after folic acid conjugation, the presence of PPG-NH₂ in addition to folic acid on the

surface may make it difficult for curcumin to securely enter the β -CD cavity and is left loosely encapsulated or entrapped on the surface. Based on these results, it is possible to optimize the release and sustain it for a longer period of time through the manipulation of the amount of PPG-NH₂, and consequently the amount of folic acid that will be on the surface.

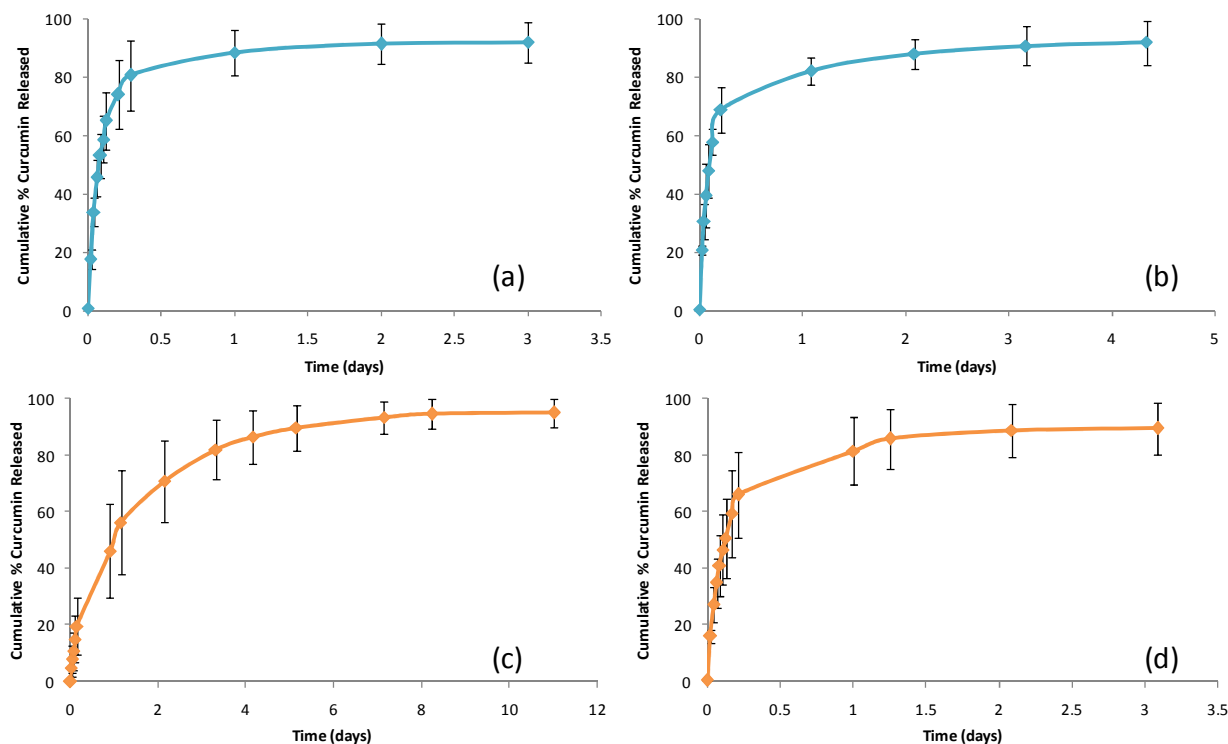


Figure 3.9: In vitro curcumin release profiles for (a) S1c, (b) S1FAC, (c) S2c, and (d) S2FAC

To further analyze the release behaviour of the drug delivery system, it may be beneficial to describe each profile using a mathematical model. The Ritger-Peppas model can be used to describe the profiles obtained for each sample using the empirical equation shown below:

$$\frac{M_t}{M_\infty} = kt^n \quad (2)$$

where M_t/M_∞ is the amount of drug released, k is the kinetic constant, t is the release time, and n is the diffusional exponent. Ritger and Peppas described controlled drug release from delivery

vehicles of different classical geometries, emphasizing the importance of the exponent, n , on the release behaviour.³²⁻³⁴ The authors summarized the results obtained for the values of the diffusional exponent for release from non-swellable systems of different geometries (Table 3.3).

Table 3.3: Diffusional exponent and diffusion mechanism for non-swellable systems of different geometries³⁴

Diffusional exponent, n			Drug Release Mechanism
Thin film	Cylindrical	Spherical	
0.50	0.45	0.43	Fickian diffusion
$0.50 < n < 1.0$	$0.45 < n < 1.0$	$0.43 < n < 1.0$	non-Fickian transport
1.0	1.0	1.0	zero-order release

The values presented in Table 3.3 describe release behaviour with the assumption of one-dimensional diffusion under perfect sink conditions. Also, the data presented by Ritger and Peppas correspond to monodisperse samples. However, with the presence of a particle size distribution, the expected values of n change. As described by Ritger and Peppas, the particle size distribution causes a significant acceleration of diffusion earlier in the release profile and a substantial retardation of release at longer times. Based on the work of Ritger and Peppas, it is possible to determine whether the samples show Fickian or non-Fickian diffusion, however, further release studies must be conducted before a conclusion can be made about whether release is diffusion driven.

3.6.4 *In vitro* Cell Studies

Breast cancer cell lines MDA-MB-231 (231) and MDA-MB-468 (468) were selected as model cancer cells for *in vitro* experiments as they are clinically relevant cell lines which are available in the laboratory. Also, these cell lines have been used in other work involving folate targeting.^{35,36} However, these previous reports suggest contradictory information regarding the expression of the folate receptor by each cell line. For this reason, it was essential to determine

which cell line overexpresses the folate receptor relative to the other using an antibody labeling technique combined with flow cytometry. Figure 3.10 shows that 468 cells exhibit higher expression of the folate receptor relative to 231 cells. Therefore, it was expected that 468 cells would show higher particle uptake in future uptake experiments. Sample S2 and S2c along with their folic acid conjugated counterparts (S2FA, and S2FAc) were selected for *in vitro* experiments due to the relatively small size compared to other samples, and more sustained release compared to sample S1c.

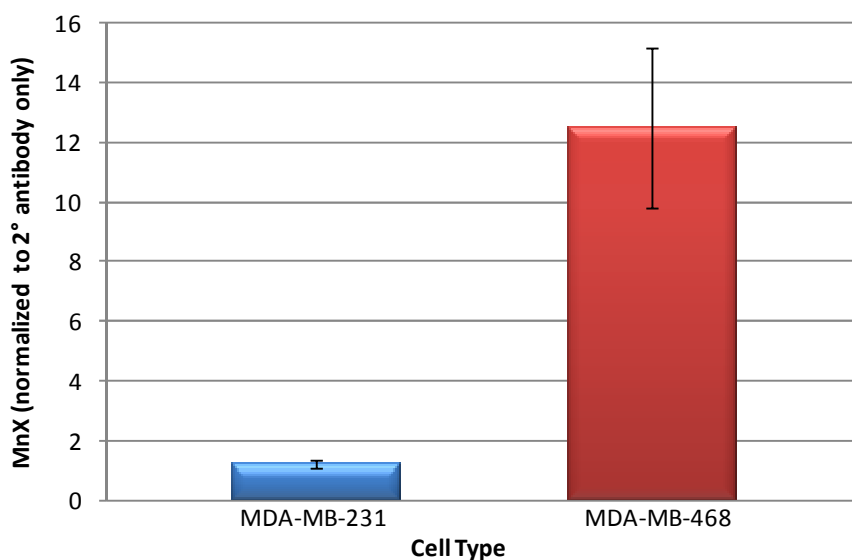


Figure 3.10: Folate receptor expression in MDA-MB-231 and MDA-MB-468 cells

Next, the uptake of FITC-labeled particles into the 231 and 468 cells were investigated. As shown in Figure 3.11, S2FA exhibited 3.2-fold greater uptake into 231 cells than S2. This might be attributed to some folate receptor present on these 231 cells. The 468 cells, exhibited a higher level of MNP uptake in general, but the uptake was 3.9-fold higher for S2FA than S2. Overall, these results are consistent with the relative folate receptor expression on these cell lines but indicate only a modest difference in folic acid mediated uptake between 231 and 468.

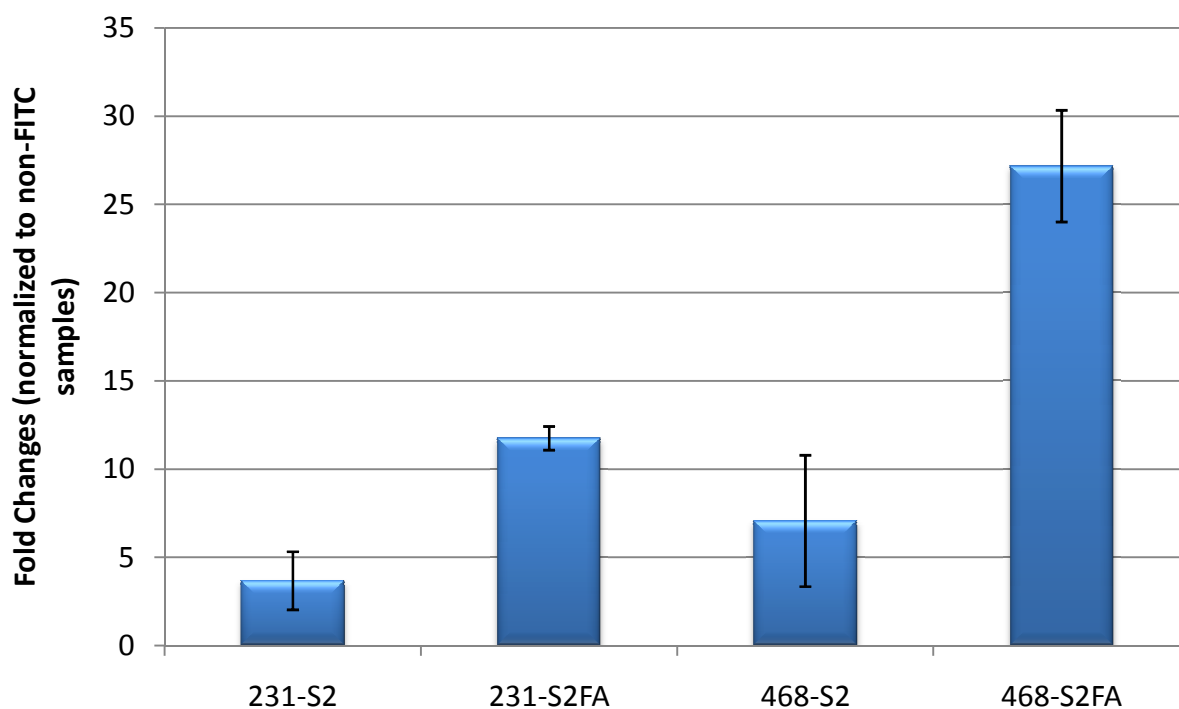


Figure 3.11: Uptake of samples S2 and S2FA by MDA-MB-231 and MDA-MB-468 cells

Before conducting cytotoxicity experiments with curcumin-loaded aggregates, a cell viability assay was performed to determine at what concentrations the “free curcumin” was toxic to the cells. As shown in Figure 3.12, curcumin was non-toxic to both cell lines at concentrations up to approximately 26 $\mu\text{g}/\text{mL}$. Higher concentrations resulted in significant levels of toxicity.

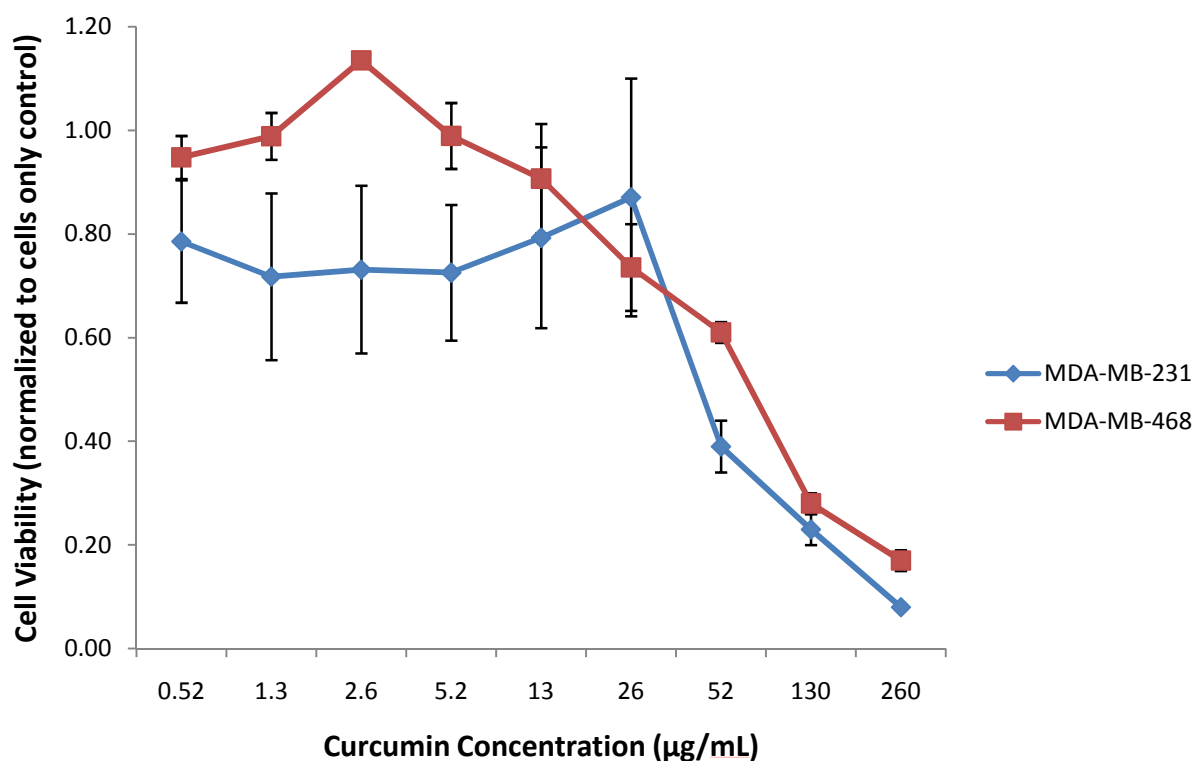


Figure 3.12: Free curcumin dose response curve

Based on these results, 231 and 468 cells were incubated with samples S2c and S2FAC at particle concentrations corresponding to curcumin concentrations in the range of 0.52 – 260 µg/mL. As shown in Figure 3.13, 231 cells treated with S2c were more resistant than 468 cells, which might result from the 231 cells being a highly aggressive breast cancer cell line.³⁷ It may also be related to the lower uptake of MNP into these cells in general. At the highest concentration tested, 231 cells treated with S2FAC showed slightly higher cell death than those treated with S2c but this difference was not statistically significant.

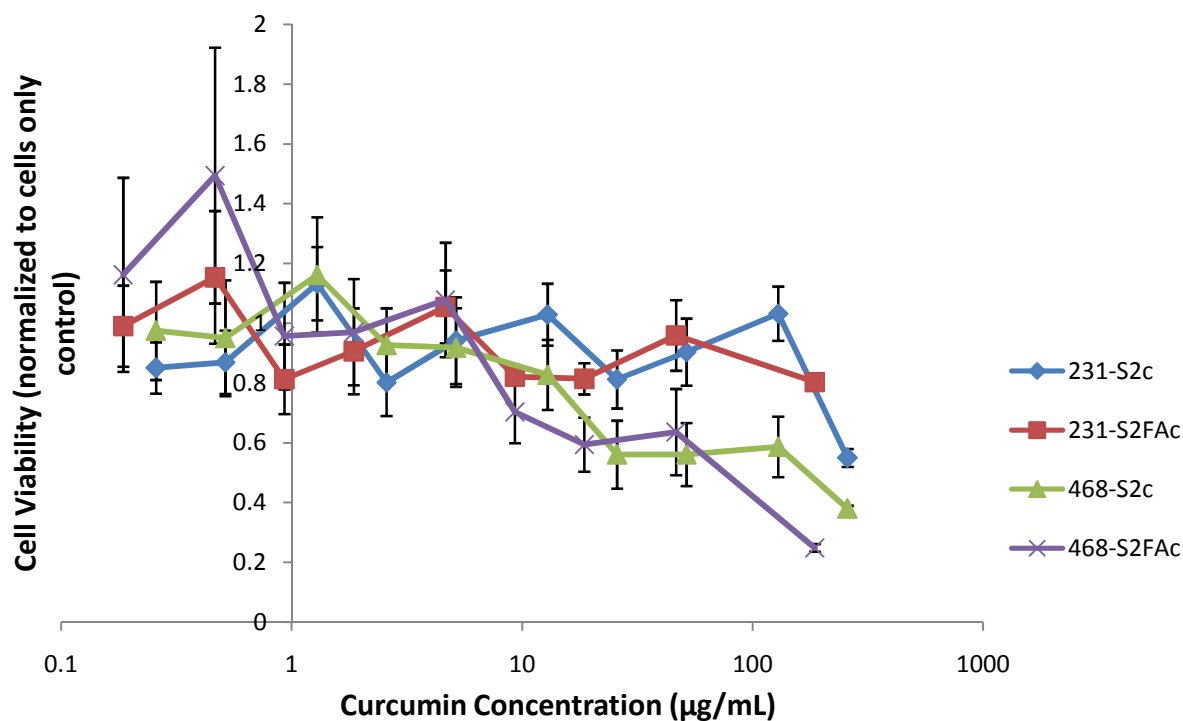


Figure 3.13: Cytotoxicity of curcumin-loaded nanoaggregates on breast cancer cells

In terms of 468 cells, death resulting from treatment with both S2c and S2FAc treated cells was very similar. This can be attributed to the general susceptibility of 468 to treatment, as well as their increased uptake of the MNPs. It was demonstrated earlier that the encapsulation efficiency of curcumin in S2FAc is less than half of that in S2c and as a result there is less drug present in S2FAc. This means that for S2FAc to deliver the equivalent dose of drug as for S2c, more than twice as many particles must be taken up by the cells. This may cancel to some extent the increase in uptake mediated by the folate.

To demonstrate that the toxicity indeed arose from curcumin rather than the MNPs itself, the toxicities of S2 and S2FA were evaluated in both 231 and 468 cells at the highest concentrations used in the above studies. As shown in Figure 3.14, at a concentration of 1000 µg/mL for both S2 and S2FA, 231 cells show no toxicity. In 468 cells, 1000 µg/mL of S2 shows slight cell death attributed to the toxic cationic charge present on the particle surfaces which is taken up by cells, however this cell death is decreased when folic acid is present (S2FA). This can be explained by the masking of this cationic charge by folic acid making the particles less toxic to cells. At a

concentration of 2000 $\mu\text{g/mL}$, more cell death was observed for both 231 and 468 cells when treated with sample S2, but this level of cell death was less than that observed in the above studies with the curcumin-loaded particles, particularly for the FA-conjugated materials.

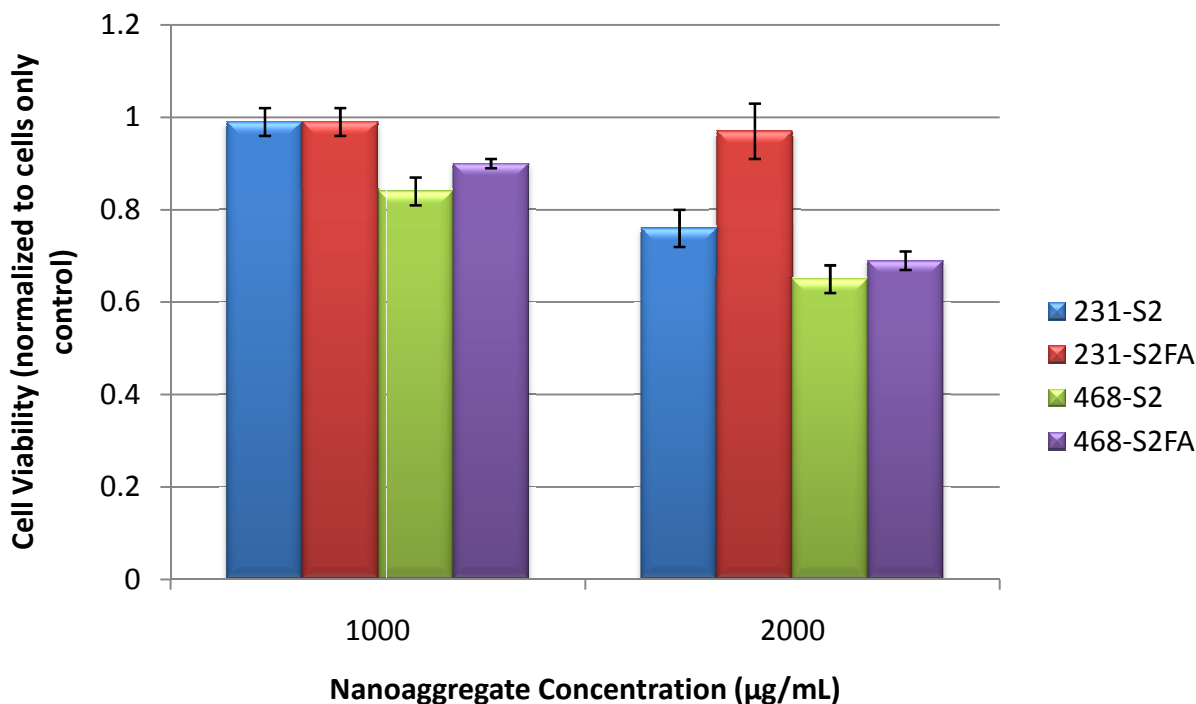


Figure 3.14: Cytotoxicity of samples S2 and S2FA

3.7 Conclusion

This chapter described the synthesis, characterization, and *in vitro* behavior of surface coated magnetite nanoparticles. Magnetic iron oxide nanoparticles were surface coated to incorporate a targeting ligand (folic acid) and a chemotherapeutic agent (curcumin). Nanoparticles were 10 – 20 nm in size as measured by DLS and were noted to form aggregates of a few hundred nanometers to microns. It was demonstrated that this aggregation decreased with increasing amounts of PPG-NH₂, however sample S2 deviated from this trend, showing the smallest aggregate size. FTIR analysis confirmed the presence of folic acid on the nanoparticles surfaces to serve as a targeting ligand for the folate receptor which is overexpressed on cancer cells surfaces. Furthermore, magnetization studies revealed that nanoaggregates retained their magnetic properties even after coating of the iron oxide core, which is required for the desired

application. *In vitro* curcumin release studies carried out on samples S1c and S2c, along with their folic acid-conjugated counterparts (S1FAc and S2FAc, respectively) demonstrated sustained release, over varying time periods. Sample S2c showed the best results in terms of controlled release, lasting for 11 days. However, sample S2FAc showed a higher burst effect than sample S2c suggesting that curcumin may have been only loosely encapsulated in sample S2FAc. Samples S1c and S1FAc showed similar release profiles, both demonstrating high burst effects and release lasting for approximately 3 days. Based on the release studies results, *in vitro* cell studies were carried out using samples S2 and S2FA on breast cancer cell lines MDA-MB-231 and MDA-MB-468. It was demonstrated that 468 cells are folate positive relative to 231 cells, and as a result, 468 cells showed higher folate-mediated uptake of nanoparticles as compared to 231 cells. Cytotoxicity studies showed higher susceptibility of 468 cells to curcumin compared to 231 cells. Also, 468 cells treated with samples S2c and S2FAc showed similar cell viability, likely because S2FAc holds approximately half the amount of drug as S2c, meaning that approximately twice the amount of S2FAc is required to deliver the same amount of curcumin as sample S2. However, the flow cytometry results still confirm that the selective targeting by folic acid in sample S2FA, suggesting that this might be translated to an effect *in vivo*, under non-static conditions. Therefore, the results obtained support the notion that magnetite nanoparticles conjugated with folic acid can potentially be used for the controlled delivery of curcumin for potential chemotherapeutic applications.

3.8 Bibliography

1. M. Salem, S. Rohani and E.R. Gillies, *RSC Advances*, 2014, **4**, 10815-10829.
2. R.M. Cornell and U. Schwertmann, *Introduction to the Iron Oxides*, in *The Iron Oxides*. 2004, Wiley-VCH Verlag GmbH & Co. KGaA. p. 1-7.
3. J.M. Perez, F.J. Simeone, Y. Saeki, L. Josephson and R. Weissleder, *Journal of the American Chemical Society*, 2003, **125**, 10192-10193.
4. A. Gupta and A.G. Curtis, *Journal of Materials Science: Materials in Medicine*, 2004, **15**, 493-496.
5. J. Gallo, N.J. Long and E.O. Aboagye, *Chemical Society Reviews*, 2013, **42**, 7816-7833.
6. L. Zhang, Y. Li and J.C. Yu, *Journal of Materials Chemistry B*, 2014, **2**, 452-470.
7. R.M. Cornell and U. Schwertmann, *Organisms*, in *The Iron Oxides*. 2004, Wiley-VCH Verlag GmbH & Co. KGaA. p. 475-489.
8. K. Yan, P. Li, H. Zhu, Y. Zhou, J. Ding, J. Shen, Z. Li, Z. Xu and P.K. Chu, *RSC Advances*, 2013, **3**, 10598-10618.
9. M.M. Yallapu, M. Jaggi and S.C. Chauhan, *Curr Pharm Des*, 2013, **19**, 1994-2010.
10. M.M. Yallapu, S.F. Othman, E.T. Curtis, B.K. Gupta, M. Jaggi and S.C. Chauhan, *Biomaterials*, 2011, **32**, 1890-905.
11. M.M. Yallapu, S.F. Othman, E.T. Curtis, N.A. Bauer, N. Chauhan, D. Kumar, M. Jaggi and S.C. Chauhan, *Int J Nanomedicine*, 2012, **7**, 1761-79.
12. M.M. Yallapu, M.C. Ebeling, S. Khan, V. Sundram, N. Chauhan, B.K. Gupta, S.E. Puumala, M. Jaggi and S.C. Chauhan, *Mol Cancer Ther*, 2013, **12**, 1471-80.
13. N. Wang, Y. Guan, L. Yang, L. Jia, X. Wei, H. Liu and C. Guo, *J Colloid Interface Sci*, 2013, **395**, 50-7.
14. J. Devkota, T.T.T. Mai, K. Stojak, P.T. Ha, H.N. Pham, X.P. Nguyen, P. Mukherjee, H. Srikanth and M.H. Phan, *Sensors and Actuators B: Chemical*, 2014, **190**, 715-722.
15. A.T. Paulino, A.G. Pereira, A.R. Fajardo, K. Erickson, M.J. Kipper, E.C. Muniz, L.A. Belfiore and E.B. Tambourgi, *Carbohydr Polym*, 2012, **90**, 1216-25.
16. A. Harada, M. Okada, J. Li and M. Kamachi, *Macromolecules*, 1995, **28**, 8406-8411.
17. Y. Liu, Y.-W. Yang, Y. Chen and H.-X. Zou, *Macromolecules*, 2005, **38**, 5838-5840.
18. Y. Lu and P.S. Low, *Journal of Controlled Release*, 2003, **91**, 17-29.

19. N. Parker, M.J. Turk, E. Westrick, J.D. Lewis, P.S. Low and C.P. Leamon, *Analytical Biochemistry*, 2005, **338**, 284-293.
20. D.M. Ragab, S. Rohani and S. Consta, *Int J Nanomedicine*, 2012, **7**, 3167-89.
21. E.R. Leite and C. Ribeiro, *Crystallization and Growth of Colloidal Nanocrystals*. 2011: Springer.
22. E.V. Shevchenko, D.V. Talapin, H. Schnablegger, A. Kornowski, O. Festin, P. Svedlindh, M. Haase and H. Weller, *J Am Chem Soc*, 2003, **125**, 9090-101.
23. Y.W. Jun, J.S. Choi and J. Cheon, *Angew Chem Int Ed Engl*, 2006, **45**, 3414-39.
24. J.D. Hu, Y. Zevi, X.M. Kou, J. Xiao, X.J. Wang and Y. Jin, *Sci Total Environ*, 2010, **408**, 3477-89.
25. B. Stuyven, Q. Chen, W.V.d. Moortel, H. Lipkens, B. Caerts, A. Aerts, L. Giebeler, B.V. Eerdenbrugh, P. Augustijns, G.V.d. Mooter, J.V. Humbeeck, J. Vanacken, V.V. Moshchalkov, J. Vermant and J.A. Martens, *Chemical Communications*, 2008, 49.
26. R.M. Cornell and U. Schwertmann, *Crystal Structure*, in *The Iron Oxides*. 2004, Wiley-VCH Verlag GmbH & Co. KGaA. p. 9-38.
27. R.M. Cornell and U. Schwertmann, *Electronic, Electrical and Magnetic Properties and Colour*, in *The Iron Oxides*. 2004, Wiley-VCH Verlag GmbH & Co. KGaA. p. 111-137.
28. J. Lee, S. Zhang and S. Sun, *Chemistry of Materials*, 2013, **25**, 1293-1304.
29. W. Cai and J. Wan, *J Colloid Interface Sci*, 2007, **305**, 366-70.
30. J. Wang, Y. Cao, B. Sun and C. Wang, *Food Chemistry*, 2011, **127**, 1680-1685.
31. C. Sun, R. Sze and M. Zhang, *J Biomed Mater Res A*, 2006, **78**, 550-7.
32. N.A. Peppas and J.J. Sahlin, *International Journal of Pharmaceutics*, 1989, **57**, 169-172.
33. P.L. Ritger and N.A. Peppas, *Journal of Controlled Release*, 1987, **5**, 37-42.
34. P.L. Ritger and N.A. Peppas, *Journal of Controlled Release*, 1987, **5**, 23-36.
35. M.S. Jhaveri, A.S. Rait, K.-N. Chung, J.B. Trepel and E.H. Chang, *Molecular Cancer Therapeutics*, 2004, **3**, 1505-1512.
36. V. Mamaeva, J.M. Rosenholm, L.T. Bate-Eya, L. Bergman, E. Peuhu, A. Duchanoy, L.E. Fortelius, S. Landor, D.M. Toivola, M. Linden and C. Sahlgren, *Mol Ther*, 2011, **19**, 1538-46.
37. H. Rochefort, M. Glondu, M.E. Sahla, N. Platet and M. Garcia, *Endocr Relat Cancer*, 2003, **10**, 261-6.

Chapter 4

4 Conclusions and Future Prospects

To reduce the side effects induced by traditional chemotherapy, this thesis demonstrated a potential means of targeted delivery for a natural chemotherapeutic agent. Specifically, magnetic magnetite nanoparticles were synthesized through a simple method, conjugated with folic acid for ligand targeted treatment, and loaded with curcumin as a chemotherapeutic agent. An extensive review was presented in Chapter 2 on the chemical properties of curcumin, its biological activity/mechanisms of action as an anti-cancer agent, and previous approaches to its delivery.

Chapter 3 described the experimental methods, results, and discussion. Synthesized magnetite nanoparticles coated with β -cyclodextrin (β -CD) and poly(propylene glycol) bis (2-aminopropyl ether) (PPG-NH₂) were characterized using various techniques, which revealed that nanoparticles were 10 – 20 nm in size and formed micron-sized aggregates. XRD analysis ensured that the synthesized iron oxide samples were in fact magnetite, and magnetic studies of both coated and uncoated particles showed that the samples retained their magnetic properties, even after the magnetite core was coated. FTIR spectra ensured the presence of both coating agents on the surface, and the successful conjugation of folic acid to PPG-NH₂.

In vitro drug release studies were conducted in buffer in order to determine the rate of curcumin release. S2c containing more PPG-NH₂, and S1c were investigated for sustained curcumin release and it was determined that S2c showed significantly better controlled release, lasting for 11 days. The presence of PPG-NH₂ likely increased the hydrophobic interactions, which must be broken for curcumin diffusion. However, for sample S2FAc the release of curcumin was faster, which was attributed to the presence of folic acid before curcumin loading, potentially making it difficult for curcumin to be entrapped securely in the β -CD cavities. Samples S1 and S1FA showed similar release profiles with high burst effects lasting for approximately 3 days. Based on these results, it may be possible to determine an optimum amount of PPG-NH₂ for folic acid conjugation which will demonstrate the most controlled curcumin release.

Sample S2 along with its folic acid conjugated (S2FA) and curcumin loaded counterparts (S2c and S2FAc) were chosen for *in vitro* experiments conducted on MDA-MB-231 (231) and MDA-MB-468 (468) breast cancer cells. It was demonstrated that 468 cells are folate receptor positive compared to 231 cells, and this was supported by the ligand-mediated uptake of folic acid-labeled magnetite samples (S2FA) by 468 cells compared to the relatively little uptake shown by 231 cells. *In vitro* cytotoxicity studies were carried out on samples S2c and S2FAc. The results demonstrated more cell death in 468 cells than 231 cells, as 231 cells were relatively folate negative and are a more treatment-resistant cell line. In addition, the amount of curcumin in folate-labeled nanoaggregates is approximately half of that present in non-labeled nanoaggregates which was why 468 cells showed similar cell death for both folic acid-labeled and non-labeled samples. In general, curcumin delivered by nanoaggregates is more toxic to 468 cells than 231 cells.

With the promising results obtained by these studies, it would be interesting to evaluate these systems *in vivo* and to investigate the effects of magnetic targeting in the enhancement of cytotoxicity in the future. Also, it would be beneficial to track these nanovehicles using MRI while simultaneously acting as a chemotherapeutic agent. In order to achieve this, it would also be ideal to reduce the degree of aggregation of the particles under physiological conditions so that they can be administered intravascularly and can exhibit prolonged circulation in the blood.

Appendix

Appendix 1: Standard XRD pattern for magnetite corresponding to ICCD card number 00-019-0629

00-019-0629 Aug 19, 2013 3:54 PM (CCPL)

Status Primary **QM:** Star (S) **Pressure/Temperature:** Ambient **Chemical Formula:** Fe +2 Fe2 +3 O4
Empirical Formula: Fe3 O4 **Weight %:** Fe72.36 O27.64 **Atomic %:** Fe42.86 O57.14
Compound Name: Iron Oxide **Mineral Name:** Magnetite, syn

Radiation: CuKα1 **λ:** 1.5406Å **Filter:** Ni Beta **Intensity:** Diffractometer **I/Ic:** 4.9

SYS: Cubic **SPGR:** Fd-3m (227)

Author's Cell [XtlCell a: 8.396Å **AuthCell Vol:** 591.86Å³ **AuthCell Z:** 8.00 **AuthCell MolVol:** 73.98]
Dcalc: 5.197g/cm³ **Dmeas:** 5.176g/cm³ **SS/FOM:** F(2θ) = 59.2(0.0129, 34)

Space Group: Fd-3m (227) **Molecular Weight:** 231.54
Crystal Data [XtlCell a: 8.396Å **XtlCell b:** 8.396Å **XtlCell c:** 8.396Å **XtlCell α:** 90.00° **XtlCell β:** 90.00°
XtlCell γ: 90.00° **XtlCell Vol:** 591.86Å³ **XtlCell Z:** 8.00] **Crystal Data Axial Ratio [a/b:** 1.000 **c/b:** 1.000]
Reduced Cell [RedCell a: 5.937Å **RedCell b:** 5.937Å **RedCell c:** 5.937Å **RedCell α:** 60.00°
RedCell β: 60.00° **RedCell γ:** 60.00° **RedCell Vol:** 147.96Å³]

πωβ: =2.42

Crystal (Symmetry Allowed): Centrosymmetric.

Pearson: cF56.00 **Prototype Structure:** Mg Al2 O4 **Prototype Structure (Alpha Order):** Al2 Mg O4
Mineral Classification: Spinel (Supergroup), 1C-oxide (Group)

Subfile(s): Primary Pattern, Forensic, Inorganic, Common Phase, Mineral Related (Mineral, Synthetic), NBS Pattern, Educational Pattern, Metals & Alloys, Pigment/Dye

Last Modification Date: 01/14/2012

00-011-0614 (Deleted), 00-026-1136 (Primary), 01-072-2303 (Alternate), 01-074-1909 (Alternate),
 01-075-0449 (Alternate), 01-075-1610 (Alternate), 01-076-1849 (Alternate), 01-079-0416 (Alternate),
 04-001-7822 (Alternate), 04-001-7909 (Alternate), 04-001-9000 (Alternate), 04-001-9328 (Alternate),
 04-002-0264 (Alternate), 04-002-0618 (Alternate), 04-002-0643 (Alternate), 04-002-1855 (Alternate),
 04-002-2487 (Alternate), 04-002-2707 (Alternate), 04-002-2709 (Alternate), 04-002-2981 (Alternate),
 04-002-3194 (Alternate), 04-002-3668 (Alternate), 04-002-5310 (Alternate), 04-002-5448 (Alternate),
 04-002-5632 (Alternate), 04-002-5683 (Alternate), 04-002-5903 (Alternate), 04-002-6866 (Alternate),
 04-002-6955 (Alternate), 04-002-8141 (Alternate), 04-002-8629 (Alternate), 04-002-9019 (Alternate),
 04-002-9635 (Alternate), 04-003-1446 (Alternate), 04-004-2838 (Alternate), 04-005-4307 (Alternate),
 04-005-4319 (Primary), 04-005-4551 (Alternate), 04-005-5733 (Alternate), 04-005-6288 (Alternate),
Cross-Ref PDF #'s: 04-005-9786 (Alternate), 04-005-9788 (Alternate), 04-005-9815 (Alternate), 04-006-0225 (Alternate),
 04-006-0425 (Alternate), 04-006-1668 (Alternate), 04-006-2406 (Alternate), 04-006-2467 (Alternate),
 04-006-2752 (Alternate), 04-006-6497 (Alternate), 04-006-6550 (Alternate), 04-006-6692 (Alternate),
 04-006-8076 (Alternate), 04-007-1427 (Alternate), 04-007-2718 (Alternate), 04-007-6010 (Alternate),
 04-007-8567 (Alternate), 04-007-8976 (Alternate), 04-007-9093 (Alternate), 04-008-0315 (Alternate),
 04-008-0777 (Alternate), 04-008-4423 (Alternate), 04-008-4511 (Alternate), 04-008-4512 (Alternate),
 04-008-8145 (Alternate), 04-009-4225 (Alternate), 04-009-8417 (Alternate), 04-009-8418 (Alternate),
 04-009-8419 (Alternate), 04-009-8420 (Alternate), 04-009-8421 (Alternate), 04-009-8422 (Alternate),
 04-009-8423 (Alternate), 04-009-8424 (Alternate), 04-009-8425 (Alternate), 04-009-8426 (Alternate),
 04-009-8427 (Alternate), 04-009-8428 (Alternate), 04-009-8429 (Alternate), 04-009-8430 (Alternate),
 04-009-8431 (Alternate), 04-009-8435 (Alternate), 04-009-8436 (Alternate), 04-009-8437 (Alternate),
 04-009-8438 (Alternate), 04-009-8439 (Alternate), 04-009-8440 (Alternate), 04-011-5952 (Alternate)

References:

Type	Reference
Primary Reference	Natl. Bur. Stand. (U. S.) Monogr. 25 5, 31 (1967).
Optical Data	Dana's System of Mineralogy, 7th Ed. I, 698.

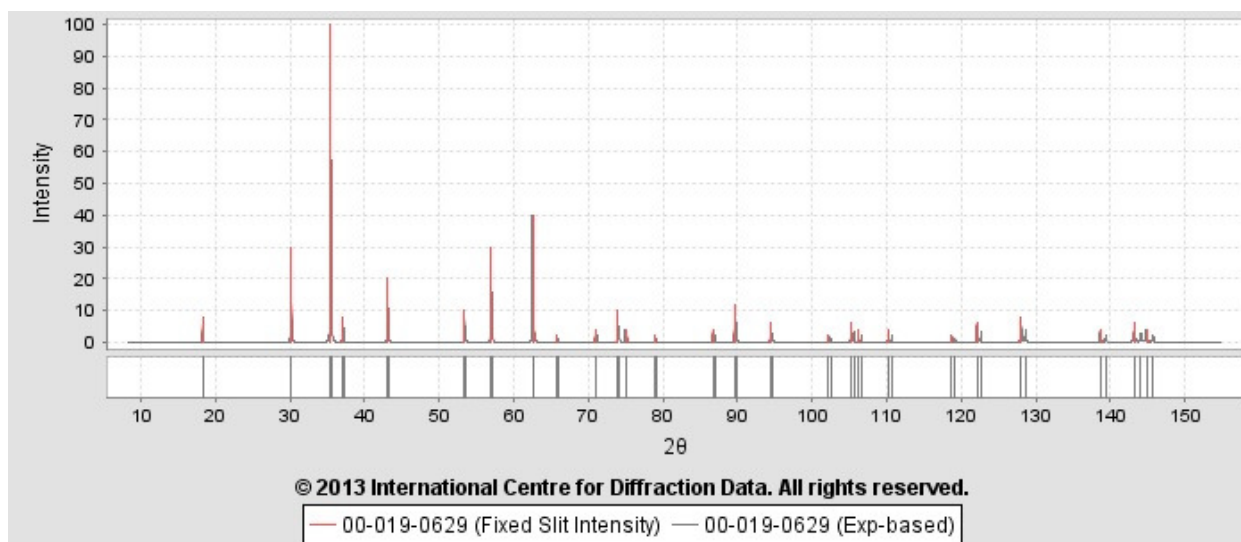
Database Comments: Additional Patterns: To replace 00-011-0614. See 00-026-1136. See 20596 (PDF 01-072-2303); 27898 (PDF 01-074-1909); 29129 (PDF 01-075-0449); 31157 (PDF 01-075-1610); 36314 (PDF 01-076-1849); 30860 (PDF 01-075-1372); 65338 (PDF 01-079-0416); 65339 (PDF 01-079-0417); 65340 (PDF 01-079-0418); 65341 (PDF 01-079-0419); 68181 (PDF 01-080-0389); 68182 (PDF 01-080-0390) and 75627 (PDF 01-082-1533). Analysis: Spectrographic analysis showed the following major impurities: 0.01 to 0.1% Co, 0.001 to 0.01% Ag, Al, Mg, Mn, Mo, Ni, Si, Ti and Zn. Color: Black. General Comments: Other data 00 025 1376. Opaque Optical Data: Opaque mineral optical data on specimen from Braastad, Norway; RR2Re=20.1, Disp.=16, VHN100=592, Color values=311, 314, . Sample Source or Locality: Sample obtained from the Columbian Carbon Co., New York, NY, USA. Temperature of Data Collection: Pattern taken at 298 K. Unit Cell: a=8.3967 refined in 1975. Unit Cell Data Source: Powder Diffraction.

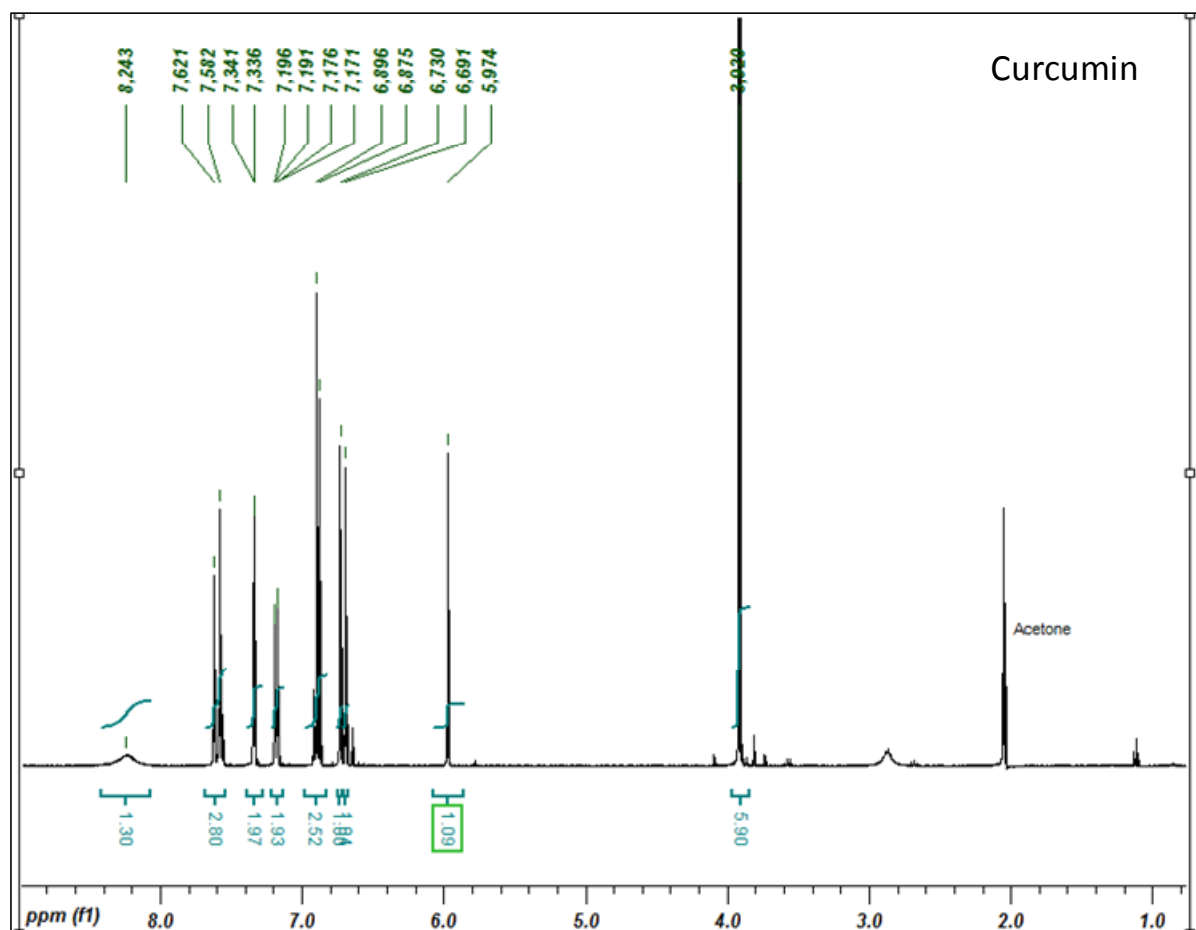
00-019-0629

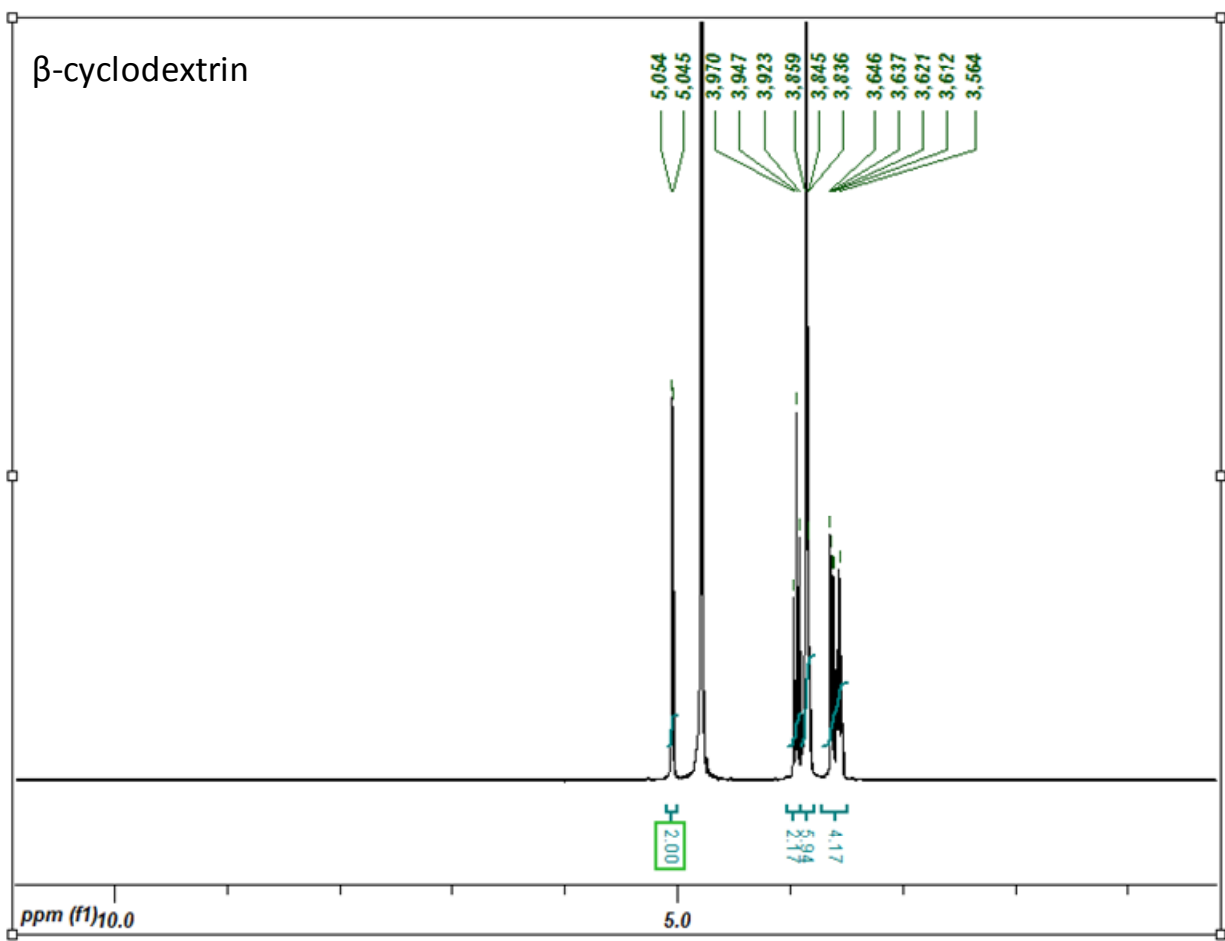
Aug 19, 2013 3:54 PM (CCPL)

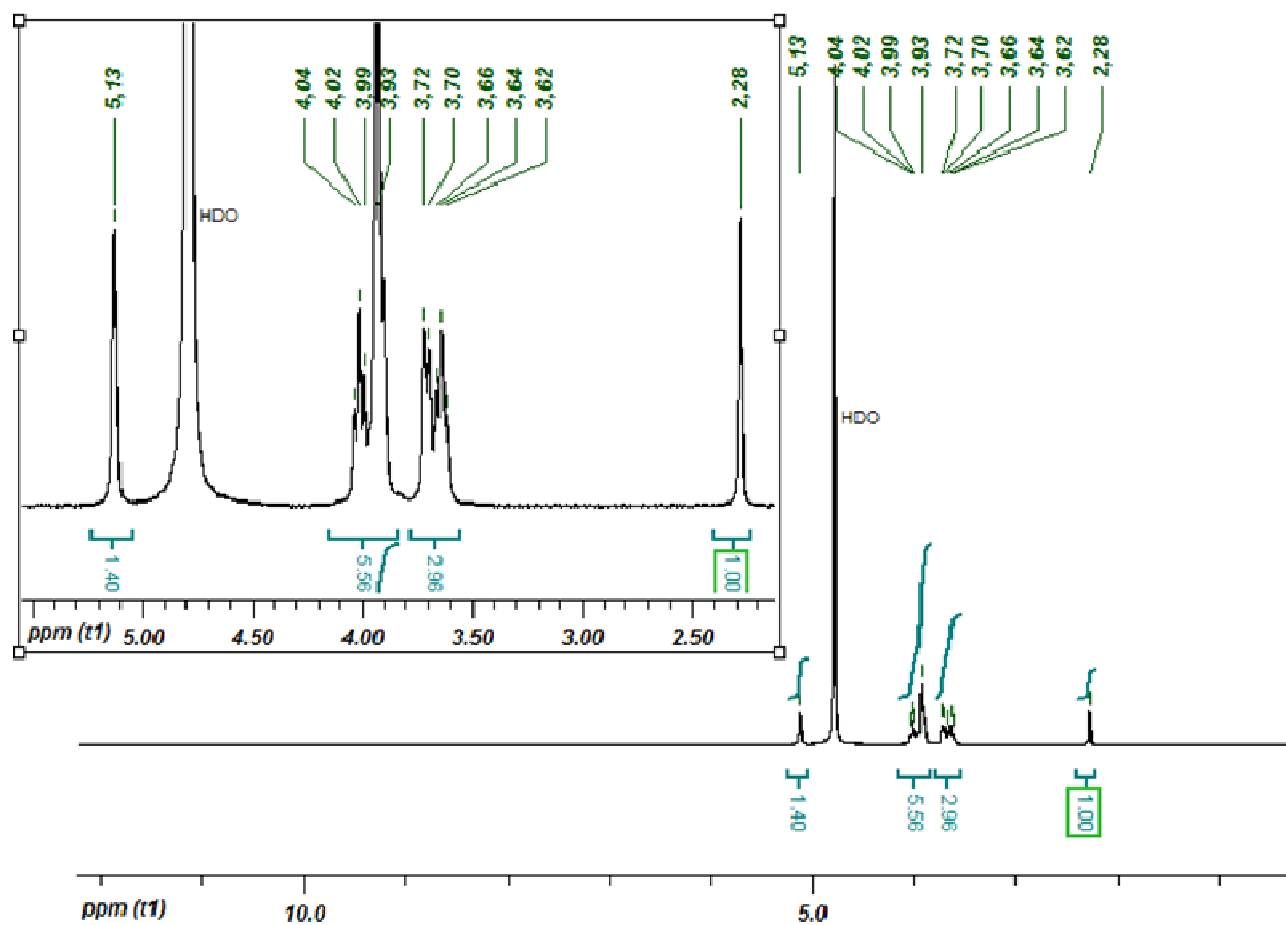
d-Spacings (2 θ) - 00-019-0629 (Fixed Slit Intensity) - Cu K α 1 1.54056Å

2 θ	d(Å)	I	h	k	l	*	2 θ	d(Å)	I	h	k	l	*	2 θ	d(Å)	I	h	k	l	*
18.2693	4.852000	8	1	1	1		70.9238	1.327700	4	6	2	0		106.2047	0.963200	4	6	6	2	
30.0945	2.967000	30	2	2	0		73.9480	1.280700	10	5	3	3		110.2686	0.938800	4	8	4	0	
35.4222	2.532000	100	3	1	1		74.9599	1.265900	4	6	2	2		118.7356	0.895200	2	6	6	4	
37.0518	2.424300	8	2	2	2		78.9286	1.211900	2	4	4	4		122.1182	0.880200	6	9	3	1	
43.0519	2.099300	20	4	0	0		86.7015	1.122100	4	6	4	2		128.0315	0.856900	8	8	4	4	
53.3908	1.714600	10	4	2	2		89.6170	1.093000	12	7	3	1		138.6508	0.823300	4	10	2	0	
56.9425	1.615800	30	5	1	1		94.4253	1.049600	6	8	0	0		143.2346	0.811700	6	9	5	1	
62.5145	1.484500	40	4	4	0		102.2241	0.989600	2	6	6	0		144.8478	0.808000	4	10	2	2	

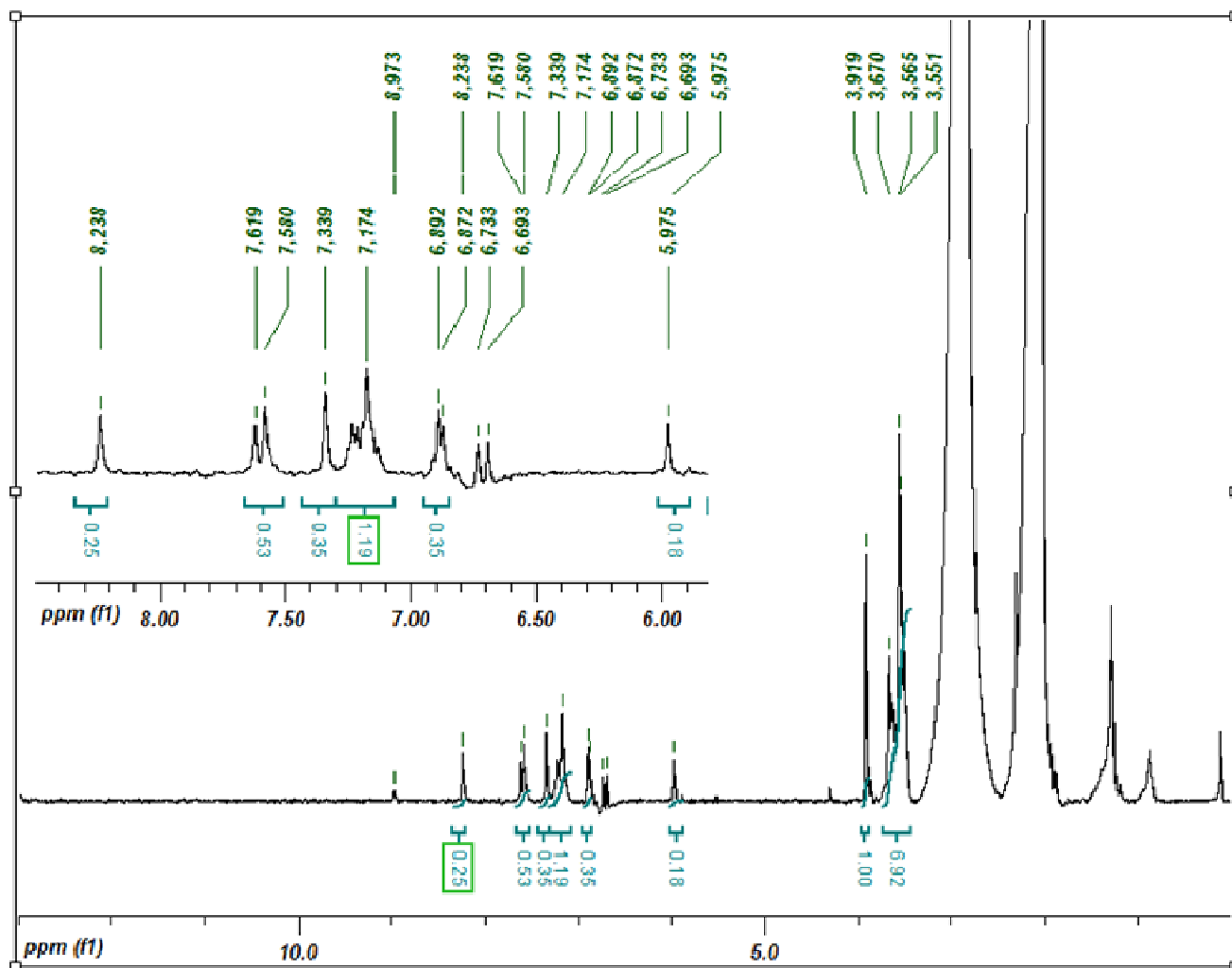


Appendix 2: ^1H NMR spectra of curcumin and β -cyclodextrin



Appendix 3: ^1H NMR of β -CD/curcumin Complex in Water

Appendix 4: ^1H NMR of β -CD/curcumin Complex in Acetone



Copyright Permissions

Chapter 2:

[M.Salem, S. Rohani, and E. R. Gillies, *RSC Advances*, 2014, **4**, 10815 – 10829] – Reproduced by permission of The Royal Society of Chemistry

<http://pubs.rsc.org/en/content/articlelanding/2014/ra/c3ra46396f#!divAbstract>

RSC | Advancing the
Chemical Sciences

Royal Society of Chemistry
Thomas Graham House
Science Park
Milton Road
Cambridge
CB4 0WF

Tel: +44 (0)1223 423 086
Fax: +44 (0)1223 423 623
Email: contracts-copyright@rsc.org

www.rsc.org

Acknowledgements to be used by RSC authors

Authors of RSC books and journal articles can reproduce material (for example a figure) from the RSC publication in a non-RSC publication, including theses, without formally requesting permission providing that the correct acknowledgement is given to the RSC publication. This permission extends to reproduction of large portions of text or the whole article or book chapter when being reproduced in a thesis.

The acknowledgement to be used depends on the RSC publication in which the material was published and the form of the acknowledgements is as follows:

- For material being reproduced from an article in *New Journal of Chemistry* the acknowledgement should be in the form:
 - [Original citation] - Reproduced by permission of The Royal Society of Chemistry (RSC) on behalf of the Centre National de la Recherche Scientifique (CNRS) and the RSC
- For material being reproduced from an article *Photochemical & Photobiological Sciences* the acknowledgement should be in the form:
 - [Original citation] - Reproduced by permission of The Royal Society of Chemistry (RSC) on behalf of the European Society for Photobiology, the European Photochemistry Association, and RSC
- For material being reproduced from an article in *Physical Chemistry Chemical Physics* the acknowledgement should be in the form:
 - [Original citation] - Reproduced by permission of the PCCP Owner Societies
- For material reproduced from books and any other journal the acknowledgement should be in the form:
 - [Original citation] - Reproduced by permission of The Royal Society of Chemistry

The acknowledgement should also include a hyperlink to the article on the RSC website.

The form of the acknowledgement is also specified in the RSC agreement/licence signed by the corresponding author.

Except in cases of republication in a thesis, this express permission does not cover the reproduction of large portions of text from the RSC publication or reproduction of the whole article or book chapter.

A publisher of a non-RSC publication can use this document as proof that permission is granted to use the material in the non-RSC publication.

Figure 2.3:

7/2/2014

Rightslink Printable License

**ELSEVIER LICENSE
TERMS AND CONDITIONS**

Jul 02, 2014

This is a License Agreement between Melessa Salem ("You") and Elsevier ("Elsevier") provided by Copyright Clearance Center ("CCC"). The license consists of your order details, the terms and conditions provided by Elsevier, and the payment terms and conditions.

All payments must be made in full to CCC. For payment instructions, please see information listed at the bottom of this form.

Supplier	Elsevier Limited The Boulevard, Langford Lane Kidlington, Oxford, OX5 1GB, UK
Registered Company Number	1982084
Customer name	Melessa Salem
Customer address	Thompson Engineering Building Rm 408 London, ON N6A5B9
License number	3420880557769
License date	Jul 02, 2014
Licensed content publisher	Elsevier
Licensed content publication	Biochimica et Biophysica Acta (BBA) - General Subjects
Licensed content title	Curcumin's pre-incubation temperature affects its inhibitory potency toward amyloid fibrillation and fibril-induced cytotoxicity of lysozyme
Licensed content author	Kuan-Nan Liu, Chia-Min Lai, Yi-Ting Lee, Sung-Ning Wang, Rita P.-Y. Chen, Jeng-Shiung Jan, Hwai-Shen Liu, Steven S.-S. Wang
Licensed content date	November 2012
Licensed content volume number	1820
Licensed content issue number	11
Number of pages	13
Start Page	1774
End Page	1786
Type of Use	reuse in a thesis/dissertation
Portion	figures/tables/illustrations
Number of figures/tables/illustrations	1
Format	both print and electronic

7/2/2014

Rightslink Printable License

Are you the author of this Elsevier article?	No
Will you be translating?	No
Title of your thesis/dissertation	Curcumin loaded magnetic nanoaggregates conjugated with folic acid for targeted cancer treatment
Expected completion date	Aug 2014
Estimated size (number of pages)	100
Elsevier VAT number	GB 494 6272 12
Permissions price	0.00 USD
VAT/Local Sales Tax	0.00 USD / 0.00 GBP
Total	0.00 USD

Curriculum Vitae

Name: Melessa Salem

Education

Bachelor of Engineering Science (Graduation with Distinction)
Biochemical Engineering (Honours Student)
Western University, London, Ontario, Canada
2008 – 2012

Master of Engineering Science
Biomedical Engineering Graduate Program
Western University, London, Ontario, Canada
2012 – 2014

Honours and Awards:

Scholarship of Distinction
2008

The Queen Elizabeth II Aiming for the Top Scholarship
2008 – 2011

Dean's Honour List
2009 – 2011

Natural Sciences and Engineering Research Council of Canada
Undergraduate Student Research Awards (NSERC USRA)
2011

Ontario Graduate Scholarship (OGS)
2013 - 2014

Related Work Experience

Teaching Assistant
Western University, London, Ontario, Canada
2012 - 2014

Publications:

M. Salem, S. Rohani, & E. R. Gillies, "Curcumin, a promising anti-cancer therapeutic: a review of its chemical properties, bioactivity and approaches to cancer cell delivery," *RSC Advances*, 10815 – 829 (2014).